University of Salford
A Greater Manchester University

SODAR calibration procedure
(final reporting on WP3, EU WISE project NNE5-2001-297)

Stuart Bradley[1,2] (ed.), Ioannis Antoniou[3], Sabine von Hünerbein[1],
Detlef Kindler[4], Manuel de Noord[5], and Hans Jørgensen[3]

[1]University of Salford, BUHU, UK
[2]University of Auckland, Physics Department, New Zealand
[3]Risø National Laboratory, Department of Wind Energy and Atmospheric Physics, DK
[4]Windtest Kaiser-Wilhelm-Koog GmbH WINDTEST, DE
[5]ECN - Energy Research Center of the Netherlands Unit Wind Energy, NL

SODAR calibration for wind energy applications

(final reporting on WP3, EU WISE project NNE5-2001-297)

Stuart Bradley (ed.)
University of Salford, BuHu, UK
University of Auckland, Physics Department, New Zealand
s.bradley@auckland.ac.nz

Ioannis Antoniou
Risø National Laboratory, Department of Wind Energy and Atmospheric Physics, DK
ioannis.antoniou@risoe.dk

Sabine von Hünerbein
University of Salford, Faculty of Science, Engineering & Environment, UK
s.vonhunerbein@salford.ac.uk

Detlef Kindler
Windtest Kaiser-Wilhelm-Koog GmbH WINDTEST, DE
kd@windtest.de

Manuel de Noord
ECN - Energy Research Center of the Netherlands Unit Wind Energy, NL
denoord@ecn.nl

Hans Jørgensen
Risø National Laboratory, Department of Wind Energy and Atmospheric Physics, DK
hans.e.joergensen@risoe.dk

The University of Salford, Greater Manchester, UK
March 2005
ISBN 0-9541649-1-1

Abstract

The method traditionally used for measuring the wind speed and direction for wind energy purposes is to record the output from cup or propeller anemometers and vanes at several heights on a mast. As turbines have grown in height, this method has become increasingly more expensive and difficult, and new methods have been sought.

One alternative method for measurement of wind speed and direction over depths of around 200m is the SODAR (SOund Detection And Ranging). This instrument is installed on the ground and every few seconds transmits a short pulse of sound upward into the atmosphere. As the sound propagates upward, some acoustic energy is continuously reflected back to the ground by the variable atmospheric turbulence encountered. By analysing the Doppler frequency shift of echoes received from sound transmitted at a small angle to the vertical, wind speed components are estimated as a function of height.

SODAR technology is well established as a tool for visualising and quantifying atmospheric dynamics in the lowest few hundred meters. At the same time, use of SODAR technology as a replacement for cup or propeller measurements in wind energy applications has a number of potential drawbacks. These include the need to calibrate much more rigorously than generally required for other applications, and the requirement that the SODAR operates with well-specified performance over the full range of atmospheric conditions relevant to wind turbine operations. Furthermore, SODAR performance should be portable from one physical site to another, and instruments supplied by a variety of manufacturers should be able to be deployed with known characteristics.

Within the WISE (WInd energy SODAR Evaluation) project (EU project number NNE5-2001-297), work package WP3 described in this report, is concerned with:

a) An estimation of the uncertainties in calibration which arise from SODAR design and operation.
b) Description of calibration procedures established by the WISE project and an evaluation of their limitations.
c) Testing of the calibration procedures against other methods of measurement.
d) Suggestions for improvements in SODAR design.

Items (a), (b), and (c) comprise Project deliverable D4 (Report on calibration of SODAR and inter-comparison before and after calibration). Item (d) comprises Project deliverable D5 (Notes on possible improvements of SODAR hardware/software for easier and better calibration).

The central conclusions of this work are

1. Care and understanding of SODAR error sources are required in order to adequately calibrate SODARs
2. A reliable calibration method is to calibrate a SODAR against a cup anemometer mounted at the top of a 40 m mast, and to use this calibration to correct SODAR wind speeds at other heights.
3. When compared with quality cup anemometers, corrected SODAR wind speeds show similar rms fluctuations to those exhibited between two cup anemometers
4. SODAR wind directions show good agreement with mast mounted vanes
5. Variations between SODARs of the same design appear to be small
6. Design changes could improve SODAR operation for wind energy applications.

Contents

Figures

Tables

1. Preface

The mechanical energy extracted from the wind by a turbine, and ultimately the electrical energy produced, depends on the wind profile throughout the sweep circle of the turbine blades. There are therefore obvious advantages for wind energy applications in wind measurements using an instrument which *profiles* continuously throughout the depth of the turbine. Traditionally this has been done using point measurements from mast-mounted anemometers, but as turbine size has grown the cost of erecting and maintaining a mast has soared. SODARs are a relatively inexpensive, robust, and proven method for remotely measuring wind speed and direction throughout an atmospheric layer near the ground. They also have the potential advantages of performing volume-averaged measurements rather than point measurements and more continuous measurements spatially.

The use of SODARs has rapidly grown for applications relating to characterising the complexity of wind and atmospheric transport processes in complex environments within the atmospheric turbulent boundary layer (the lowest few hundred meters). However, most of these applications do not require absolute measurements of wind speed and direction to the degree of accuracy normally available from well-calibrated cup anemometers mounted on a mast.

In the following we deal with issues relating to absolute calibration of SODARs and the relationship between wind estimates from SODARs and from cups. The emphasis is on obtaining highly precise windspeed measurements, and so considerable effort is applied to a theoretical and statistical analysis of SODAR signal production, reception, and signal processing for a range of SODAR configurations.

2. Principles of SODAR operation

The principles of SODAR operation, with particular reference to wind energy applications, have been described in detail by Antoniou et al. (2003). Here we give a brief resume of SODAR design characteristics and parameters which relate to calibration issues.

2.1 SODAR beams

SODARs send successive pulses of sound in a number of beam directions, generally including a vertical beam and several beams tilted at 15°-25° to the vertical. At least three beams in differing directions are needed in order to obtain measurements of the 3D wind velocity (see later for more detail). When one of these sound pulses is transmitted, sound is scattered by turbulent refractive index changes at all heights, and acoustic energy scattered back to the ground is collected by microphones. Usually the speakers which transmit the pulse are also used as microphones. This process gives a continuous time record of echo strength related to turbulent intensity. Knowledge of the local speed of sound, c, allows the time, t, elapsed since transmitting to be interpreted in terms of the height, z, from which an echo originated using

$$z = \frac{ct}{2}. \qquad (2.1)$$

The result is a height profile of a measure of turbulent intensity.

If the scattering turbulence has a component of motion parallel to the beam direction, this changes the acoustic frequency of the echo ('Doppler shift'). Analysis of the frequency spectrum of the received back-scattered signal allows estimation of the speed of the turbulence parallel to the beam as a function of inferred height.

Some seconds after the pulse is transmitted the echo signals are too weak to be detected above the background electrical and acoustic noise, because of spherical spreading of the energy and also

atmospheric absorption. At this time the next acoustic pulse is transmitted, generally in a different direction so that a different component of the wind is estimated. The upward propagation of an acoustic pulse is illustrated in Figure 1.

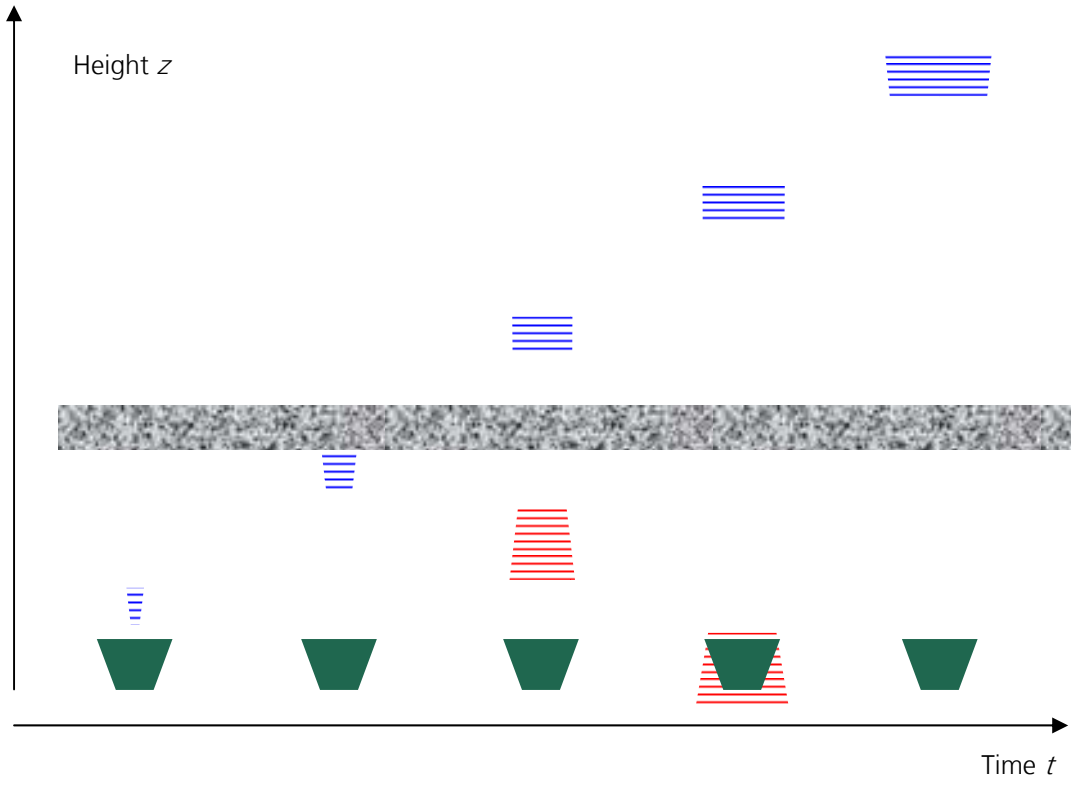

Figure 1. The position, at successive time steps, of an acoustic pulse transmitted vertically. The blue shows the upward propagating pulse and the red shows the downward propagating reflection from a turbulent layer shown the grey.

It is clear from this figure that: the volume occupied by the transmitted acoustic pulse increases as it progresses vertically; the echo from height z is received after travelling distance $2z$; and a scattering layer of finite thickness lengthens the received signal. For an acoustic pulse duration of τ and half beam width of $\Delta\varphi$, the effective volume over which wind speed averaging takes place is $c\tau[\pi(z\,\Delta\varphi/2)^2]/2$ where c is the speed of sound and z is the height. In practice it takes some time T to sample the echo signal for each frequency spectrum, and this time may be the dominant time in determining the averaging volume. In any case, it can be seen that the wind speed and direction estimates have a vertical spatial resolution of $c\tau/2$ or $cT/2$ and a horizontal spatial resolution of approximately $z\,\Delta\varphi/2$. Since the various beams are generally tilted at angle φ to the vertical, but in different directions, they are also horizontally separated by a distance of $z\varphi$ to $2z\varphi$ and this imposes some limitation because the separate wind components are not being estimated within the same volume.

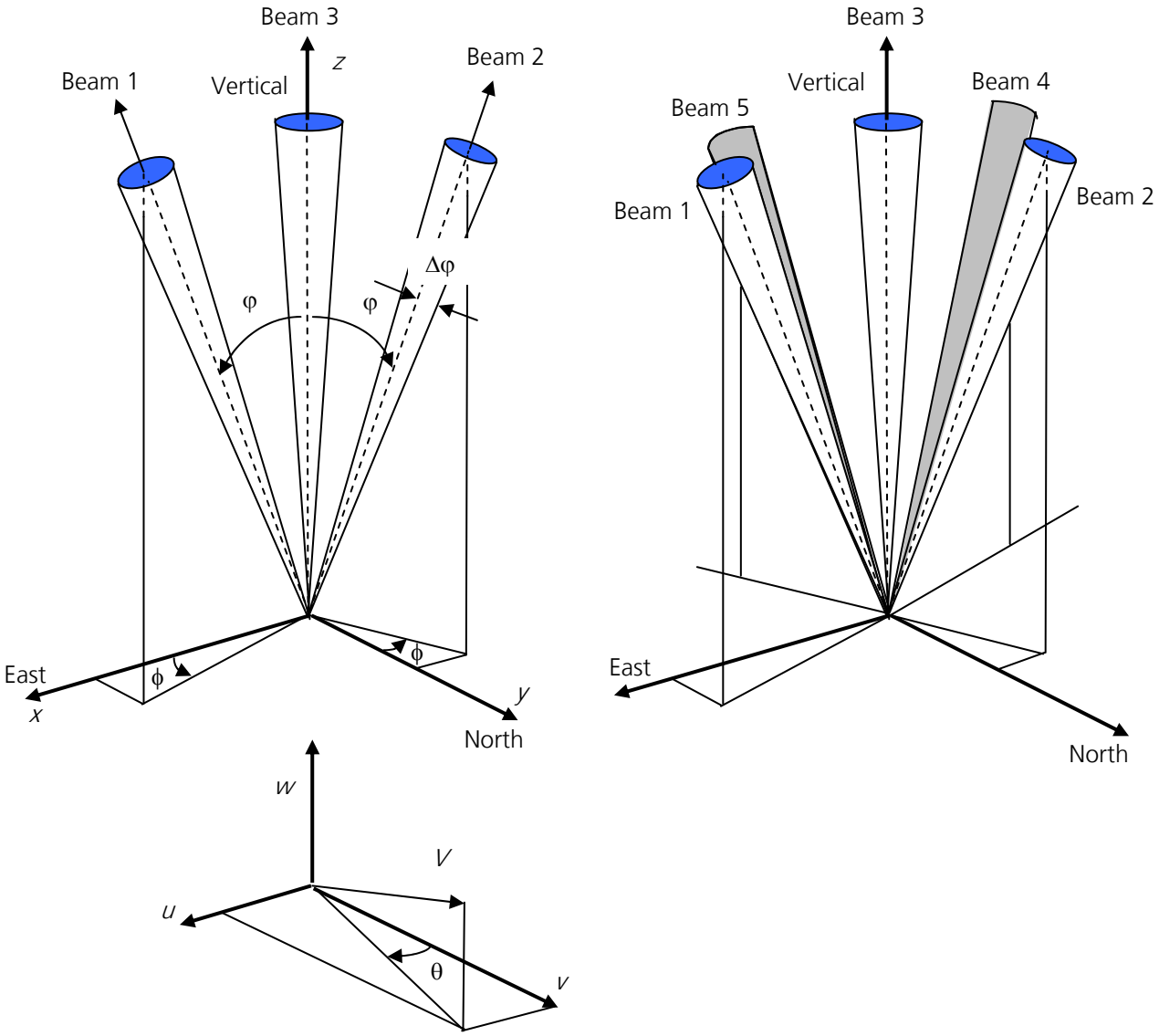

Figure 2. Typical beam geometries for a 3-beam and a 5-beam system, showing the relationship to wind components. The transmission in a particular beam direction, and the analysis of the echoes from that beam, is usually completed before transmission in the next beam direction.

Figure 2 shows typical beam configurations for (a) a 3-beam SODAR, and (b) a 5-beam SODAR. The planes defined by the beam axes and the vertical are generally orthogonal. Here beams are numbered 1-5 and the tilt angle φ, typically 15°-20°, is generally the same for the various tilted beams. Each tilted beam is also partly sensitive to the vertical wind. When the SODAR is installed, there will generally be an orientation angle ϕ between beam planes and North, East, West and South, so that it is not necessarily possible to identify individual beams with the easterly (u), northerly (v), vertical (w), westerly ($-u$), and southerly ($-v$) wind components, although each beam half-width is typically 4°. The wind speed is V and the wind direction is θ.

The beam directions for SODARs are generally selected electronically using phased arrays of speakers and microphones. The antenna is therefore a regular N_A x N_A grid of speakers each separated by spacing d. The interference pattern from this 2D array produces intensity approximately proportional to

$$\left[\frac{\sin\left(N_A k \frac{d}{2}\sin\theta\right)}{\sin\left(k\frac{d}{2}\sin\theta\right)}\right]^2 \tag{2.2}$$

where θ is the zenith angle, and $k = \frac{2\pi}{\lambda}$ is the wavenumber for transmitted sound of wavelength λ (see Werkhoven and Bradley, 1997, for details). By employing a phase shift increment of $\Delta\phi$ between each row of speakers the transmitted wavefront is tilted by

$$\varphi \approx \frac{\Delta\phi}{kd} = \frac{c}{2\pi f_T d}\Delta\phi \tag{2.3}$$

where f_T is the transmitting frequency. Typically $\Delta\phi$=90°. As an example an AeroVironment 4000 SODAR has d = 0.06 m and f_T = 4500 Hz so, with c = 340 m s^{-1} the tilt angle is 340x90/(2π4500x0.06)=18°. This angle is dependent both on transmitted frequency f_T and speed of sound c. In Figure 2 the beams are shown as having finite spread into cones. Eq. (2.2 gives the distribution of intensity into these cones, and the beam half-width is an angle of about

$$\Delta\varphi = \frac{c}{2fdN_A}. \tag{2.4}$$

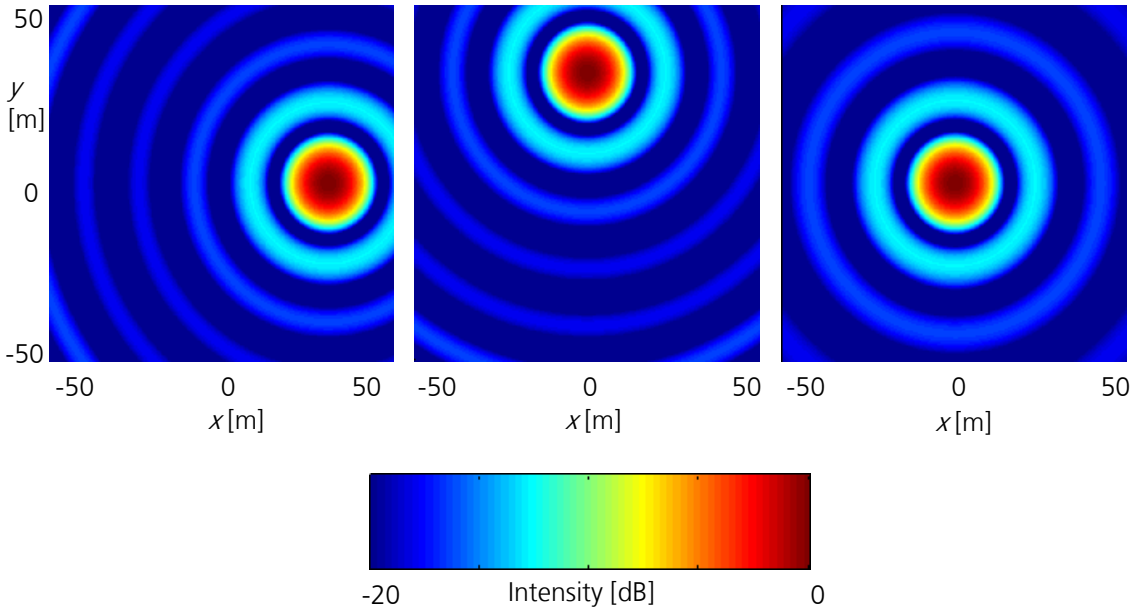

Figure 3. The relative intensity patterns from an AeroVironment 4000 at 100 m height. The effect of acoustics baffles has been ignored.

For example, the AeroVironment 4000 with N_A=8 gives a beam width of about 5°. The result is a *weighting* on wind speed estimates resulting from different regions of the beam according to this intensity pattern. This weighting produces spread in the Doppler peak of the echo frequency spectrum, and also some bias, as discussed later in Section 3.3. The relative intensities for the AeroVironment case are shown as dB in Figure 3.

2.2 Frequency spectrum

The frequency content in the received signal includes electronic and background acoustic noise, Doppler shifted echo signals at frequencies near the transmitted frequency f_T, and echoes from nearby solid objects such as buildings or masts at the frequency f_T. The received signal is demodulated and sampled giving a Doppler FFT spectrum at discrete frequencies

$$f_i = i\frac{f_s}{N_f} \qquad i = -\frac{N_f}{2}+1, -\frac{N_f}{2}+2, \ldots, \frac{N_f}{2}-1, \frac{N_f}{2} \tag{2.5}$$

where the spectrum contains N_f points sampled at a rate f_s. Each spectrum is therefore acquired over a time interval of $T=N_f/f_s$ equivalent to a height interval of $cN_f/2f_s$. This height resolution for wind component estimation is typically Δz = 10 m, giving spectral estimates separated by about $\Delta f = 170/\Delta z = 17$ Hz. A transmitted pulse of duration τ = 50 ms gives a spectral peak of half width around 20 Hz, but the returned echo signal is accompanied by noise so a *peak detection* algorithm is required and the estimated Doppler shift frequency is subject to uncertainty. It is usual to average over perhaps 5 to 10 minutes to obtain an improved signal-to-noise ratio (SNR). This can be done by averaging the frequency spectrum obtained at each sampled height, or range gate, separately for each beam. Since noise is random and the echo signal not, an improvement by a factor $\sqrt{N_s}$ is obtained in the SNR of the power spectrum if N_s spectra are averaged. Note however that the SNR may be considered too low in some cases and individual spectra excluded from the average, so that N_s may be different for each beam and each height over a particular averaging period.

2.3 Wind component estimation

The five beams shown in Figure 2 have directions given by unit vectors

$$\begin{aligned}
\underline{b_1} &= (\sin\varphi\cos\phi \quad \sin\varphi\sin\phi \quad \cos\varphi) \\
\underline{b_2} &= (-\sin\varphi\sin\phi \quad \sin\varphi\cos\phi \quad \cos\varphi) \\
\underline{b_3} &= (0 \quad 0 \quad 1) \\
\underline{b_4} &= (-\sin\varphi\cos\phi \quad -\sin\varphi\sin\phi \quad \cos\varphi) \\
\underline{b_5} &= (\sin\varphi\sin\phi \quad -\sin\varphi\cos\phi \quad \cos\varphi)
\end{aligned} \tag{2.6}$$

If the wind vector $\underline{V}$ has components u, v, and w, in the x, y, and z directions, respectively, then the projections of the wind onto the beam directions are

$$\begin{aligned}
v_{r1} &= \underline{V}\bullet\underline{b_1} = u\sin\varphi\cos\phi + v\sin\varphi\sin\phi + w\cos\varphi \\
v_{r2} &= \underline{V}\bullet\underline{b_2} = -u\sin\varphi\sin\phi + v\sin\varphi\cos\phi + w\cos\varphi \\
v_{r3} &= \underline{V}\bullet\underline{b_3} = w \\
v_{r4} &= \underline{V}\bullet\underline{b_4} = -u\sin\varphi\cos\phi - v\sin\varphi\sin\phi + w\cos\varphi \\
v_{r5} &= \underline{V}\bullet\underline{b_5} = u\sin\varphi\sin\phi - v\sin\varphi\cos\phi + w\cos\varphi
\end{aligned} \tag{2.7}$$

These radial velocity components give Doppler shifted echoes with frequency spectrum power at

$$\Delta f_j = -\frac{2v_{rj}}{c}f_T \qquad j = 1, 2, 3, 4, 5\,. \tag{2.8}$$

Given the presence of noise, a peak detection algorithm is then used to determine the best estimate of Δf_j and hence solve the system (2.7) for the wind components (u, v, w).

2.4 Signal Processing

The SODAR incorporates signal-processing software to determine

- The position in the spectrum of the signal peak (corresponding to Doppler shift)
- The averages over a number of profiles (to improve SNR).

The methods for achieving these tasks vary a little between manufacturers, as follows.

Metek

Metek average N_s spectra for each beam and each range gate. Each recorded value in a spectrum is the sum (P_E+ P_G) of the echo P_E from turbulence and the Gaussian noise P_G which has zero mean and variance σ_P^2 . The signal-to-noise-ratio, or SNR, from a single spectral estimate is

$$SNR_1 = \frac{P_E}{\sigma_P}.$$

If N_s spectra are averaged, the average spectral estimate becomes $P_E + \frac{1}{N_s}\sum_1^{N_s} P_G$, and the variance in this estimate is $\mathrm{var}\left(\frac{1}{N_s}\sum_1^{N_s} P_G\right) = \frac{1}{N_s}\sigma_P^2$. The SNR is therefore

$$SNR_{N_s} = \sqrt{N_s}\,\frac{P_E}{\sigma_P}. \qquad (2.9)$$

In the Metek SODAR, 32 complex Fourier amplitudes are obtained over N_s = 20-60 profiles, giving 32 averaged spectral intensities. Two noise spectra measurements are made shortly before each pulse is transmitted and these are averaged to obtain an estimate of P_G at each frequency in the Fourier spectrum. These averaged noise intensities are subtracted from the averaged intensities received after the pulse, to give residual power spectra at each range gate. It is assumed that the noise-free signal power spectrum has a Gaussian shape

$$\frac{P_0 \Delta f}{\sqrt{2\pi}\sigma_f} e^{-\frac{1}{2}\left(\frac{f-\hat{f}}{\sigma_f}\right)^2}$$

where $\Delta f = \frac{1}{T}$ is the frequency resolution. If logarithms of the spectral estimates are used,

$$L = \ln\left(\frac{P_0 \Delta f}{\sqrt{2\pi}\sigma_f}\right) - \frac{1}{2}\left(\frac{f-\hat{f}}{\sigma_f}\right)^2 \qquad (2.10)$$

which is a quadratic in f. Using Least Squares, the moments P_0 , $\hat{f}$, and σ_f can be estimated. In practice, only n spectral points within ¼ height (6dB) of the main peak are included in the Least Squares fit. Simulations based on this scheme show that, for high SNR and with N_s>40, the uncertainty in the peak position $\hat{f}$ is about 0.06 spectral bin widths and the uncertainty in σ_f is about 0.2 spectral bins. If all cases are rejected which have SNR below a certain critical threshold, then this accuracy is expected. With Δz =20m and f_T=1675Hz, the error in the radial velocity component is $\sigma_{v_r} = \sigma_{\hat{f}} \Delta z$ = 0.1 m s^{-1} and the error in the estimate of the width of the velocity spectrum is 0.17 m s^{-1}. For a tilt angle of φ = 20°, and given that the two horizontal velocity components are generally comparable and dominate over the vertical component,

$\sigma_V \approx \frac{\sqrt{2}\sigma_{v_r}}{\sin\varphi}$ = 0.4 m s^{-1}. Similar analysis gives the uncertainty σ_θ in the wind direction as about 6° for V=5 m s^{-1}.

AeroVironment

The AeroVironment system performs peak-detection on each individual 64-point spectrum (128-point spectra can also be user-selected). This is done by finding the highest power in any contiguous 5-spectral-point group (or 7-point for a 128-point spectrum) across the frequency spectrum. The SNR is then defined as the 5-point power divided by the power in the remaining 59 points normalized by multiplying by 59/5. Finally, averaging the accepted peak positions over N_s profiles gives the estimated Doppler shift for the particular range gate and beam. Note that if the user selects the option to use Beam 3 data, then a rejected beam 3 spectrum causes the Beam 1 and Beam 2 peak estimates to also be rejected at that range gate for that profile (i.e. the system does not default to a 2-beam configuration which might give averages of mixed 2-beam and 3-beam calculations). Numbers of accepted Beam 1, Beam 2, and Beam 3 peak estimates in each averaging interval are output for the user.

The system also employs an adaptive noise threshold as part of the decision to accept/reject a spectrum. This threshold is determined by sampling the background noise prior to the transmit pulse, and appropriately scaling this threshold to account for spherical beam divergence with altitude. This option can be disabled or enabled by the user. If this option is disabled the system uses a fixed noise threshold which is applied at every altitude.

Statistical analysis shows that the uncertainty in each estimate of the position of the spectral peak in this scheme depends on $(SNR_1)\left(\frac{\Delta f}{\sigma_f}\right)^3$.

3. Sources of calibration error

The above brief outline of SODAR operating principles indicates a number of possible sources of errors in derived wind speeds and directions. These errors fall into three main categories:

1. geometrical
    i. Height estimation errors
    ii. Errors in tilt angle
    iii. Errors in scattering angle
2. bias in wind estimation
    i. Uncertainties in the standard against which calibrations are conducted
    ii. Incomplete beam data
    iii. Variance in SODAR averages from varying numbers of samples
    iv. Separation of sampling volumes
    v. Different averaging schemes for SODAR and standard
3. noise problems
    i. Spectral peak position errors
    ii. Loss of signal in noise

Some of these errors are also "operational problems" in the sense that they can cause a change in the calibration depending on siting or conditions or Sodar operating parameters.

3.1 Uncertainties in the calibration 'standard'

Cup anemometers and sonic anemometers are two 'standards' against which SODARs might be calibrated in the field. Both have instrumental and siting errors (see Antoniou et al., 2003 for a description of cup errors). Additionally when a comparison is made there will be fluctuations in wind speed and direction which will not be identical at the 'standard' site and the SODAR site. This

means that calibrations are conducted against a 'standard' which also contains errors, some of which could be systematic. These errors are called 'Type A errors'. If a calibration could be conducted against an error-free standard, then corrections and uncertainties would be identified due to the SODAR design. Such errors are called 'Type B errors'. However, conducting a calibration against a real 'standard' which has inherent Type A errors can cause the Type A errors to be included into the calibration as Type B errors. This would then mean that whenever the 'calibrated' SODAR was subsequently used, it would give wrong data because it also included errors from the 'standard'. To illustrate, imagine that a SODAR was calibrated against a cup which always read 5% too low, but that the SODAR recorded wind speeds accurately. Then a wind speed of 10 m s^{-1} would be recorded by the cup as 9.5 m s^{-1} and by the SODAR as 10 m s^{-1}. A SODAR calibration would then be found as $V_{true}=0.95\,V_{SODAR}$. When the SODAR is used subsequently in the field it will always read 5% too low.

This transference of Type A to Type B error can be minimised in three ways. The first is to take every precaution in calibrating and siting the 'standard'. The second is to identify the possible sources of calibration error which arise *because* of the calibration configuration (rather than because of the characteristics of the SODAR). Finally, weighted least squares fitting should include uncertainty weighting on *both* the SODAR and the 'standard'. There is an established method, 'orthogonal least squares' for handling errors in both the dependent and independent variables. Dissanaike et al, 2003 describe this technique and an improved algorithm.

In the paragraphs below we identify errors arising both because of calibration setup and because of the particular nature of SODAR design.

3.2 Height estimation errors

The simple assumption in Eq. 2.1, which allows comparison between SODAR determined winds and winds determined by other means, depends on knowledge of the speed of sound. In practice, each beam also drifts with the wind, but this is considered separately below.

The sound speed, for a constant rate of change of temperature with height (this gradient is known as the "lapse rate") and echo return time t, is

$$2\frac{dz}{dt} = c \approx c_0 + \frac{1}{2}\frac{c_0}{T_0}\frac{dT}{dz}z \tag{3.1}$$

giving

$$\ln\left(1+\frac{1}{2T_0}\frac{dT}{dz}z\right) = \frac{1}{2T_0}\frac{dT}{dz}\frac{c_0}{2}t\,.$$

The height estimated from (2.1) is, in terms of the actual echo height

$$\hat{z} \approx z\left(1-\frac{1}{4T_0}\frac{dT}{dz}z\right). \tag{3.2}$$

For example, $\frac{dT}{dz}$ = 0.01 K m^{-1} gives a negligible 0.3 m error at a range of 200 m. In comparison, a 15 K error in surface air temperature used to estimate c_0 gives a 5 m height error over the range 200 m. This error is readily corrected by measuring, or even estimating climatologically, the surface air temperature. If it is assumed that the return time for an echo from 200 m with a beam tilted at 18° is the same as that for a vertical beam, then the height error is 10 m. This error is also easily, although not necessarily, corrected by all SODAR manufacturers.

3.3 Errors in tilt angle

The tilt angle φ is vitally important in connecting the Doppler shifted spectral peaks to the individual wind velocity components through (2.7) and (2.8). The magnitude of the error can be estimated by assuming the tilt angle is actually $\varphi+\Delta\varphi$ but that it is assumed in analysis of the winds

that the tilt angle is φ. Then, for w=0, and just considering Beam 1, the estimated wind component is

$$\hat{u} = \frac{v_{r1}}{\sin\varphi} = \frac{u\sin(\varphi+\Delta\varphi)}{\sin\varphi} \approx u\left(1+\frac{\Delta\varphi}{\tan\varphi}\right). \tag{3.3}$$

For a typical beam tilt angle of 18°, this represents a 5% error in wind speed for each 1° error in tilt angle. This order of error is unacceptable for wind energy applications which would normally require errors to be less than 1% overall.

There are two principal sources of error: temperature changes affecting beam formation; and the SODAR being out-of-level.

Tilt angle dependence on temperature

Most SODARs form their acoustic beams using a phased 2D matrix of speakers/microphones. From (2.3) the change in tilt angle with temperature is

$$\frac{\partial\varphi}{\partial T} = \frac{\varphi}{c}\frac{\partial c}{\partial T} = \frac{\varphi}{2T} \tag{3.4}$$

or about 1° tilt change for 33°C change in temperature (1.5% wind speed error for every 10°C change in temperature). Such errors should also be corrected by either measuring the surface air temperature or using a climatology.

Out-of-level errors

When a vector $\underline{b}$ is rotated angle $\Delta\varphi$ about the vector $\underline{n}$ to give a new vector $\underline{b'}$

$$\underline{b'} = \underline{b}\cos\Delta\varphi + (1-\cos\Delta\varphi)(\underline{b}\bullet\underline{n})\underline{n} + (\underline{n}\times\underline{b})\sin\Delta\varphi\,.$$

If the SODAR is not level, but is rotated by angle $\Delta\varphi$ about the y axis, this formula gives

$$\begin{aligned}
\underline{b'_1} &= (\sin[\varphi+\Delta\varphi] \quad 0 \quad \cos[\varphi+\Delta\varphi]) \\
\underline{b'_2} &= (\cos\varphi\sin\Delta\varphi \quad \sin\varphi \quad \cos\varphi\cos\Delta\varphi) \\
\underline{b'_3} &= (\sin\Delta\varphi \quad 0 \quad \cos\Delta\varphi) \\
\underline{b'_4} &= (-\sin[\varphi-\Delta\varphi] \quad 0 \quad \cos[\varphi-\Delta\varphi]) \\
\underline{b'_5} &= (\cos\varphi\sin\Delta\varphi \quad -\sin\varphi \quad \cos\varphi\cos\Delta\varphi)
\end{aligned} \quad .$$

Here, for simplicity, we have used an orientation angle ϕ = 0. The radial velocity components are

$$\begin{aligned}
v_{r1} &= \underline{V}\bullet\underline{b'_1} = u\sin[\varphi+\Delta\varphi] + w\cos[\varphi+\Delta\varphi] \\
v_{r2} &= \underline{V}\bullet\underline{b'_2} = u\cos\varphi\sin\Delta\varphi + v\sin\varphi + w\cos\varphi\cos\Delta\varphi \\
v_{r3} &= \underline{V}\bullet\underline{b'_3} = u\sin\Delta\varphi + w\cos\Delta\varphi \\
v_{r4} &= \underline{V}\bullet\underline{b'_4} = -u\sin[\varphi-\Delta\varphi] + w\cos[\varphi-\Delta\varphi] \\
v_{r5} &= \underline{V}\bullet\underline{b'_5} = u\cos\varphi\sin\Delta\varphi - v\sin\varphi + w\cos\varphi\cos\Delta\varphi
\end{aligned} \quad .$$

For a 3-beam system, the winds estimated are

$$u' = \frac{v_{r1} - v_{r3}\cos\varphi}{\sin\varphi} = u\cos\Delta\varphi - w\sin\Delta\varphi$$
$$v' = \frac{v_{r2} - v_{r3}\cos\varphi}{\sin\varphi} = v \qquad . \qquad (3.5)$$
$$w' = v_{r3} = u\sin\Delta\varphi + w\cos\Delta\varphi$$

In some cases, for example if the return from the vertical beam is corrupt, it is assumed that w=0 and the horizontal components are found from

$$u' = \frac{v_{r1}}{\sin\varphi} = u\left(\cos\Delta\varphi + \sin\Delta\varphi\cot\varphi\right)$$
$$v' = \frac{\eta_2}{\sin\varphi} = v + u\sin\Delta\varphi\cot\varphi \qquad . \qquad (3.6)$$

Five beam systems produce estimates

$$u' = \frac{v_{r1} - v_{r4}}{2\sin\varphi} = u\cos\Delta\varphi - w\sin\Delta\varphi$$
$$v' = \frac{v_{r2} - v_{r5}}{2\sin\varphi} = v \qquad . \qquad (3.7)$$
$$w' = v_{r3} = u\sin\Delta\varphi + w\cos\Delta\varphi$$

The interesting result is that there is no difference between the wind component estimates from 3-beam and 5-beam systems, providing the w component is used in the calculations. If the entire SODAR is tilted, then the change in radial velocity component on a tilted beam is accompanied by a change in the radial velocity on beam 3: when the w contribution is subtracted from a tilted beam, the tilt error is largely cancelled.

However, the errors in (3.6) are exactly those calculated in (3.3) i.e. 5% wind component error for each 1° of tilt error. The conclusion is that if the beam 3 spectral peak determination is considered unreliable then it is better to NOT include the (3.6) calculation in forming an average over some period of time.

Bias due to beam spread

As indicated from (2.2), each acoustic beam has finite angular width. This means that the Doppler power spectrum is due to a spread of φ and ϕ in (2.7) and (2.8). The contribution to the power spectrum for Beam 1 from a small volume around position (r,φ,ϕ) has angular dependence proportional to

$$I_1(\varphi,\phi)\sin\varphi d\varphi d\phi\left(u\sin\varphi\cos\phi + v\sin\varphi\sin\phi + w\cos\varphi\right) \qquad (3.8)$$

at a Doppler shift of

$$f_1 = -\frac{2\left(u\sin\varphi\cos\phi + v\sin\varphi\sin\phi + w\cos\varphi\right)f_T}{c} \qquad (3.9)$$

where $I_1(\varphi,\phi)$ is the angular intensity pattern. Adding up all such contributions which result in power in a particular frequency interval gives the Doppler spectrum. Spread in the beam pattern $I_1(\varphi,\phi)$ is weighted by the $\sin^2\varphi$ factor, giving bias to the tilt angle. Near the tilted beam axis at $\varphi \approx \overline{\varphi}$, a reasonable approximation is a Gaussian shape

$$I_1(\varphi,\phi) = I_0(\phi)\exp\left(-\frac{1}{2}\left[\frac{\sin\varphi - \sin\overline{\varphi}}{\sigma_\varphi}\right]^2\right) \qquad (3.10)$$

where the beam width σ_φ is about 7/9 of $\Delta\varphi$ given in (2.4). Along the ϕ = 0 line, the power spectrum contributions are proportional to

$$f_1^2 \exp\left(-\frac{1}{2}\left[\frac{f_1 - \bar{f}_1}{\sigma_{f_1}} \right]^2 \right)$$

where $\bar{f}_1 = -\frac{2uf_T}{c}\sin\bar{\varphi}$ and $\sigma_{f_1} = \frac{2uf_T}{c}\sigma_\varphi$. The spectrum peak occurs at

$$\frac{d}{df_1}\left\{ f_1^2 \exp\left(-\frac{1}{2}\left[\frac{f_1 - \bar{f}_1}{\sigma_{f_1}} \right]^2 \right) \right\} = 0$$

or

$$f_1 = \bar{f}_1 + 2\frac{\sigma_{f_1}^2}{\bar{f}_1}. \tag{3.11}$$

The estimated wind speed component, neglecting beam spread weighting, is

$$\hat{u} = u\left(1 + \frac{2\sigma_\varphi^2}{\sin^2\bar{\varphi}} \right) \tag{3.12}$$

This error clearly increases with beam width and is less for greater tilt angles. For example, assuming a SODAR having f_T = 4500 Hz, $kd/2$ = 2.5, and N_A = 8, and concentrating on the central part of a tilted beam, gives a design tilt angle of 18.32°, but a weighted tilt angle, estimated from (2.4) and (3.11) of 19.61°. This gives a 7% overestimate of wind speeds.

3.4 Errors in scattering angle

The Doppler formula (2.8) is more complicated than first might be thought, since it derives from reflections from a moving target in a moving medium travelling at an angle to the receiver. The situation can be visualised as the acoustic pulse being blown downwind. Scattered sound must then be directed further upwind in order to reach and be received by the SODAR. Both the upward and downward wind refraction effects cause extra Doppler effects and lead to a correction to the simple Doppler shift formula.

Georges and Clifford (1972) first gave a treatment for the bi-static case and then extended this with examples for the mono-static situation (Georges and Clifford, 1974). Unfortunately their formula for Doppler shift does not reduce to the simple 1D text book case when the transmitter, receiver and wind are in line. This means also that numerical simulations based on the Georges and Clifford formulae by Phillips et al. (1977) and Schomburg and Englich (1998) are suspect. More recently, Ostashev (1997) has treated the 2D (x, z) case, and has found that the error in wind speed calculated using the 2D version of (2.7) and (2.8) is $\Delta V = \frac{V^2}{c}\sin\varphi$. This is in contrast to Georges and Clifford, who find that there is no refractive correction (to 2nd order) when the wind is entirely horizontal. Given the confusion in these various treatments, and the need for a 3D correction formula, we now give a basic derivation of 'beam drift' effects.

Assume there is a SODAR at (0,0,0) and a patch of turbulence at $\underline{r_0} = (x_0, y_0, z_0)$. The SODAR emits a sound wave crest at time = 0 and in the direction having unit vector $\hat{\underline{b}} = (\sin\varphi\cos\phi, \sin\varphi\sin\phi, \cos\varphi)$. In time t_1 the turbulent patch will have moved to $\underline{r_1} = \underline{r_0} + \underline{V}t_1$ and

the crest will meet the turbulent patch at this time if $\underline{r}_1 = \left(c\underline{\hat{b}} + \underline{V}\right)t_1$. This means that $\underline{r}_0 = ct_1\underline{\hat{b}}$ or $ct_1 = \underline{r}_0 \bullet \underline{\hat{b}}$.

At time T a second crest is emitted. This crest meets the turbulent patch at time t_2 if

$$\underline{r}_2 = \underline{r}_0 + \underline{V}t_2 = \left(c\underline{\hat{b}'} + \underline{V}\right)(t_2 - T) \tag{3.13}$$

since the time taken to reach the turbulent patch is t_2-T. The period of the sound at the turbulent patch is therefore $T' = t_2 - t_1$. Note that $\underline{\hat{b}'}$ is in general different from $\underline{\hat{b}}$, since the beam must be aimed a little further downstream to meet the same turbulent patch. From (3.13) $\underline{r}_0 + \underline{V}T = c\underline{\hat{b}'}(t_2 - T)$ so

$$\begin{aligned} (ct_2 - cT)^2 &= \left(\underline{r}_0 + \underline{V}T\right) \bullet \left(\underline{r}_0 + \underline{V}T\right) \\ c^2t_2^2 - r_0^2 &= 2\left(c^2t_2 + \underline{r}_0 \bullet \underline{V}\right)T - \left(c^2 - V^2\right)T^2 \end{aligned}. \tag{3.14}$$

Also the initial height of the turbulent patch was $z_0 = \underline{r}_0 \bullet \underline{\hat{z}} = ct_1\underline{\hat{b}} \bullet \underline{\hat{z}}$ so

$$\underline{r}_0 = \frac{z_0}{\underline{\hat{b}} \bullet \underline{\hat{z}}}\underline{\hat{b}}. \tag{3.15}$$

At time t_1 the first crest is scattered into all directions by the turbulent patch at position $\underline{r}_1$. This scattered crest will meet the SODAR at time t_3 if

$$-\underline{r}_1 = \left(c\underline{\hat{b}''} + \underline{V}\right)(t_3 - t_1) \tag{3.16}$$

where the part of the scattered wave which reaches the SODAR is initially scattered in direction $\underline{\hat{b}''}$. Similarly, at time t_2 the second crest is scattered when the turbulent patch is at position $\underline{r}_2$ and the part of the wavefront directed in direction $\underline{\hat{b}'''}$ will meet the SODAR at time t_4 where

$$-\underline{r}_2 = \left(c\underline{\hat{b}'''} + \underline{V}\right)(t_4 - t_2). \tag{3.17}$$

The period of the scattered sound reaching the SODAR is $T'' = t_4 - t_3$. From (3.16), $c\underline{\hat{b}''}(t_3 - t_1) = -\underline{r}_1 - \underline{V}(t_3 - t_1) = -\left(c\underline{\hat{b}}t_1 + \underline{V}t_3\right)$ or $c^2(t_3 - t_1)^2 = \left(c\underline{\hat{b}}t_1 + \underline{V}t_3\right) \bullet \left(c\underline{\hat{b}}t_1 + \underline{V}t_3\right)$. This gives

$$t_3 = 2ct_1\frac{\left(\underline{V} \bullet \underline{\hat{b}} + c\right)}{c^2 - V^2} = \frac{2\left(\underline{r}_0 \bullet \underline{\hat{b}}\right)\left(\underline{V} \bullet \underline{\hat{b}} + c\right)}{c^2 - V^2}. \tag{3.18}$$

From (3.13) and (3.17), $-\underline{r}_0 = c\underline{\hat{b}'''}(t_4 - t_2) + \underline{V}t_4 = c\underline{\hat{b}'''}(T'' + t_3 - t_2) + \underline{V}(T'' + t_3)$. Therefore $c^2(T'' + t_3 - t_2)^2 = \left[\underline{r}_0 + \underline{V}(T'' + t_3)\right] \bullet \left[\underline{r}_0 + \underline{V}(T'' + t_3)\right]$, or

$$\left(c^2 - V^2\right)(T'' + t_3)^2 - 2\left(c^2t_2 + \underline{r}_0 \bullet \underline{V}\right)(T'' + t_3) + \left(c^2t_2^2 - r_0^2\right) = 0. \tag{3.19}$$

Multiplying by $\frac{c - V}{c + V}$ and rearranging,

$$[(c-V)T'']^2 + 2[(c-V)T''][(c-V)t_3] + [(c-V)t_3]\left[(c-V)t_3 - 2\frac{c^2t_2 + \underline{r}_0 \bullet \underline{V}}{c+V}\right]$$
$$- 2\frac{c^2t_2 + \underline{r}_0 \bullet \underline{V}}{c+V}[(c-V)T''] + 2\frac{(c^2t_2 + \underline{r}_0 \bullet \underline{V})(c-V)T}{c+V} - (c-V)^2T^2 = 0$$

giving

$$\left[(c-V)(T''+t_3) - \frac{c^2t_2 + \underline{r}_0 \bullet \underline{V}}{c+V}\right]^2 = \left[\frac{c^2t_2 + \underline{r}_0 \bullet \underline{V}}{c+V} - (c-V)T\right]^2 .$$

The positive root must be taken, giving

$$(c-V)T'' = 2\frac{c^2t_2 + \underline{r}_0 \bullet \underline{V} - (\underline{r}_0 \bullet \hat{\underline{b}})(\underline{V} \bullet \hat{\underline{b}} + c)}{c+V} - (c-V)T \ . \qquad (3.20)$$

Finally, substitution from (3.14) for t_2 and from (3.15) for $\underline{r}_0$ gives,

$$(c^2 - V^2)T''\cos\varphi = (c^2 + V^2)T\cos\varphi + 2cz_0\left\{\left[1 + 2\frac{\underline{VT}\cos\varphi}{z_0} \bullet \hat{\underline{b}} + \left(\frac{VT\cos\varphi}{z_0}\right)^2\right]^{\frac{1}{2}} - 1\right\} . \qquad (3.21)$$

This result is *exact* for a constant wind, and gives the period T'' of the sound received at the SODAR. For 1D sound transmission in line with the wind, this gives a Doppler shift of $\Delta f = f'' - f_T = \frac{1}{T''} - \frac{1}{T} = -2\frac{V}{c+V}f_T$ as expected.

In general $VT << z_0$. For example, V=20 m s^{-1}, T=0.5 ms, so VT = 10^{-2}, whereas the first range gate $z_0 > 5$ m. Therefore

$$\left(1 - \frac{V^2}{c^2}\right)T'' \approx \left(1 + 2\frac{\underline{V}}{c} \bullet \hat{\underline{b}} + \frac{V^2}{c^2}\right)T$$

or, after rearranging

$$\frac{\Delta f}{f_T} = \frac{-2\frac{\underline{V} \bullet \hat{\underline{b}}}{c} - 2\frac{V^2}{c^2}}{1 + 2\frac{V}{c}\hat{\underline{V}} \bullet \hat{\underline{b}} + \frac{V^2}{c^2}} \qquad (3.22)$$

to within 0.2%. Here $\hat{\underline{V}}$ is a unit vector in the direction of the wind. The Doppler shift is usually calculated from (2.8) and the velocity components estimated from $-2\frac{\underline{V}_e \bullet \hat{\underline{b}}}{c}f_T$. The estimated velocity $\underline{V}_e$ in terms of true velocity $\underline{V}$ is therefore

$$\underline{V}_e \bullet \hat{\underline{b}} = \frac{\underline{V} \bullet \hat{\underline{b}} + \frac{V^2}{c}}{1 + 2\frac{V}{c}\hat{\underline{V}} \bullet \hat{\underline{b}} + \frac{V^2}{c^2}} . \qquad (3.23)$$

A further approximation can be made that $V<<c$, giving

$$\underline{V_e} \bullet \underline{\hat{b}} \approx \underline{V} \bullet \underline{\hat{b}} + \frac{V^2}{c}\left[1 - 2\left(\underline{\hat{V}} \bullet \underline{\hat{b}}\right)^2\right]. \tag{3.24}$$

Generally $2\left(\underline{\hat{V}} \bullet \underline{\hat{b}}\right)^2 < 0.2$ so

$$\underline{V_e} \bullet \underline{\hat{b}} = \underline{V} \bullet \underline{\hat{b}} + \frac{V^2}{c}. \tag{3.25}$$

This predicts a larger effect than the treatment by Ostashev (1997).

For a 3-beam SODAR system,

$$\begin{aligned} v_{r1} &= u_e \sin\varphi\cos\phi + v_e \sin\varphi\sin\phi + w_e \cos\varphi = u \sin\varphi\cos\phi + v \sin\varphi\sin\phi + w\cos\varphi + \frac{V^2}{c} \\ v_{r2} &= -u_e \sin\varphi\sin\phi + v_e \sin\varphi\cos\phi + w_e \cos\varphi = -u \sin\varphi\sin\phi + v \sin\varphi\cos\phi + w\cos\varphi + \frac{V^2}{c}, \\ v_{r3} &= w_e = w + \frac{V^2}{c} \end{aligned} \tag{3.26}$$

or

$$\begin{aligned} u_e \sin\varphi + w_e \cos\varphi(\cos\phi - \sin\phi) &= u \sin\varphi + w\cos\varphi(\cos\phi - \sin\phi) + \frac{V^2}{c}(\cos\phi - \sin\phi) \\ v_e \sin\varphi + w_e \cos\varphi(\cos\phi + \sin\phi) &= v \sin\varphi + w\cos\varphi(\cos\phi + \sin\phi) + \frac{V^2}{c}(\cos\phi + \sin\phi) \end{aligned}.$$

If the estimate of the vertical wind, w_e, is used in the solution for u_e and v_e, then

$$\begin{aligned} u_e &= u + \frac{V^2}{c}\frac{(\cos\phi - \sin\phi)(1-\cos\varphi)}{\sin\varphi} = u + \sqrt{2}\frac{V^2}{c}\sin\left(\frac{\pi}{4} - \phi\right)\tan\frac{\varphi}{2} \\ v_e &= v + \frac{V^2}{c}\frac{(\cos\phi + \sin\phi)(1-\cos\varphi)}{\sin\varphi} = v + \sqrt{2}\frac{V^2}{c}\sin\left(\frac{\pi}{4} + \phi\right)\tan\frac{\varphi}{2} \end{aligned}. \tag{3.27}$$

The wind speed estimated without beam drift corrections is

$$V_e = \sqrt{u_e^2 + v_e^2} = V\left[1 + \sqrt{2}\frac{V}{c}\sin\left(\theta + \phi + \frac{\pi}{4}\right)\tan\frac{\varphi}{2}\right]. \tag{3.28}$$

The corrections are <1% for $V \leq 15$ m s^{-1}. If, on the other hand, the vertical radial wind information is not used, and $w = 0$, then

$$V_e = \sqrt{u_e^2 + v_e^2} = V\left[1 + \sqrt{2}\frac{V}{c\sin\varphi}\sin\left(\theta + \phi + \frac{\pi}{4}\right)\right]. \tag{3.29}$$

These corrections are generally much larger, as shown in Figure 4.

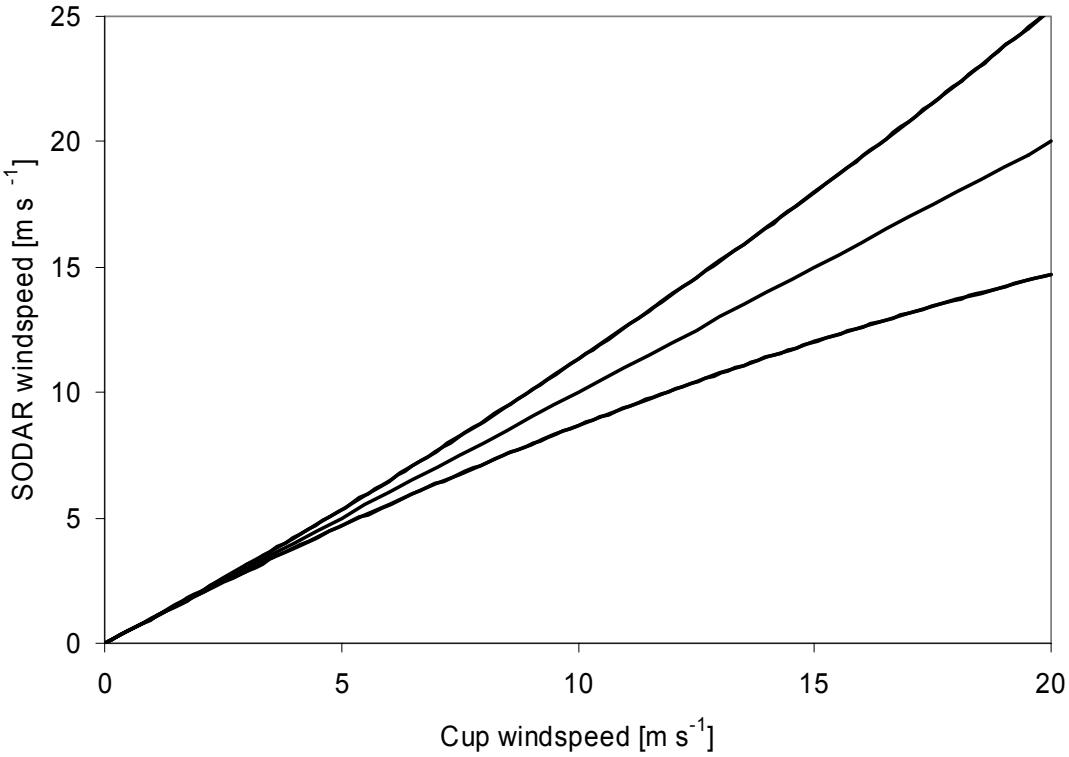

Figure 4. Wind speeds estimated for a 2-beam SODAR vs those which would be recorded by a cup anemometer. The upper and lower curves are the two extreme limits and the straight line shows 1:1.

Corrected wind directions can be found similarly.
The true wind components can be recovered from the estimated components of (3.29) by

$$V \approx V_e\left[1-\sqrt{2}\,\frac{V_e}{c\sin\varphi}\sin\left(\theta+\phi+\frac{\pi}{4}\right)\right]. \tag{3.30}$$

For a 5-beam SODAR system, winds are estimated from

$$\frac{(v_{r1}-v_{r4})\cos\phi-(v_{r2}-v_{r5})\sin\phi}{2\sin\varphi}=u_e=u$$
$$\frac{(v_{r1}-v_{r4})\sin\phi+(v_{r2}-v_{r5})\cos\phi}{2\sin\varphi}=v_e=v$$

In this case the $\frac{V^2}{c}$ errors cancel for *u* and *v*, and no correction for wind drift is required. However, *w* still has the error given in (3.26). Clearly, for estimation of *horizontal winds* the 5-beam system is inherently much superior, provided valid data is recorded in all four tilted beams (see detailed discussion in section 3.5).
The error in the vertical velocity component, *w*, is about 0.3 m s^{-1} for all beam configurations when *V*=10 m s^{-1}, so can be a major source of error. Also, there is error propagation into σ_w via

$$\sigma_{w'}^2=\sigma_w^2+\left(\frac{V}{c}\right)^2\sigma_V^2\,. \tag{3.31}$$

System	Correction term for V	Maximum error at V=5 m s^{-1}	Maximum error at V=10 m s^{-1}	Maximum error at V=20 m s^{-1}
2-beam	$\frac{V^2}{c}\sqrt{2}\sin\left(\theta+\phi+\frac{\pi}{4}\right)\frac{1}{\sin\varphi}$	±7	±14 %	±27 %
3-beam	$\frac{V^2}{c}\sqrt{2}\sin\left(\theta+\phi+\frac{\pi}{4}\right)\tan\frac{\varphi}{2}$	±0.3 %	±0.7 %	±1.3 %
5-beam	0	0	0	0

Table 1. Summary of beam-drift errors, assuming tilt angle $\varphi = \pi/10$.

3.5 Calculating wind components from incomplete beam data

In the presence of noise, one or more beams may have missing data at some range gate. "Missing data" is generally defined in some way by the SODAR manufacturer in terms of software switches which select various "filters" or consistency checks (see Section 5.3 below). This means that (2.7) and (2.8), or the equivalent for a 3-beam system, may not be able to be used.
Two questions arise:

1. how should a reduced set of equations be solved to obtain estimates of wind components u, v and w?
2. what is the effect on the uncertainties in an averaged wind when reduced data are used?

These questions relate to both calibration and operational issues because of the need to obtain the best possible data from a SODAR.

Suitable reductions are based on (2.7). The standard deviations when orientation $\phi = 0$ are, based on the standard deviation in estimation of Δf, and from the smallest to the largest,

$$\begin{aligned}
\sigma_A &= \frac{c}{2\sqrt{2}f_T\cos\varphi}\sigma_{\Delta f}\\
\sigma_B &= \frac{c}{2f_T}\sigma_{\Delta f}\\
\sigma_C &= \frac{c}{2\sqrt{2}f_T\sin\varphi}\sigma_{\Delta f}\\
\sigma_D &= \frac{c}{2f_T\sin\varphi}\sigma_{\Delta f}\\
\sigma_E &= \frac{c\sqrt{3}}{2\sqrt{2}f_T\sin\varphi}\sigma_{\Delta f}\\
\sigma_F &= \frac{c\sqrt{1+\cos^2\varphi}}{2f_T\sin\varphi}\sigma_{\Delta f}
\end{aligned} \qquad (3.32)$$

giving the results in Table 2.

beam	u	±	V	±	w	±
all	$(v_{r1}-v_{r4})/2\sin\varphi$	C	$(v_{r2}-v_{r5})/2\sin\varphi$	C	v_{r3}	B
2345	$(v_{r3}\cos\varphi-v_{r4})/\sin\varphi$	F	$(v_{r2}-v_{r5})/2\sin\varphi$	C	v_{r3}	B
1345	$(v_{r1}-v_{r4})/2\sin\varphi$	C	$(v_{r3}\cos\varphi-v_{r5})/\sin\varphi$	F	v_{r3}	B
1245	$(v_{r1}-v_{r4})/2\sin\varphi$	C	$(v_{r2}-v_{r5})/2\sin\varphi$	C	$\dfrac{v_{r1}+v_{r2}+v_{r4}+v_{r5}}{4\cos\varphi}$	
1235	$(v_{r1}-v_{r3}\cos\varphi)/\sin\varphi$	F	$(v_{r2}-v_{r5})/2\sin\varphi$	C	v_{r3}	B
1234	$(v_{r1}-v_{r4})/2\sin\varphi$	C	$(v_{r2}-v_{r3}\cos\varphi)/\sin\varphi$	F	v_{r3}	B
123	$(v_{r1}-v_{r3}\cos\varphi)/\sin\varphi$	F	$(v_{r2}-v_{r3}\cos\varphi)/\sin\varphi$	F	v_{r3}	B
124	$(v_{r1}-v_{r4})/2\sin\varphi$	C	$2[v_{r2}-v_{r1}-v_{r4}]/2\sin\varphi$	E	$(v_{r1}+v_{r4})/2\cos\varphi$	A
125	$[2v_{r1}-v_{r2}-v_{r5}]/2\sin\varphi$	E	$(v_{r2}-v_{r5})/2\sin\varphi$	C	$(v_{r2}+v_{r5})/2\cos\varphi$	A
134	$(v_{r1}-v_{r4})/2\sin\varphi$	C			v_{r3}	B
135	$(v_{r1}-v_{r3}\cos\varphi)/\sin\varphi$	F	$(v_{r3}\cos\varphi-v_{r5})/\sin\varphi$	F	v_{r3}	B
145	$(v_{r1}-v_{r4})/2\sin\varphi$	C	$[v_{r1}+v_{r4}-2v_{r5}]/2\sin\varphi$	E	$(v_{r1}+v_{r4})/2\cos\varphi$	A
234	$(v_{r3}\cos\varphi-v_{r4})/\sin\varphi$	F	$(v_{r2}-v_{r3}\cos\varphi)/\sin\varphi$	F	v_{r3}	B
235			$(v_{r2}-v_{r5})/2\sin\varphi$	C	v_{r3}	B
245	$[v_{r2}+v_{r5}-2v_{r4}]/2\sin\varphi$	E	$(v_{r2}-v_{r5})/2\sin\varphi$	C	$(v_{r2}+v_{r5})/2\cos\varphi$	A
12	$v_{r1}/\sin\varphi$	D	$v_{r2}/\sin\varphi$	D		
13	$(v_{r1}-v_{r3}\cos\varphi)/\sin\varphi$	F			v_{r3}	B
14	$(v_{r1}-v_{r4})/2\sin\varphi$	C				
15	$v_{r1}/\sin\varphi$	D	$-v_{r5}/\sin\varphi$	D		
23			$(v_{r2}-v_{r3}\cos\varphi)/\sin\varphi$	F	v_{r3}	B
24	$-v_{r4}/\sin\varphi$	D	$v_{r2}/\sin\varphi$	D		
25			$(v_{r2}-v_{r5})/2\sin\varphi$	C		
34	$(v_{r3}\cos\varphi-v_{r4})/\sin\varphi$	F			v_{r3}	B
35			$(v_{r3}\cos\varphi-v_{r5})/\sin\varphi$	F	v_{r3}	B
45	$-v_{r4}/\sin\varphi$	D	$-v_{r5}/\sin\varphi$	D		

Table 2. Formulae for computing velocity components from multi-beam SODARs when orientation ϕ=0. For the definition of beam numbers refer to Figure 2.

Which gives less uncertainty: a 3-beam or a 5-beam system?

It is evident from the above that many combinations may occur in practice, with differing error contributions to the final averaged wind. The 5-beam system is more robust in terms of providing some measure of all three wind components, but acquisition of 5 beams takes 5/3 times as long as acquisition of 3 beams, so there will generally be 5/3 times as many wind estimates obtained at each range gate for a 3-beam system, giving a nominal $\sqrt{1.7}=1.3$ times improvement in SNR.

Assume, because of noise, a random fraction f of spectra at a particular range gate produce acceptable data. For a 3-beam system the probability of obtaining acceptable spectra from Beams 1 and 2, and thereby obtaining a wind speed estimate, is f^2. For a 5-beam system, the probability of obtaining acceptable data from beams 1 and 2, or 1 and 5, or 2 and 4, or 4 and 5 is $f^5+5f^4(1-f)+7f^3(1-f)^2+4f^2(1-f)^3=f^2(4-5f+3f^2-f^3)$ (the different terms on the left corresponding to the probabilities of the acceptable combinations when 5 beams, 4 beams, 3

beams and 2 beams have acceptable data). Overall, the ratio of acceptable 5-beam wind speeds to acceptable 3-beam wind speeds will be

$$\frac{3}{5}\left(4 - 5f + 3f^2 - f^3\right). \tag{3.33}$$

This is unity at f≈0.7 and increases for smaller f. This implies that a 3-beam system will generally give better quality data when data availability is higher (for example, closer to the ground), but worse when data availability is reduced (for example, further above the ground) as shown in Figure 5.

In addition, if full 3-beam data or full 5-beam data are available (the SNR is high) then Table 2 shows that the ratio of spectrum peak position errors is

$$\frac{\sigma_F}{\sigma_c} = \sqrt{1+\cos^2\varphi}\sqrt{2} \approx 2 \tag{3.34}$$

so that a 5-beam system will be more accurate in this regime. A much more complex analysis using the probability of success of each beam combination times the estimated peak error gives the second curve in Figure 5, but the conclusion is effectively not changed.

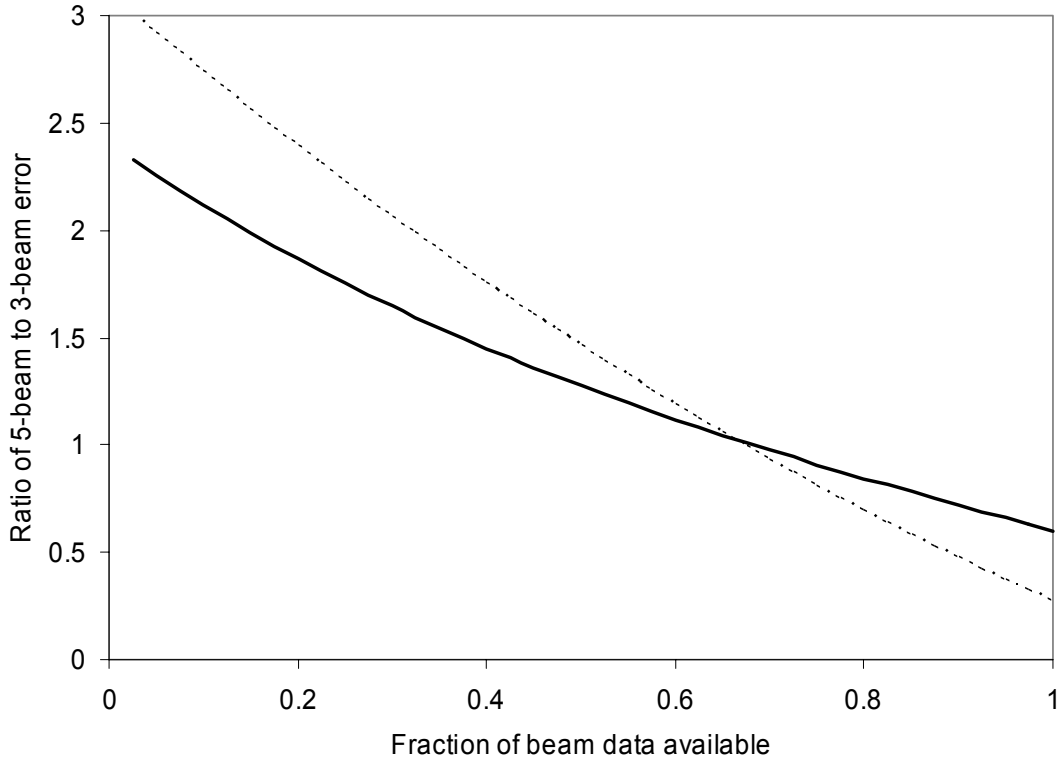

Figure 5. Estimated wind speed errors from a 5-beam system compared to a 3-beam system, as a function of fraction of individual spectra acceptable. Solid curve: neglecting peak position error dependence on SNR. Dashed curve: including peak position error.

3.6 Variance in SODAR average wind speed and direction

Generally wind data from a number of profiles are averaged. In the following we will restrict attention to the horizontal wind components. The i^{th} profile may contain an acceptable u_i wind component and/or an acceptable v_i component. This results, after an averaging period, in N_u east-west components and N_v north-south components. The means and variances from a single averaging period are

$$\begin{aligned} \bar{u} &= \frac{1}{N_u}\sum_{i=1}^{N_u} u_i \qquad & \sigma_u^2 &= \frac{1}{N_u}\sum_{i=1}^{N_u}\left(u_i-\bar{u}\right)^2 = \frac{1}{N_u}\sum_{i=1}^{N_u} u_i^2 - \left(\bar{u}\right)^2 \\ \bar{v} &= \frac{1}{N_v}\sum_{i=1}^{N_v} v_i \qquad & \sigma_v^2 &= \frac{1}{N_v}\sum_{i=1}^{N_v} v_i^2 - \left(\bar{v}\right)^2 \end{aligned} \quad . \tag{3.35}$$

Some analysis is needed because some SODAR software gives $\bar{u}$, $\bar{v}$, σ_u, σ_v, and the mean speed $\bar{V}$ and direction $\bar{\theta}$, but not the errors $\sigma_{\bar{V}}$ or $\sigma_{\bar{\theta}}$.

The wind speed V_i can only be calculated from those N_V profiles where both u_i and v_i are available so $N_V \le N_u$, $N_V \le N_v$. Also

$$\begin{aligned} V_i &= \left(u_i^2 + v_i^2\right)^{\frac{1}{2}} \\ \theta_i &= \tan^{-1}\frac{u_i}{v_i} \end{aligned} \quad . \tag{3.36}$$

Note that the wind direction needs to be calculated using four quadrants. The average wind speed and variance in wind speed are just found in the usual way

$$\bar{V} = \frac{1}{N_V}\sum_{i=1}^{N_V}\left(u_i^2 + v_i^2\right)^{\frac{1}{2}} \qquad \sigma_V^2 = \frac{1}{N_V}\sum_{i=1}^{N_V}\left(u_i^2 + v_i^2\right) - \left(\bar{V}\right)^2 \tag{3.37}$$

or

$$\sigma_V^2 \approx \frac{N_u}{N_V}\left[\sigma_u^2 + \left(\bar{u}\right)^2\right] + \frac{N_v}{N_V}\left[\sigma_v^2 + \left(\bar{v}\right)^2\right] - \left(\bar{V}\right)^2 . \tag{3.38}$$

Also,

$$\sigma_{\bar{V}}^2 \approx \frac{\sigma_V^2}{N_V} = \frac{N_u}{N_V^2}\left[\sigma_u^2 + \left(\bar{u}\right)^2\right] + \frac{N_v}{N_V^2}\left[\sigma_v^2 + \left(\bar{v}\right)^2\right] - \frac{1}{N_V}\left(\bar{V}\right)^2 \tag{3.39}$$

is the variance in the mean wind speed over the averaging period.

The direction needs to be found from the accumulated wind runs in each component, since otherwise averaging could result in a nearly 0° direction being interpreted as nearly 180°. So

$$\bar{\theta} \approx \tan^{-1}\frac{\bar{u}}{\bar{v}} . \tag{3.40}$$

This is why, for the AeroVironment SODAR, no "number of recorded values" is given for the direction.
The variance in direction is

$$
\begin{aligned}
\sigma_{\bar{\theta}}^2 &= \sum_{i=1}^{N_u}\left(\frac{\partial\bar{\theta}}{\partial u_i}\right)^2\sigma_u^2 + \sum_{i=1}^{N_v}\left(\frac{\partial\bar{\theta}}{\partial v_i}\right)^2\sigma_v^2 \\
&= \sum_{i=1}^{N_u}\left(\frac{\partial\tan\bar{\theta}}{\partial u_i}\frac{1}{1+\tan^2\bar{\theta}}\right)^2\sigma_u^2 + \sum_{i=1}^{N_v}\left(\frac{\partial\tan\bar{\theta}}{\partial v_i}\frac{1}{1+\tan^2\bar{\theta}}\right)^2\sigma_v^2 \\
&= \left(\frac{(\bar{v})^2}{(\bar{u})^2+(\bar{v})^2}\right)^2\frac{1}{(N_v\bar{v})^2}\left[N_u\sigma_u^2 + N_v\sigma_v^2\left(\frac{N_u\bar{u}}{N_v\bar{v}}\right)^2\right] \\
&= \frac{N_u}{N_v}\frac{\sigma_u^2 + \frac{N_u}{N_v}\sigma_v^2\tan^2\bar{\theta}}{N_v(\bar{v})^2\left[\tan^2\bar{\theta}+1\right]^2}
\end{aligned}
\quad . \tag{3.41}
$$

3.7 Peak position detection errors

The Doppler spectrum for each beam at each range gate comprises an echo power spectrum accompanied by noise. Each manufacturer has their own proprietary method (such as described in Section 2.4) for detecting the position of the Doppler shifted peak in the presence of noise, but these methods are not generally divulged since they are central to the operational advantages of the SODAR compared to competitors.

Nevertheless, we can estimate likely uncertainties as follows. It is assumed that voltage amplitudes are sampled and spectral estimates are obtained at N_f frequencies f_i each separated by f_s/N_f as in (2.5). The spectral amplitudes A_i have a mean value $\overline{A_i}$ determined by the Fourier transform of the noise-free echo pulse and a standard deviation σ_A due to the Gaussian noise. The probability for A_i is therefore

$$
p(A_i) = \frac{1}{\sqrt{2\pi}\sigma_A}e^{-\frac{1}{2}\left(\frac{A_i-\overline{A_i}}{\sigma_A}\right)^2} .
$$

In practice power spectral estimates $P_i = A_i^2$ are generally used, with probabilities

$$
p(P_i) = \frac{1}{\sqrt{2\pi P_i}\,\sigma_A}e^{-\frac{1}{2}\left(\frac{\sqrt{P_i}-\overline{A_i}}{\sigma_A}\right)^2} . \tag{3.42}
$$

From (3.39) the mean and variance of the power spectral estimates are

$$
\begin{aligned}
\overline{P_i} &= \left(\overline{A_i}\right)^2 + \sigma_A^2 \\
\sigma_i^2 &= 2\sigma_A^2\left[2\left(\overline{A_i}\right)^2 + \sigma_A^2\right].
\end{aligned} \tag{3.43}
$$

If the noise-free power spectrum is essentially Gaussian of the form

$$
\left(\overline{A_i}\right)^2 = \frac{\hat{P}}{\sqrt{2\pi}\sigma_f}e^{-\frac{1}{2}\left(\frac{f_i-\Delta f}{\sigma_f}\right)^2} \tag{3.44}
$$

then a suitable definition of the SNR is

$$
SNR = \frac{\hat{P}}{\sigma_A^2} . \tag{3.45}
$$

The general method for peak detection is to somehow identify the likely frequency index *i* close to the signal peak (perhaps on the basis of power over a some bandwidth interval, compared to noise power estimated from spectral wings or distant range gates), and then fit some function to the spectral estimates to find the optimum peak position. For example, a 5-point quadratic might be fit through the five closest points to where the peak is thought to lie. This technique gives an error estimate for the Doppler shift. In the 5-point quadratic, this is, approximately

$$\sigma_{\Delta f} \approx \frac{14}{\sqrt{SNR}} \left(\frac{\sigma_f}{f_s / N_f} \right)^2 . \tag{3.46}$$

This means that the error in frequency estimation increases for low SNR or if the width of the signal peak is wide compared to the frequency intervals in the FFT. The term in brackets is, however, fixed for a particular SODAR.

The errors in frequency estimation from (3.43) propagate into velocity component estimation as in (3.27), (3.36) and (3.38).

3.8 Loss of signal in noise

One of the principal problems of SODAR calibration and use in connection with wind turbines is the poorer data availability at greater heights, and the fact that data availability depends on meteorological conditions. The SODAR equations can be written

$$P = P_E + P_F + P_P + P_N \tag{3.47}$$

where P is the total received power, P_E is the power scattered from turbulence, P_F is the power reflected from fixed objects such as masts, P_P is the power scattered from precipitation, and P_N is noise power. The required signal is from P_E and the remaining terms on the right lead to reduced SNR.

Generally P_F may be reduced by selecting the orientation of the SODAR to minimise power transmitted toward the fixed object. If P_F is still present, then it can often be identified because it has zero Doppler shift and its spectral width may be different from that of P_E. While fixed echoes remain an *operational problem*, for calibration purposes, those range gates affected can simply be ignored. This is discussed further later.

Echoes from precipitation are an operational problem for SODARs, but can effectively be eliminated from calibration data because the presence of rainfall can be sensed via other means or from the increased vertical velocities detected by the SODAR.

External noise remains the main difficulty during calibration. Both P_E and P_N can be variable. Expanding (3.47),

$$P_E = 3x10^{-4} P_T G A_e \, \tau \, f_T^{\frac{1}{3}} \left[\frac{c^{\frac{2}{3}}}{T^2} \right] \left[\frac{e^{-2\alpha z}}{z^2} \right] C_T^2 \tag{3.48}$$

where P_T is the transmitted acoustic power, G the antenna gain in the beam direction, A_e the effective area of the antenna for receiving power from the beam direction, τ the transmitted pulse duration, f_T the transmitted frequency, c the speed of sound, T the atmospheric temperature, α the atmospheric acoustic absorption, z the range, and C_T^2 the structure function for turbulent temperature fluctuations. Terms before the first square bracket are instrumental, and the first square bracket contains terms weakly dependent on atmospheric temperature profile variations. The C_T^2 term represents the echo signal generation and the second square bracket contains terms representing signal loss due to absorption and spherical spreading. The absorption is generally not very large, so most signal loss is through the unavoidable inverse-square reduction with height. For

example, the inverse square loss between 10 m and 100 m is 20 dB whereas the absorption loss is around 0.6 dB for a 1 kHz SODAR and 6 dB for a 4.5 kHz SODAR.
C_T^2 is related to the strength of turbulence, which depends on both site (surface roughness) and atmospheric stability. It can be expressed in terms of the turbulent energy dissipation rate ε, and on ε_θ, the dissipation rate for heat.

$$C_T^2 = \frac{0.106}{0.033}\varepsilon^{-\frac{1}{3}}\varepsilon_\theta \tag{3.49}$$

where

$$\varepsilon_\theta = K_h\left(\frac{d\bar{\theta}}{dz}\right)^2 \tag{3.50}$$

and

$$\varepsilon = K_h\left(\frac{d\bar{u}}{dz}\right)^2\left(Pr - Ri\right). \tag{3.51}$$

The Prandtl number $Pr = \frac{K_m}{K_h} \approx 0.7$, K_h is the eddy diffusion coefficient for temperature, K_m is the coefficient of eddy viscosity, $\frac{d\bar{\theta}}{dz}$ is the potential temperature gradient, and $\frac{d\bar{u}}{dz}$ is the wind speed gradient. The Richardson number *Ri* is a measure of the rate of mechanical work done in creating turbulent eddies compared to the rate of destruction of turbulence energy. In practice it is found if a critical Richardson number of $Ri > 0.25$ is exceeded, then turbulence does not occur. Note that if *Ri* is negative, then the temperature profile is unstable.

Atmospheric stability is usually characterised by either the Richardson number *Ri* or the Monin-Obhukov length *L* and neither of these is directly connected with C_T^2. The Monin-Obhukov length is an estimate of the height at which the turbulent energy dissipation rate ε becomes zero. Definitions are

$$Ri = \frac{g}{\bar{T}}\frac{\frac{d\bar{\theta}}{dz}}{\left(\frac{d\bar{u}}{dz}\right)^2} \tag{3.52}$$

$$L = \frac{\rho c_p u_*^3 \bar{T}}{\kappa g H} \tag{3.53}$$

where *g* is the acceleration due to gravity, $\bar{T}$ is mean layer temperature, ρ is air density, c_p is the specific heat at constant pressure, $\kappa \approx 0.4$ is the von Karman constant, u_* is the friction velocity, and *H* is the heat flux. The two are closely related, since when $z = L$ then $Ri = Pr$.
The heat flux *H* can be written in terms of the temperature gradient through

$$H = -c_p \rho K_h \frac{d\bar{\theta}}{dz} \tag{3.54}$$

and the friction velocity can be expressed in terms of wind speed gradient through

$$u_*^2 = K_m \frac{d\bar{u}}{dz}. \tag{3.55}$$

$$L = -\frac{K_m^2 \bar{T}}{\kappa g K_h} \frac{\left(\frac{d\bar{u}}{dz}\right)^{\frac{3}{2}}}{\frac{d\bar{\theta}}{dz}}. \tag{3.56}$$

From (3.52) and (3.56),

$$L \bullet Ri = -\frac{K_m^2}{\kappa K_h}\left(\frac{d\bar{u}}{dz}\right)^{-\frac{1}{2}}$$

$$L(Ri)^{\frac{3}{4}} = -\frac{K_m^2}{\kappa K_h}\left(\frac{g}{\bar{T}}\right)^{-\frac{1}{4}}\left(\frac{d\bar{\theta}}{dz}\right)^{-\frac{1}{4}} \tag{3.57}$$

so

$$\varepsilon_\theta = K_h\left(\frac{K_m^8 \bar{T}}{g\kappa^4 K_h^4 L^4 Ri^3}\right)^2$$

$$\varepsilon = K_h\left(\frac{K_m^4}{\kappa^2 K_h^2 L^2 Ri^2}\right)^2 (Pr - Ri)$$

and it is possible to write C_T^2 in terms of L and Ri:

$$C_T^2 = \frac{0.106}{0.033}\frac{K_m^{\frac{40}{3}} \bar{T}^2}{g^2 \kappa^{\frac{20}{3}} K_h^6} L^{-\frac{20}{3}} Ri^{-\frac{14}{3}} (Pr - Ri)^{-\frac{1}{3}}. \tag{3.58}$$

A clearer picture emerges if it is assumed that the wind shear is largely determined by the site, and variations in C_T^2 are mostly due to variations in temperature gradient. Then

$$C_T^2 = \frac{0.106}{0.033} K_h^{\frac{2}{3}}\left(\frac{d\bar{u}}{dz}\right)^{\frac{10}{3}}\left(\frac{\bar{T}}{g}\right)^2 \frac{Ri^2}{(Pr - Ri)^{\frac{1}{3}}} \tag{3.59}$$

or

$$C_T^2 = \frac{0.106}{0.033}\frac{K_h^{-\frac{4}{3}} K_m^4 \bar{T}^2}{\kappa^2 g^2}\left(\frac{d\bar{u}}{dz}\right)^{3-2/3} \frac{1}{L^2\left(Pr + \frac{K_m^2}{\kappa K_h}\sqrt{\frac{d\bar{u}}{dz}}\frac{1}{L}\right)^{\frac{1}{3}}} \tag{3.60}$$

In this case, if data availability is determined by SNR values (with some spread since noise and signal will both be variable), then comparable levels of data availability occur for constant $\frac{C_T^2}{z^2}$. Figure 6 shows two contours of constant $\frac{C_T^2}{z^2}$ superimposed on the data availability diagram reported by Kindler et al. (2004). Near neutral conditions, this theory appears to hold, but for larger absolute

values of *Ri* there seems to be little dependence on *Ri*. Instead, above about 100 m, availability is roughly proportional to $1/z$ rather than $\sqrt{C_T^2}/z$. This is shown in Figure 7. Similarly, availability is shown as a function of z/L in Figure 8 and Figure 9 for L computed at two different heights. While Figure 6 and Figure 8 are qualitatively similar, as predicted by (3.57), the 20 m L gives quite different patterns in Figure 9, possibly because this is in a different scaling and turbulence regime.

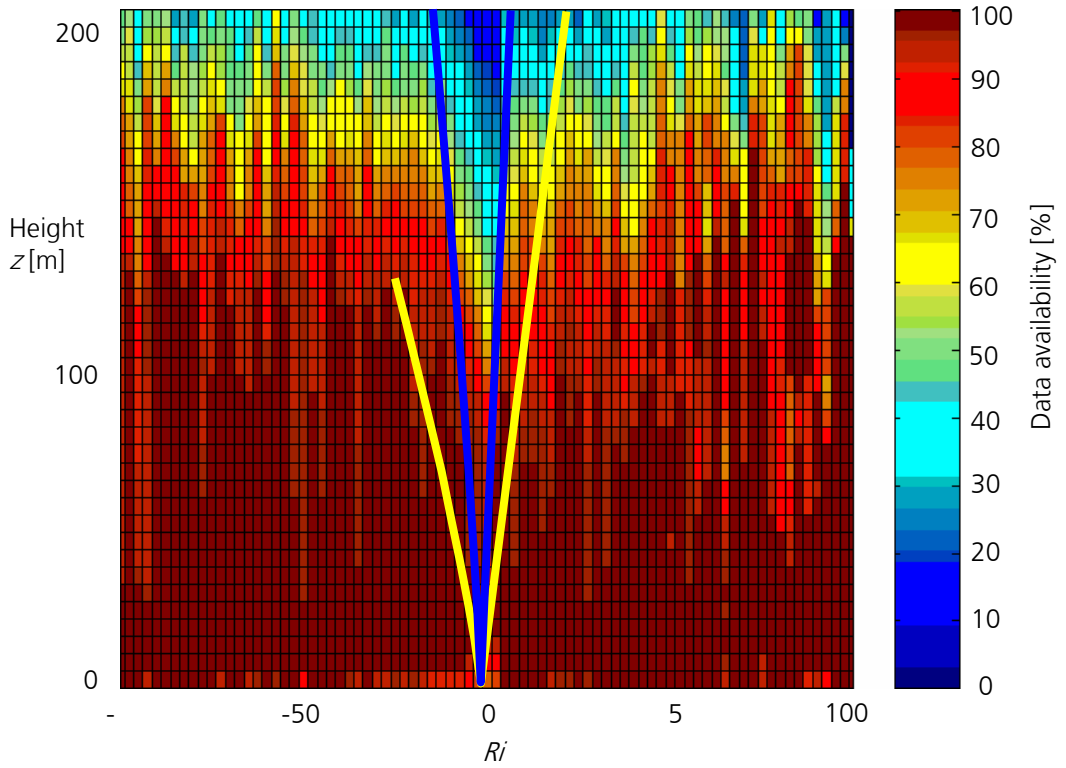

Figure 6. Percentage of relative data yield of Scintec SODAR receptions, plotted against height z of the SODAR range gates and against the Richardson number *Ri* based meteorological mast measurements at 100 m. The solid yellow and blue lines are two contours of constant $\frac{C_T^2}{z^2}$.

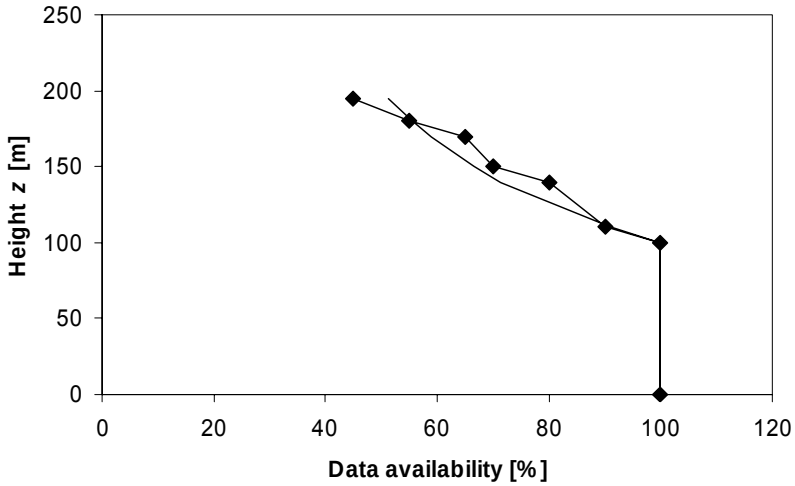

Figure 7. Data availability based on Figure 6 and on $1/z$ for heights above 100 m.

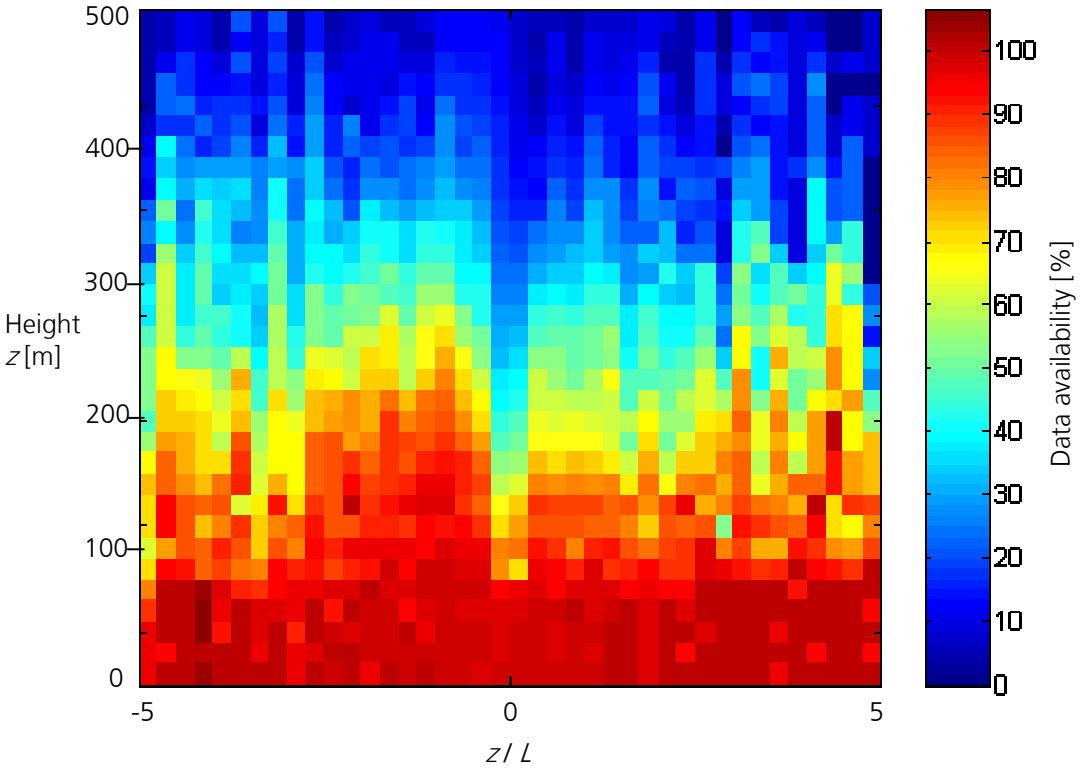

Figure 8. Data availability for the Metek SODAR based on Monin-Obhukov length *L* estimated from a sonic anemometer at 20 m height

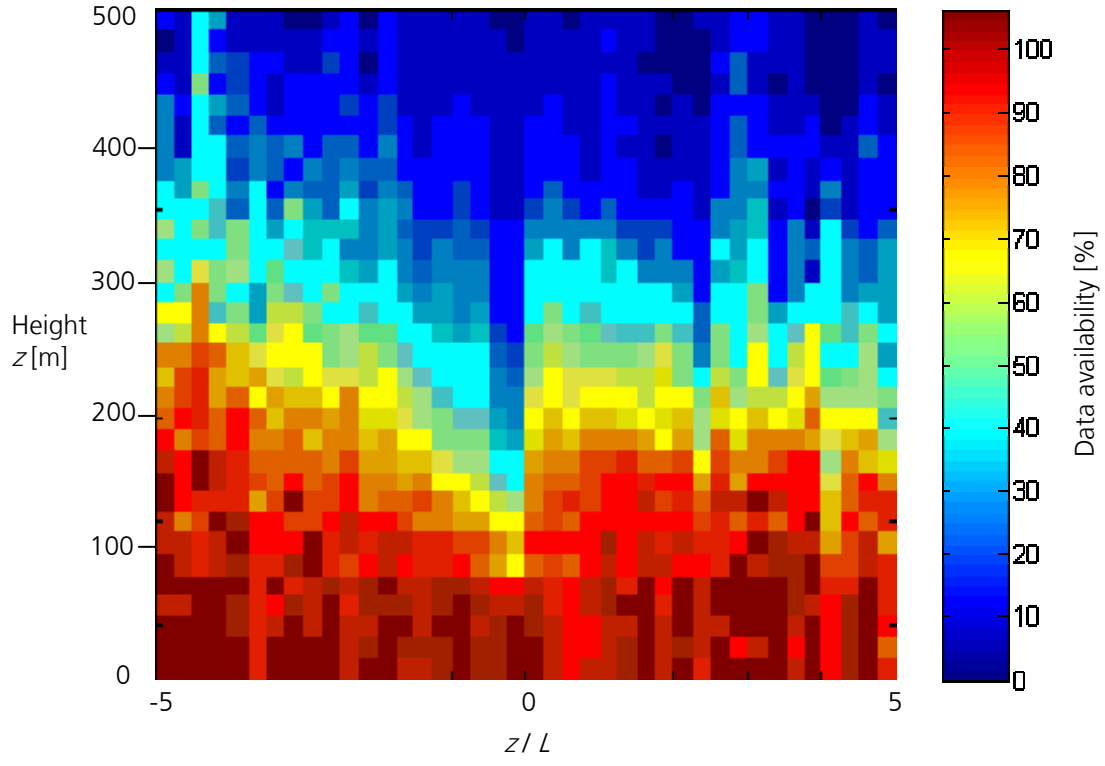

Figure 9. Data availability for the Metek SODAR based on Monin-Obhukov length *L* estimated from a sonic anemometer at 100 m height

The above shows that systematic bias can occur in calibration and operationally due to reduced data availability with extended height and during near-neutral conditions. For calibration purposes this can potentially be corrected by doing weighted least-squares fitting against the 'standard wind measurements' with the weighting determined as described in Sections 3.4 and 3.5 above.
In this section we have attempted to find a measurable and commonly used parameter (either Ri or L) which can be used in a functional relationship of the form

Data availability = f(Ri, z) or Data availability = g(L,z).

If successful, this approach would allow inversion of the function to give a prediction of availability under different atmospheric conditions. On the basis of Figs. 6-9 neither Ri nor L give a complete description and further work clearly needs to be done. The problem is that we essentially are attempting to predict C_T^2 from Ri or L, since availability should be closely correlated with echo strength, which is directly proportional to C_T^2. Ideally, perhaps, C_T^2 would be measured independently of the SODAR, and used to predict the SODAR data availability, but this approach would require purpose-designed mast installations. Another approach would be to use a complex boundary layer model to predict C_T^2, but this would be an entire new research effort.

3.9 Spatial and temporal separation of sampling volumes

The SODAR estimates wind components u, v, and w from at least three separated volumes, as described in Section 2.1 and Figure 2 and Figure 3. For example, at 100 m the data from u and v are separated by typically 40-50 m and 1.5-7 s (depending on the overall range). Assuming Taylor's frozen field hypothesis, the times 1.5-7 s correspond to distances of wind travel of 15 to 70 m at 10 m s^{-1}. The question arises as to how well correlated wind components are over these times and distances.
However, the distances characteristic of the SODAR operation are comparable or less than those applying in practice when a SODAR is used in conjunction with a wind turbine. Also, if calibrations are carried out against a mast, then such distances are also involved between the SODAR and mast. For calibration purposes, any fluctuations due to spatial and temporal separations will appear as added variance and uncertainty in fitted parameters.
Antoniou and Jørgensen (2003) and Antoniou et al. (2004) have shown that the distance between mast and SODAR is not a concern for a site which is on flat terrain.

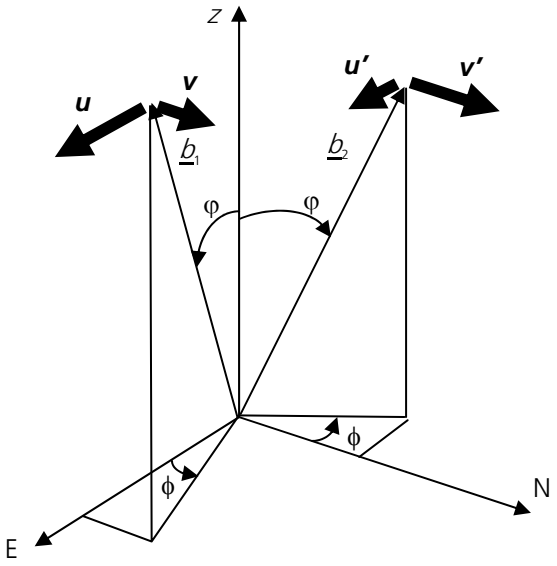

Figure 10. Geometry for Beams 1 and 2, showing different measured wind components

For a 3-beam SODAR, assuming the vertical velocity is w=0, the radial velocities recorded from tilted beams 1 and 2 are

$$\begin{aligned} v_{r1} &= (u\cos\phi + v\sin\phi)\sin\varphi \\ v_{r2} &= (-u'\sin\phi + v'\cos\phi)\sin\varphi \end{aligned} \tag{3.61}$$

where φ is the beam tilt angle and ϕ is the SODAR orientation angle with respect to North (see Figure 10). Because of spatial separation of the sampling volumes, the velocity components measured from each beam will not in general be exactly the same for a particular profile.

The components u and v are required, and also velocity components are averaged over a number of profiles. If solution for u and v is done on each profile *before* averaging, then

$$\begin{aligned} \hat{u} &= \frac{v_{r1}\cos\phi - v_{r2}\sin\phi}{\sin\varphi} \\ \hat{v} &= \frac{v_{r1}\sin\phi + v_{r2}\cos\phi}{\sin\varphi} \end{aligned} \tag{3.62}$$

are the estimated components for each profile. This gives

$$\begin{aligned} \hat{u} &= u\cos^2\phi + u'\sin^2\phi \\ \hat{v} &= v'\cos^2\phi + v\sin^2\phi \end{aligned} . \tag{3.63}$$

The square of the overall wind speed estimated from a single profile would be

$$\hat{V}^2 = \hat{u}^2 + \hat{v}^2 = \left(u^2 + v'^2\right)\cos^4\phi + 2(uu' + vv')\sin^2\phi\cos^2\phi + \left(u'^2 + v^2\right)\sin^4\phi$$

If this is now averaged,

$$\overline{\hat{V}^2} = \overline{u^2 + v'^2}\cos^4\phi + 2\left(\overline{uu'} + \overline{vv'}\right)\sin^2\phi\cos^2\phi + \overline{u'^2 + v^2}\sin^4\phi$$

$$\overline{\hat{V}^2} \approx \overline{V^2}\cos^4\phi + 2\left(\overline{uu'} + \overline{vv'}\right)\sin^2\phi\cos^2\phi + \overline{V^2}\sin^4\phi$$

where $\overline{V^2}$ is the average of the square of the true wind. It is assumed that the average winds at the two sampling volume positions are the same, but that winds at both locations are fluctuating. The terms $\overline{uu'}$ and $\overline{vv'}$ represent cross-correlations between wind components at each sampling volume. We will assume they can be written as

$$\begin{aligned} \overline{uu'} &= \rho\overline{u^2} \\ \overline{vv'} &= \rho\overline{v^2} \end{aligned} \tag{3.64}$$

where ρ is a correlation coefficient. Also we assume $\overline{uu'} + \overline{vv'} \approx \rho\overline{V^2}$. The result is

$$\overline{\hat{V}^2} \approx \overline{V^2}\left[\cos^4\phi + 2\rho\sin^2\phi\cos^2\phi + \sin^4\phi\right] = \overline{V^2}\left[1 - (1-\rho)\sin^2 2\phi\right]. \tag{3.65}$$

The estimated wind speed can be expected to be increasingly smaller than the actual wind speed as the two sample volumes become more separated and ρ decreases. This would be expected to give a lower correlation slope with mast measurements with increasing height.

If, as with the AeroVironment and Metek SODARs (see Section 2.4), the radial components or spectra are averaged, then post-processing gives

$$\begin{aligned} \overline{\hat{u}} &= \overline{u}\cos^2\phi + \overline{u'}\sin^2\phi = \overline{u} \\ \overline{\hat{v}} &= \overline{v'}\cos^2\phi + \overline{v}\sin^2\phi = \overline{v} \end{aligned}$$

so that there will be no beam-separation effect on wind speed estimates.

For a 5-beam SODAR, there are two extra beams, 4 and 5, tilted in the opposite directions to Beams 1 and 2. Similarly to above

$$\begin{aligned}\hat{u} &= \frac{(v_{r1}-v_{r4})\cos\phi-(v_{r2}-v_{r5})\sin\phi}{\sin\varphi}=\frac{u+u'}{2}\\ \hat{v} &= \frac{(v_{r1}-v_{r4})\sin\phi-(v_{r2}-v_{r5})\cos\phi}{\sin\varphi}=\frac{v+v'}{2}\end{aligned} \tag{3.66}$$

with the difference that there is no SODAR orientation dependence. Again there is a beam separation effect *only* if the wind speed estimates are obtained *before* averaging. Then

$$\begin{aligned}\hat{V}^2 &= \hat{u}^2+\hat{v}^2=\frac{1}{4}\left[V^2+2(uu'+vv')+V'^2\right]\\ \overline{\hat{V}^2} &= \overline{V^2}\left[1-\frac{1}{2}(1-\rho)\right]\end{aligned} \tag{3.67}$$

giving a similar expected decrease in slope with height, but without the orientation effect.

3.10 Different averaging schemes for SODAR and standard

Cup anemometers represent one 'standard' against which SODARs might be calibrated. As pointed out by Antoniou and Jørgensen (2003) cup anemometers measure wind run and divide by averaging time to obtain wind speed. Thus

$$V_{cup}=\frac{1}{T}\int_0^T V dt=\frac{1}{T}\int_0^T\sqrt{u^2+v^2}\,dt \tag{3.68}$$

whereas a SODAR obtains wind speed from the averaged u and the averaged v components:

$$V_{SODAR}=\sqrt{\left(\frac{1}{T}\int_0^T u dt\right)^2+\left(\frac{1}{T}\int_0^T v dt\right)^2}\ . \tag{3.69}$$

To allow for the sampled nature of the SODAR (a sample each profile), assume that the wind is essentially in the $+x$ direction with small perturbations:

$$\begin{aligned}u &= U+u_i\\ v &= v_i\end{aligned}\qquad (i-1)\Delta t<t\le i\Delta t\ . \tag{3.70}$$

Then

$$\begin{aligned}V_{cup} &= \frac{1}{N}\sum_{i=1}^N\sqrt{(U+u_i)^2+v_i^2}\\ &= \frac{U}{N}\sum_{i=1}^N\sqrt{1+\frac{2u_i}{U}+\frac{u_i^2+v_i^2}{U^2}}\\ &\approx \frac{U}{N}\sum_{i=1}^N\left(1+\frac{u_i}{U}+\frac{u_i^2+v_i^2}{2U^2}\right)\\ &\approx U+\frac{1}{N}\sum_{i=1}^N u_i+\frac{1}{2NU}\sum_{i=1}^N\left(u_i^2+v_i^2\right)\end{aligned} \tag{3.71}$$

and

$$
\begin{aligned}
V_{SODAR} &= \sqrt{\left(U+\frac{1}{N}\sum_{i=1}^{N}u_i\right)^2+\left(\frac{1}{N}\sum_{i=1}^{N}v_i\right)^2} \\
&= U\sqrt{1+\frac{2}{N}\sum_{i=1}^{N}\frac{u_i}{U}+\left(\frac{1}{N}\sum_{i=1}^{N}\frac{u_i}{U}\right)^2+\left(\frac{1}{N}\sum_{i=1}^{N}\frac{v_i}{U}\right)^2} \\
&\approx U\left[1+\frac{1}{N}\sum_{i=1}^{N}\frac{u_i}{U}+\frac{1}{2}\left(\frac{1}{N}\sum_{i=1}^{N}\frac{u_i}{U}\right)^2+\frac{1}{2}\left(\frac{1}{N}\sum_{i=1}^{N}\frac{v_i}{U}\right)^2\right] \\
&\approx U+\frac{1}{N}\sum_{i=1}^{N}u_i+\frac{1}{2N^2U}\sum_{i=1}^{N}\left(u_i^2+v_i^2\right)+\frac{1}{2N^2U}\sum_{i=1}^{N}\sum_{j\neq i=1}^{N}\left(u_iu_j+v_iv_j\right)
\end{aligned}
\quad . \tag{3.72}
$$

This gives

$$
V_{cup} \approx V_{SODAR}+\frac{1}{2U}\left[\frac{1}{N}\sum_{i=1}^{N}\left(u_i^2+v_i^2\right)\right] \tag{3.73}
$$

for large N. So $V_{cup} > V_{SODAR}$. Antoniou and Jørgensen (2003) describe a method for estimating the difference between the two measurements. Panofsky et al. (1977) show that

$$
\frac{1}{N}\sum_{i=1}^{N}\left(u_i^2+v_i^2\right)\approx\left(2.5u_*\right)^2
$$

where u_* is the friction velocity, and assuming a log wind profile

$$
U=\frac{u_*}{\kappa}\ln\frac{z}{z_0}
$$

where $\kappa\approx0.4$ is the von Karman constant and z_0 is the roughness length. Since $V_{SODAR}\approx U$,

$$
V_{cup} \approx V_{SODAR}\left(1+\frac{1}{2\left(\ln\frac{z}{z_0}\right)^2}\right). \tag{3.74}
$$

For example, over pasture having z_0=0.05 m, the correction is 1% at 50 m height. For rougher terrain or greater heights the correction is smaller. The results of comparison between field trials and this theory have been inconclusive, possibly because of the limited height range and atmospheric conditions under which a log wind profile usually is observed.

4. Calibration methods

Calibration of a SODAR for wind measurements, in the context of wind engineering, means generating a set of instructions on how to obtain, from the SODAR data, wind speed and direction at a number of known heights and with known and sufficient accuracy. These instructions will not simply be a regression equation, but will also include how to set the SODAR up and apply any necessary data filtering so that the regression equation applies.

Only wind information is required, and not echo amplitude or turbulence data (at this stage). In order that SODARs can be used instead of cup anemometers on masts, the accuracy obtained from the calibration should be comparable to the accuracy of the cups. Sufficient accuracy is probably better than 1% of wind speed which translates roughly into 1% in direction. This gives an accuracy of 3% in wind power. The required height range should extend above the maximum height reached by current turbines, so 150-200 m should be the design aim. Reliable measurements should be available in wind turbine sites, which include offshore and hilly terrain (near the hill crests). Data availability should be maximised, although it should not strictly be necessary to obtain good wind data in *all* conditions (such as during high winds or heavy rainfall).

The calibration *method* should be easily replicated and checked. Calibration between several SODARs should obviously be consistent (it is undesirable to have distinct calibration methods for different SODAR models).

4.1 Calibrations against various potential standards

Atmospheric Research and Technology Ltd produce SODAR self 'calibration' tools (http://www.sodar.com/prod02.htm). These however check the basic functionality of a SODAR rather than conducting a calibration. For example, the frequency transmitted is checked and the ability of the SODAR to detect peaks, but there is no check on the beam pattern and directivity nor is there any check on actual response to winds.
The Salford Group have considered construction of a transponder which essentially detects the sound generated by the SODAR over a wide solid angle and produces a delayed, Doppler shifted, response which has noise added based on real atmospheric echoes. The response would be based on the SODAR equation. Such a transponder would require distributed microphones and speakers mounted above the SODAR on some kind of thin framework and in the far field (perhaps 10 m distance). This would check most of the functions of the SODAR and the error conditions described in Section 3, but levelling of this device would also be critical.

Wind speed and direction have often been measured by free flying wind-sonde balloons (with RADAR reflectors or GPS) and compared with the SODAR output. The difficulty is that the balloon profiles are very transitory compared to a typical wind profile averaging time of 5-10 minutes for a SODAR. The nominal ascent rate of a Vaisala sonde is 4 m s^{-1} so the balloon will return data from the lowest 200 m for 50 s: this corresponds to about 7 complete cycles around the beams of a 5-beam SODAR. During these 50 s the balloon will have also drifted 500 m downwind if the wind speed is 10 m s^{-1}. These problems mean that free balloons are never going to provide adequate calibration for SODARs.

Some tethered balloon systems also record winds. For example, the Vaisala DigiCora tethersonde system (http://www.vaisala.com/) has up to six wind sensors on the tether (say with spacing 30 m for a 200 m line) with accuracy of 0.1 m s^{-1} and 1° in direction. In practice though, swinging of the sensors might be expected to give much reduced accuracy in the field. Because they also require a huge amount of manpower for operation they can only be used intermittently. Therefore, systems of this sort are not intended to be primary standards.

The expense of routine calibration against cup anemometers on a tall (≥ 100 m) mast precludes this method except as verification that a short-mast calibration method is satisfactory and that there is not some calibration problem unaccounted for. This was the focus of the PIE field trials described below.

Many of the calibration problems referred to above can be resolved by calibrating the SODAR against a cup anemometer and/or sonic mounted on a short (40 m, say) mast. Of the errors listed at the start of Section 3, the geometric errors can be eliminated and the estimation bias largely reduced, leaving only the difficulties if the SNR is inadequate. The preferred situation is shown in Figure 11.

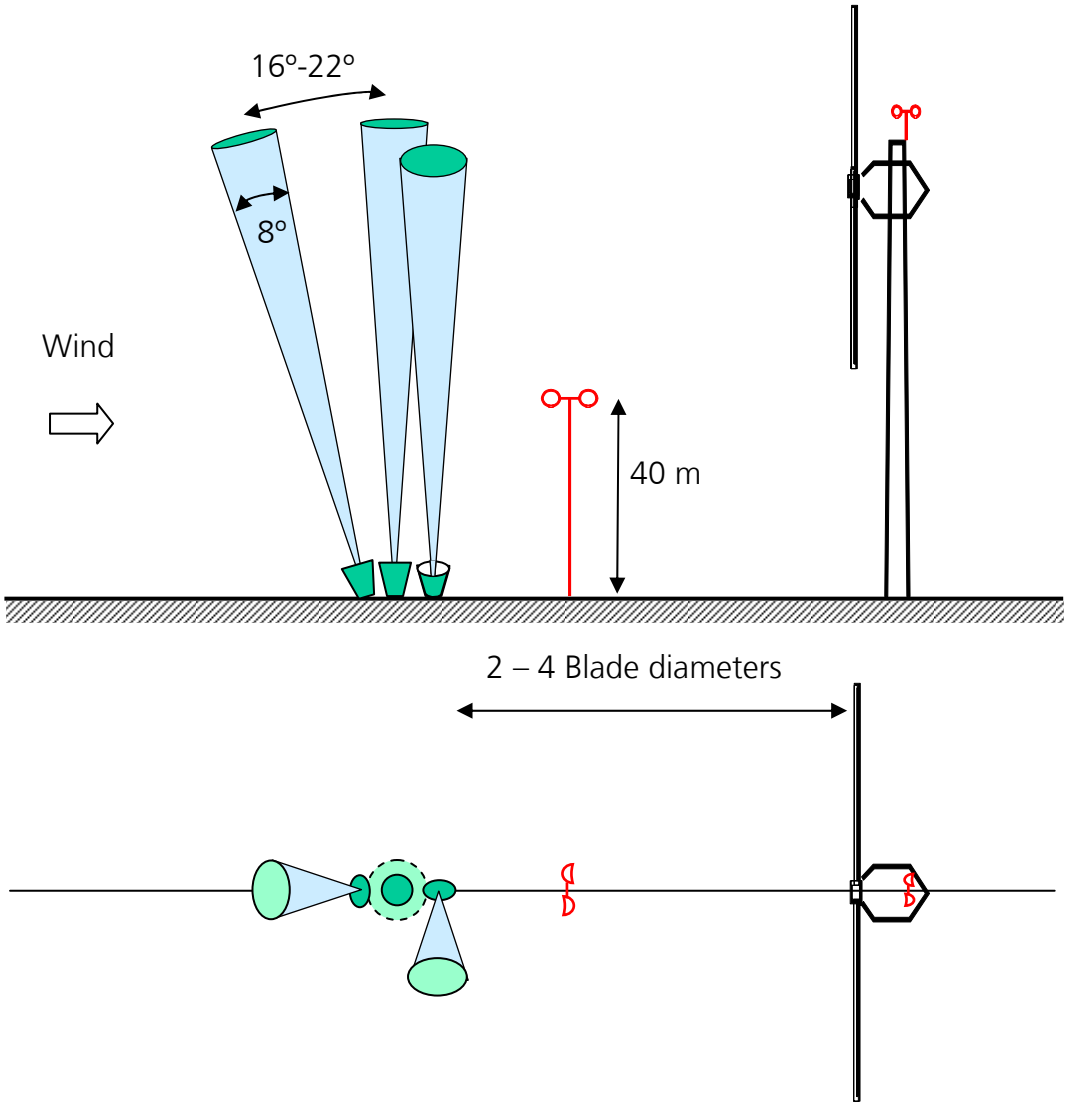

Figure 11. Preferred calibration configuration. A SODAR is situated in the prevailing upwind direction from the turbine and at a distance of 2-4 diameters. The acoustic beams are aimed away from the turbine and mast to minimise fixed echoes.

5. Calibration results

5.1 The PIE experiment setup

The Profiler Intercomparison Experiment (PIE) was conducted in order to test the calibration of a range of SODARs against a well-instrumented 120 m mast. The SODARS were operated at sufficiently different frequencies to not interfere with each other.

SODAR types and characteristics

SODAR	Operated by	f_T Hz	Transducers	Beams	Δz m
AeroVironment 4000*	RISØ	4500	50	3	10
Metek PCS2000-64 with 1290MHz RASS	Salford	1674	64	5	15
Scintec SFAS	WINDTEST KWK	2540-4850	64	9	5

Table 3. Summary of the main features of the SODARs deployed.

*This unit had a Model 3000 enclosure, which may have modified the beam shape and tilt.

Site Description

The test site is the National Danish Test Station for Large Wind Turbines situated in the northwest of Denmark close to the North Sea. The test site is flat, surrounded by grassland, with no major obstacles in the immediate neighbourhood and at a distance of 1.7 km from the west coast of Denmark. The prevailing wind direction is from the west. The general site locality is shown in Figure 12.

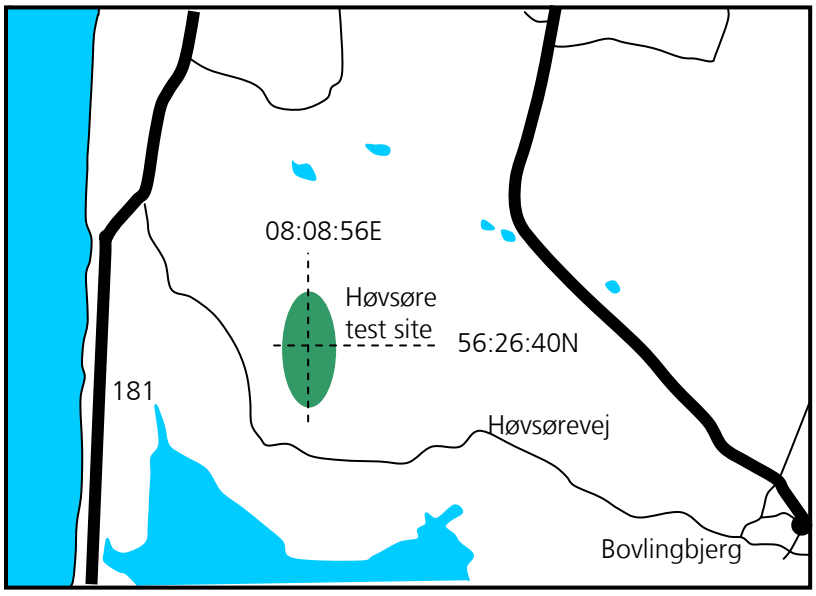

Figure 12. The locality, with the site indicated by the dashed oval

The site includes five turbine test stands, as shown in Figure 13, where five wind turbines are presently installed. The stands are placed in the north-south direction at a distance from each other of 300m with stand 5 the southernmost one. In front of every test stand and at a distance of 240 m in the prevailing wind direction, a met mast is situated, with a hub height equal to the turbine height at the corresponding stand.

Figure 13. The test site, the met tower and the SODARs (wind blowing from the east)

At the south of the turbine row, a met tower (Stand 6) is located at 200 m from Stand 5. Its instrumentation is described in Figure 14. The rain sensor was not installed from the start of the test period and shortly after its installation it failed. Later on a tipping bucket rain sensor was installed. Likewise the 100 m wind direction sensor was not available from the beginning of the measurement period due to a lightning strike. Four phased-array SODARs were located to the southwest of the met tower (see Figure 15), but due to intermittent availability the high-frequency Metek SODAR was not used for calibrations.

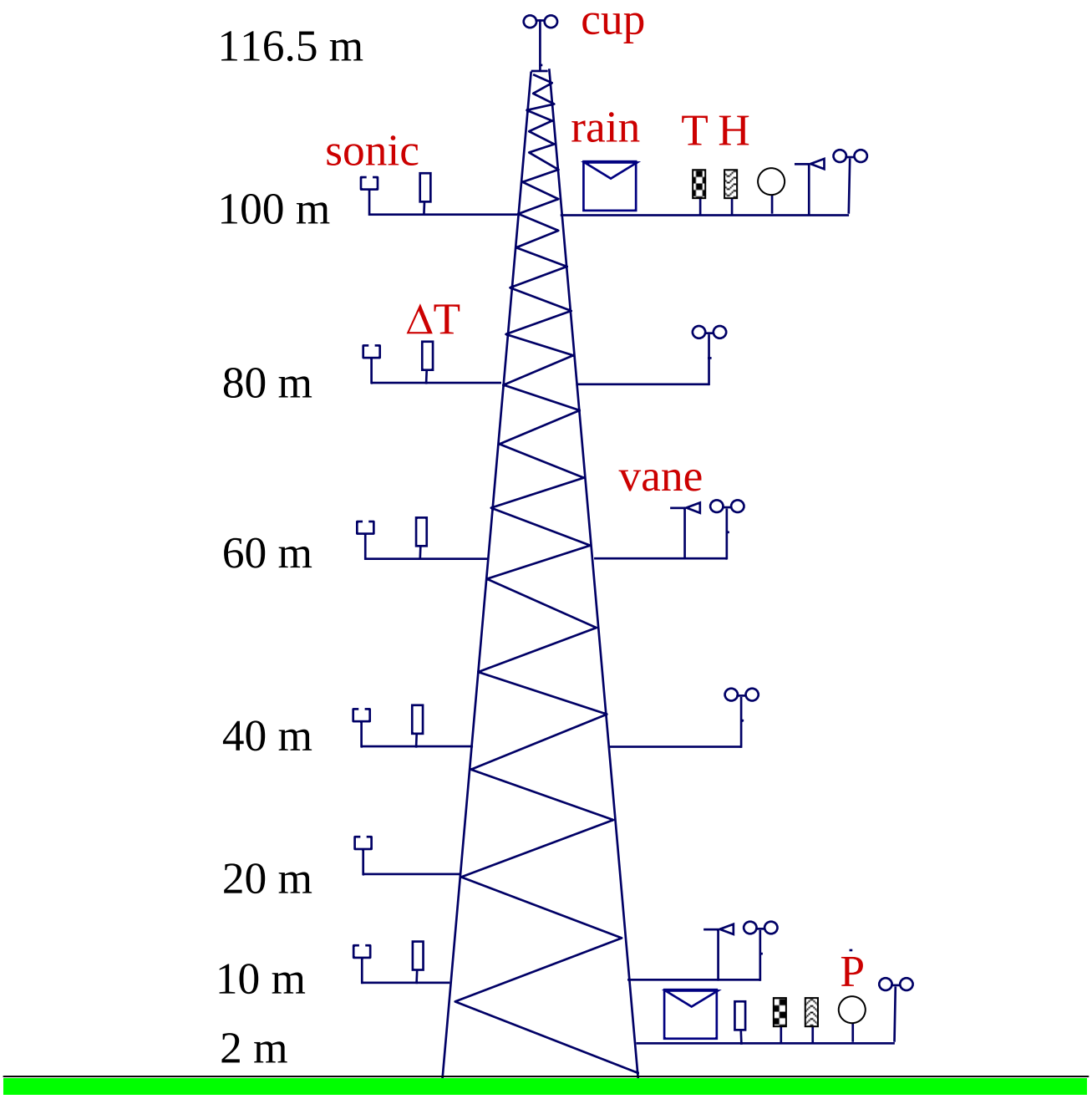

Figure 14. Schematic of the tower instrumentation (looking to the tower from the west). Instruments consist of cup anemometers ('cup'), wind vanes ('vane'), sonic anemometers ('sonic'), differential temperature transducers ('ΔT'), absolute temperature transducer 'T', humidity sensors 'H' and pressure sensors 'P'.

Figure 15. The three SODARs used for calibration. From upper left: Scintec SFAS (octogonal baffle), AV4000 (small square baffle), and Metek SODAR/RASS (large square baffle). The fourth SODAR, lowermost in the picture, was not used for calibration.

5.2 Raw SODAR data versus mast

Initial plots of raw SODAR windspeed vs cup windspeed show a number of problems, typified by Figure 16.

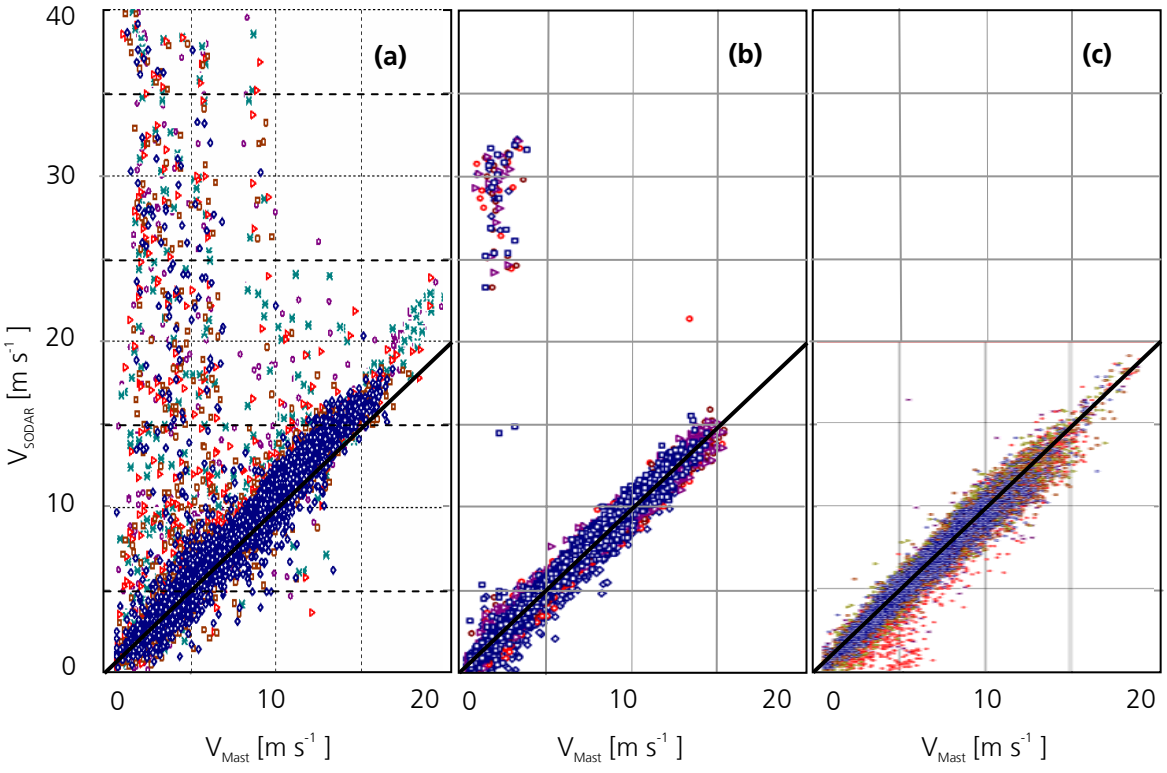

Figure 16. Mast windspeeds vs raw SODAR windspeeds. (a) AV4000, O=40m, ✱=60m, Δ=80m, ◘=100m, ◇=116m; (b) Scintec, ◘=40m, O=60m, Δ=80m, O=100m, ◇=116m; (c) Metek, ◇=40m, ◘=60m, Δ=80m, O=100m, X=116m.

The raw plots have obvious outlier data-points. For the AV4000 and the Scintec, high apparent SODAR winds at low mast winds are caused by rain. The particular filtering options selected for the various SODARs in these examples remove more of these points for the Scintec and virtually all rain points for the Metek, but other choices could give the opposite results.
A second cause of outliers is fixed echoes. These points exhibit low apparent winds from the SODAR and higher winds from the cup anemometers, as evident by the red points in Figure 16 (c).

5.3 Numerical procedures for calibrations

Filtering

The SODAR data first must be filtered to remove rain data, fixed echo data, and any other bad data due to external noise. The discussion which follows is very brief since this topic is treated more fully in the Operational Characteristics part of the WISE Project.

Measurement sector

The mast anemometers are known to have a sector from which winds do not give good data because of shielding by the mast. In the case of the PIE trial, the wind direction sector from 325°-90° gave potentially contaminated cup data. The Scintec SODAR-Mast data set was filtered to remove these data, but much of the data shown for the other two SODARs includes all wind directions (however, see the detailed analysis below for the Metek SODAR).

Rain detection

During rain the signal is backscattered against falling raindrops, resulting in a relatively large negative vertical velocity. This velocity contaminates the horizontal wind calculations and can lead to predictions of high windspeeds.
Rain gauges were part of the mast instrumentation, but it is also possible to filter the SODAR data based on just SODAR observations to remove most of the rain contamination. This is a desirable approach, since it removes the need for yet another instrument when SODARs are used as autonomous wind sensors at wind energy installations.
Each SODAR has methods for detection of 'bad data' and in many cases the menu-guided user choices can allow for automatic removal of rain-contaminated data. Additionally, or independently, it is possible to use the routinely available diagnostic information provided by the SODAR output to construct a rain-rejection filter.
For example, the AV4000 outputs a quantity called IW, the intensity of the echo from the vertical ($\langle w \rangle$ beam, and a corresponding SNR for that beam called SNRW. During rain IW will generally be higher and SNRW lower, so the ratio IW/SNRW is a possible rain discriminator. On the AV4000 dry periods typically show IW/SNRW=20-50, whereas in rain IW/SNRW may rise to ~100. During snowfall there is some evidence that IW/SNRW is *lower* than the dry figure. A test was run at the ECN EWTW site, using a tipping bucket rain gauge for comparison. Figure 17 shows IW/SNRW vs windspeed during dry periods, and Figure 18 for raining periods. It can be seen from these figures that IW/SNRW is only indicative of the possibility of rain occurring. This analysis suggests that, without further research, rain gauges should be deployed to indicate possible contamination of wind data by rainfall.

Fixed echo detection

Echoes from hard, static, non-atmospheric objects ('fixed echoes') result in a peak at zero frequency shift which, depending on atmospheric signal strength, can be wrongly interpreted as a radial wind speed of 0 m s^{-1}. SODAR manufacturers generally have some fixed echo detection and removal filters which can be applied with some success. Recently, this was also the focus of another EU project (MEPROS).

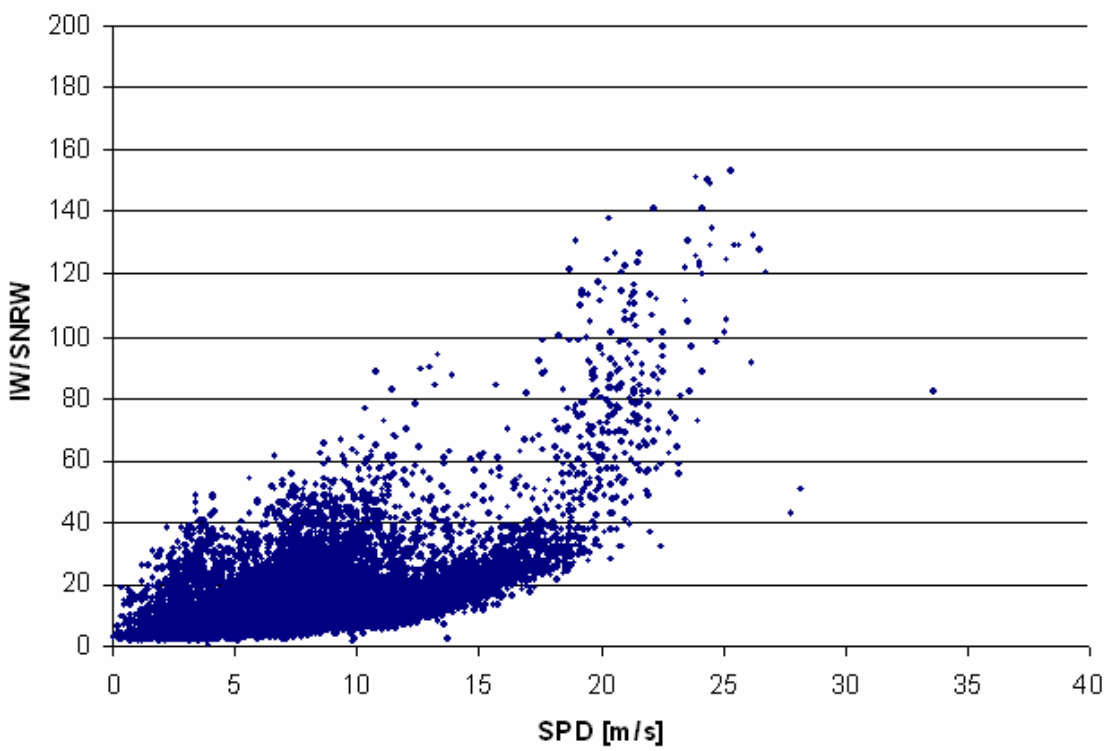

Figure 17. Vertical beam intensity IW divided by SNR vs wind speed during dry periods.

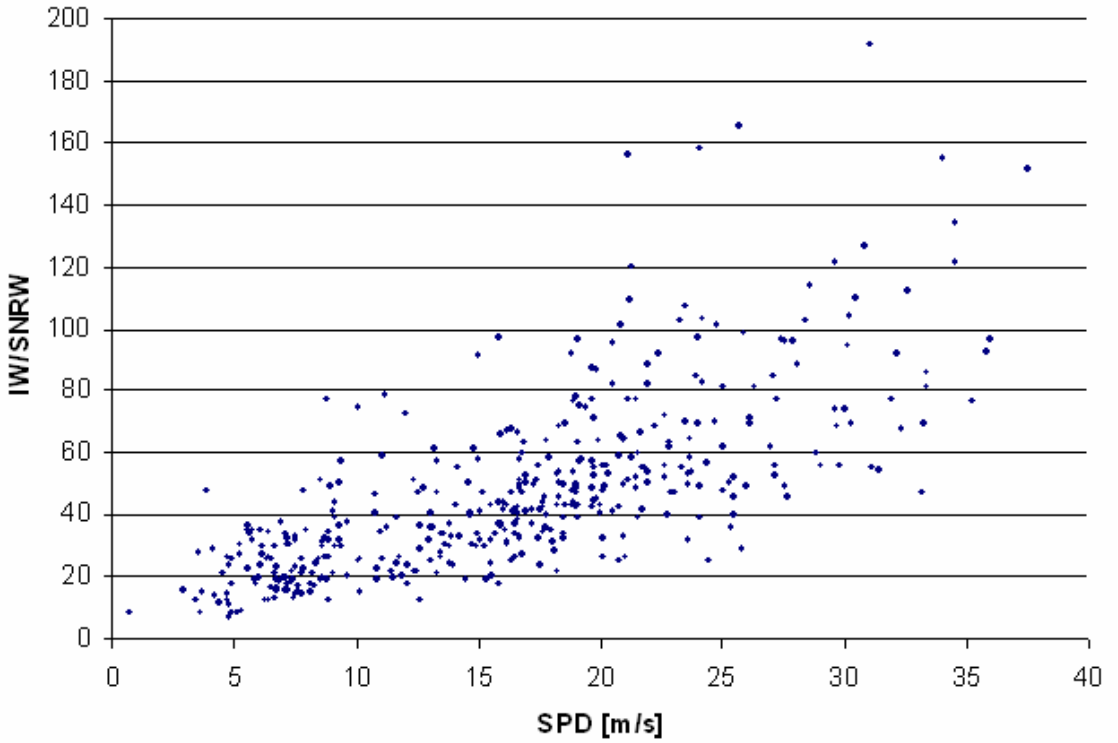

Figure 18. Vertical beam intensity divided by SNR vs windspeed during raining periods

There are two steps required to filter the data completely:

1. The parameters of the SODAR manufacturer's software need to be chosen so that most of the faulty data points are filtered out before any manual data analysis is undertaken. There is no general rule as to which parameters to choose as these vary between different SODARs and sites. The parameters depend on the digital signal processing that is used for data acquisition. For that reason it has so far been impossible to agree on a common filter standard for all SODAR manufacturers and models.
2. In a second step the data set has to be evaluated manually to include filters that depend on external measurement parameters such as the sector filtering and the rain effects mentioned earlier.

Correlation method

In performing a correlation between SODAR wind speeds and mast (i.e. cup) windspeeds, a regression model is required. If we initially ignore the correction due to beam-drift, then the SODAR wind speed V_s can be expected to be a linear function of the cup wind speed V_c. Moreover, it is known that a SODAR will produce a windspeed estimate of zero when there is no wind, so a linear model without offset is most appropriate:

$$V_s = mV_c + \varepsilon \tag{5.1}$$

where m is the slope and ε is the error, assumed to be random and normally distributed with zero mean and variance $\sigma^2_{V_s}$. Although there are errors associated with the cup measurements, orthogonal regression does not seem to offer new insights while inherently using the assumption that the cup errors are *equal* to the SODAR errors. Consequently, we use linear least squares regression.

If N wind speeds V_{s_i}, V_{c_i} are available at a particular height, the residuals are

$$\varepsilon_i = V_{s_i} - mV_{c_i} \qquad i = 1, 2, ..., N \tag{5.2}$$

and least squares minimises $\sum_{i=1}^{N} \varepsilon_i^2$, to give an estimate

$$\hat{m} = \frac{\sum_{i=1}^{N} \frac{V_{c_i} V_{s_i}}{\sigma_i^2}}{\sum_{i=1}^{N} \frac{V_{c_i}^2}{\sigma_i^2}} \tag{5.3}$$

of the slope, with variance

$$\sigma_m^2 = \frac{1}{\sum_{i=1}^{N} \frac{V_{c_i}^2}{\sigma_i^2}} . \tag{5.4}$$

Here σ_i^2 is the variance in V_{s_i}. There is evidence that availability, and hence $\sigma^2_{V_s}$, varies with height, but there is not strong evidence (for example from Figure 16) for $\sigma^2_{V_s}$ depending on V_s. Hence we assume that the SODAR measurement error is independent of V_s at a particular height, and all $\sigma_i^2 = \sigma^2_{V_s}$.

The central calibration question is as follows. Given a SODAR windspeed measurement, V_s, what is the best estimate of the true windspeed, V, and what is the uncertainty, σ_V, in that estimate?

From the above, the best estimate of the true windspeed is

$$\hat{V} = \frac{V_s}{\hat{m}} . \tag{5.5}$$

Also,

$$\begin{aligned} \sigma_V^2 &= \left(\frac{\partial \hat{V}}{\partial V_s}\right)^2 \sigma_{V_s}^2 + \left(\frac{\partial \hat{V}}{\partial \hat{m}}\right)^2 \sigma_m^2 \\ &= \frac{\sigma_{V_s}^2}{\hat{m}^2} + \hat{V}^2 \frac{\sigma_m^2}{\hat{m}^2} \end{aligned} . \tag{5.6}$$

Note that

$$\sigma_{V_s}^2 \approx \frac{1}{N}\sum_{i=1}^{N} \varepsilon_i^2 . \tag{5.7}$$

Finally, quality of regression is often judged by the correlation coefficient

$$r = \frac{\sum_{i=1}^{N}\left(V_{s_i} - \overline{V_s}\right)\left(V_{c_i} - \overline{V_c}\right)}{\sqrt{\sum_{i=1}^{N}\left(V_{s_i} - \overline{V_s}\right)^2 \sum_{i=1}^{N}\left(V_{c_i} - \overline{V_c}\right)^2}} . \tag{5.8}$$

From (5.1), (5.3), (5.4), (5.7), and (5.8), it can be shown that

$$\frac{\sigma_m^2}{\hat{m}^2} = \frac{1-r^2}{r^2 N}\left(1 - \frac{\overline{V_c}^2}{\frac{1}{N}\sum_{i=1}^{N} V_{c_i}^2}\right) = \frac{1-r^2}{r^2 N}\,\frac{\frac{1}{N}\sum_{i=1}^{N}\left(V_{c_i} - \overline{V_c}\right)^2}{\frac{1}{N}\sum_{i=1}^{N}\left(V_{c_i} - \overline{V_c}\right)^2 + \overline{V_c}^2} .$$

If observed windspeeds are uniformly distributed between 0 and V_{max} then

$$\frac{\sigma_m^2}{\hat{m}^2} = \frac{1-r^2}{4r^2 N} \tag{5.9}$$

which is useful in relating correlation coefficient to uncertainty in slope.

Similar equations are used to correlate wind directions.

Distribution of wind speed data

During the calibration period the wind speeds will not be uniformly distributed (it could be a particularly windy period or a particularly calm period). Also the cup anemometers have a "starting wind speed" required to overcome their inertia and, in the current case cup data indicating wind speeds of less than 4 m s^{-1} are generally excluded because the cup calibration is considered unreliable. What are the implications for calibration of the probability distribution of wind speed?

For the linear model of (5.1), if $V_{s_i} \approx V_{c_i}$, as is expected here, then (5.3) predicts that the estimated slope *m* will not depend much on the distribution of wind speeds. On the other hand, (5.4) shows that σ_m^2 will be smaller if the wind speed distribution is more dominated by higher winds. Consequently, the inferences about the *quality* of the model fit (i.e. the uncertainty in the slope) would be expected to vary seasonally and depending on the duration of the calibration period. In the present case, the probability distribution is shown for 60 m height in Figure 19.

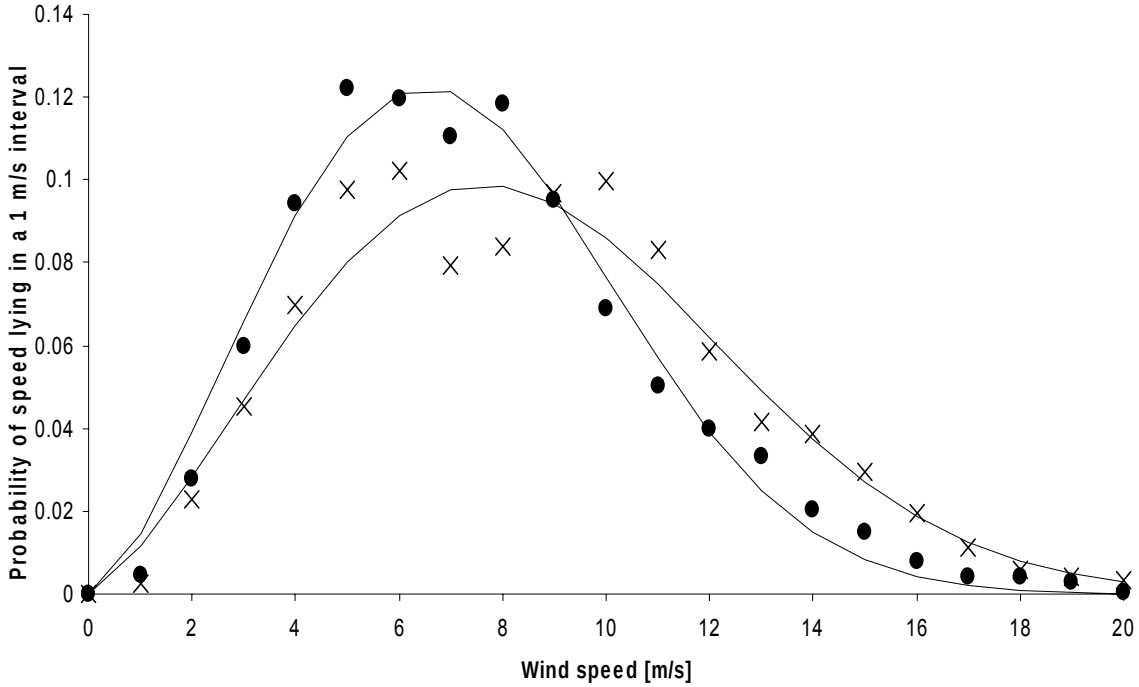

Figure 19. The wind speed probability at two heights during the calibration period. Solid circles: 40 m; crosses: 100 m. Solid lines: Weibull distribution fits with shape and scale parameters (2.44, 8.1 m s^{-1}) and (2.34, 9.7 m s^{-1}) respectively.

From (5.4),

$$\sigma_m^2 = \frac{\sigma_{V_s}^2}{Nc^2\left(1+\frac{2}{k}\right)}$$

for a Weibull distribution having scale parameter *c* and shape parameter *k*. For the example above from the PIE data, if *N* were the same at both heights

$$\frac{\sigma_{m_{100}}^2}{\sigma_{m_{40}}^2} = \left(\frac{8.1}{9.7}\right)^2 \frac{1+2/2.44}{1+2/2.34} = 0.7$$

giving not much difference in predicted slopes errors. As seen from Table 4, there are around 20% fewer acceptable data at 100 m compared to 40 m, so the difference in slope erros should be even smaller. Extreme differences in wind distribution, such as (*k*, *c*) = (2, 5 m s^{-1}) and (5, 15 m s^{-1}) would give a ratio of slope errors of around 0.2. For the PIE data, we would expect σ_m to be *less* at greater altitudes due to this effect, since wind speeds are generally higher.

5.4 Mast-SODAR correlations for wind speed

Regression slope

Figure 20 shows correlations between each of the three SODARs and the mast cup anemometers at a number of heights corresponding to the sites on the mast shown in Figure 14. The regression results are summarized in Table 4. It may be seen that

- Scatter of data increases with height
- There are fewer data points and fewer high-wind points at greater heights
- Slopes are not within 5%
- Correlation is high with values of ≥ 0.96.

System	Parameter	40m	60m	80m	100m	120m
AV4000	N	6580	6555	6281	5453	4676
	$\hat{m}$	1.082	1.085	1.083	1.079	1.080
	$\hat{m}/\hat{m}_{40}$	1	1.002	1.001	0.997	0.960
	σ_m	0.0009	0.0009	0.0009	0.0012	0.0016
	r^2	0.983	0.984	0.982	0.972	0.960
Metek	N	9454	9429	9408	8232	8292
	$\hat{m}$	0.944	0.935	0.928	0.923	0.936
	$\hat{m}/\hat{m}_{40}$	1	0.991	0.983	0.978	0.991
	σ_m	0.0012	0.0012	0.0012	0.0017	0.0014
	r^2	0.949	0.947	0.945	0.908	0.935
Scintec	N	6580	6555	6281	5453	4676
	$\hat{m}$	1.013	0.984	0.978	0.961	0.942
	$\hat{m}/\hat{m}_{40}$	1	0.971	0.966	0.949	0.930
	σ_m	0.0008	0.0008	0.0009	0.0010	0.0013
	r^2	0.982	0.982	0.979	0.977	0.965

Table 4. Results of regression of SODAR windspeeds against mast windspeeds.

The N values indicate that the Metek SODAR data may not have been filtered as strongly as the data from the other two SODARs. This is also suggested from the data spread in Figure 20. One consequence is that some fixed echo data has been included in the Metek regression at 100m, as can be seen from low SODAR windspeeds compared to mast windspeeds. This also explains the significantly lower m value for that regression. For example, exclusion of points with $V_s < 3$ m s^{-1} which also have $V_c - V_s > 2$ m s^{-1} leads to a regression with $m = 0.9285$ instead of 0.923.
Note that σ_m is *not* generally lower at greater heights, and this does not agree with the Weibull estimation above, even when the effect of differing N values is included. It is concluded, therefore, that there is a genuine greater spread in data at greater heights. This is not really unexpected, however, since the lower data availability implies greater errors.

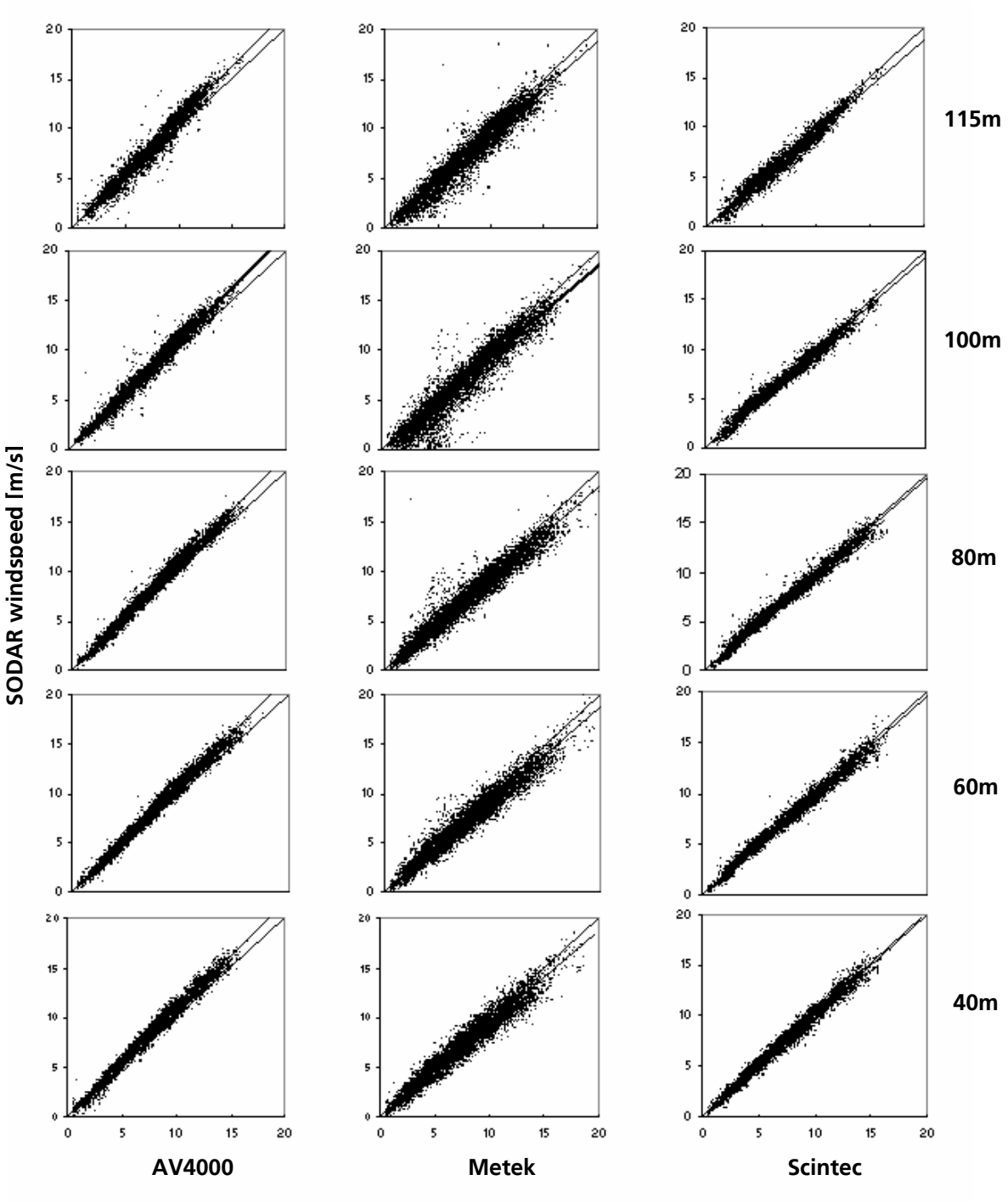

Figure 20. Regressions of SODAR windspeeds against mast windspeeds. Rows (from top): 120 m, 100 m, 80 m, 60 m, 40 m. Columns (from left): AV4000, Metek, Scintec

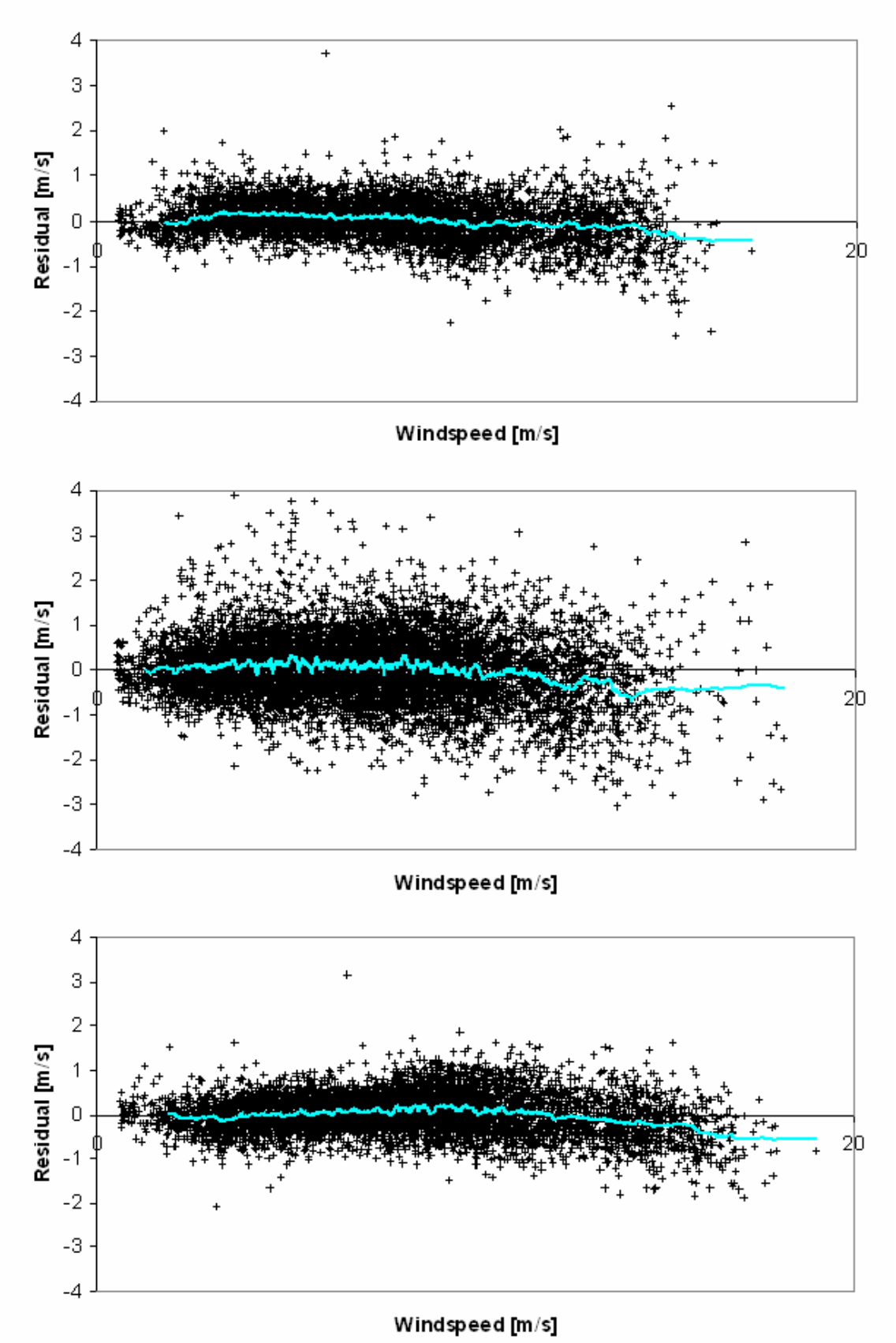

Figure 21. Residual plots for AV4000 (lower), Metek (centre), and Scintec (upper) at 60 m. Superimposed line: running average of 100 points.

Figure 21 shows typical residual plots (ε vs. V_c) for each SODAR. A running average is also shown in each case, where the average is over 100 points (monotonically sorted in increasing V_c). Variation with V_c is apparent for V_c above about 12 m s^{-1} with the non-linearity about 2% at 18 m s^{-1}. Referring to Table 1 this is too high to be explained by beam drift effects. A more likely explanation is that the higher winds come from a different sector, on average, than the lower winds, and the errors apparent in all three SODARs are therefore not only a function of wind direction, but also of wind speed. Referring to Eq. (5.6), Table 4, and Figure 21 we find that $\sigma_{V_s}^2 >> \hat{V}^2\sigma_m^2$ and so $\sigma_V \approx \sigma_{V_s}$, which is not unexpected. SODAR manufacturers generally quote the uncertainty in windspeed measurement expected with their system. For example, in the discussion in Section 2.4, Metek estimate σ_{V_s} = 0.4 m s^{-1}, which is consistent with the data in Figure 21. Also, the standard deviation of residuals for the AV4000 at 40m is 0.40 m s^{-1}. Scintec specifications quote 0.1 to 0.3 m s^{-1} accuracy for their horizontal winds, but it is clear from the data set displayed in Figure 21 that the SFAS system is not achieving that level of accuracy in this comparison.

How much of these residuals is due to variations in the wind itself over the separation distance between the SODAR and mast? In Figure 22 the residuals are plotted from a linear least-squares fit of the 80 m mast wind speed to the 60 m mast wind speed. Little difference is evident between this plot and those of Figure 21.

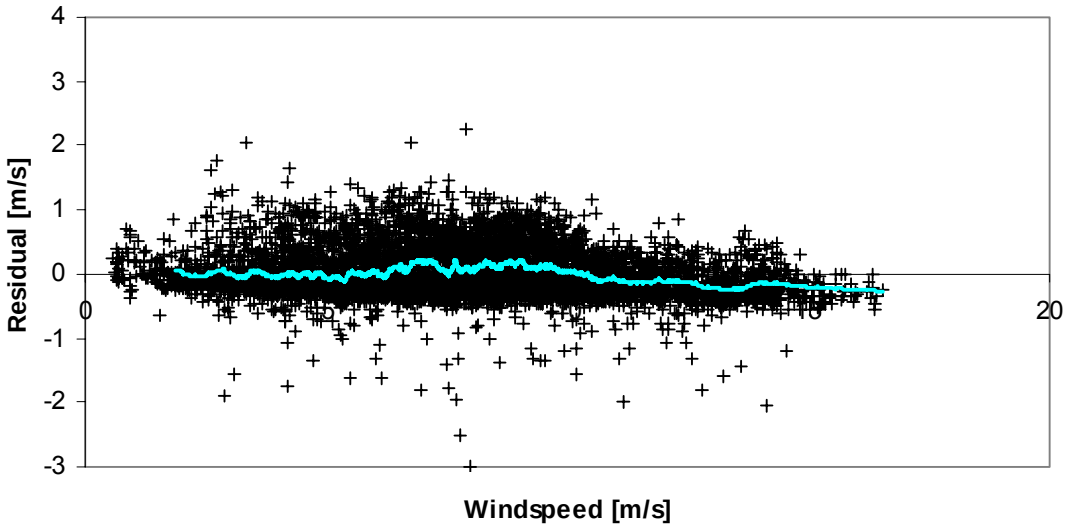

Figure 22. Residuals in a linear fit of 80 m mast wind speed to 60 m mast wind speed.

Figure 23 shows the rms error in the residuals for the AV4000 at 60 m height, as a function of windspeed, together with the rms residuals of the 80 m mast vs 60 m mast wind speed fit. For the SODAR-mast fit there is an indication of a small increase in uncertainty with increasing windspeed, but an estimate of 0.4-0.5 m s^{-1} is again reasonable. This means that the variation in wind speed measured by mast and SODAR is around 4% at 10 m s^{-1} and 2-3% at 20 m s^{-1}, for these 10-minute averages. Longer averages would reduce this error, providing the atmosphere was stationary over the averaging period: for times beyond about 20 minutes in convective conditions this assumption is probably not valid.

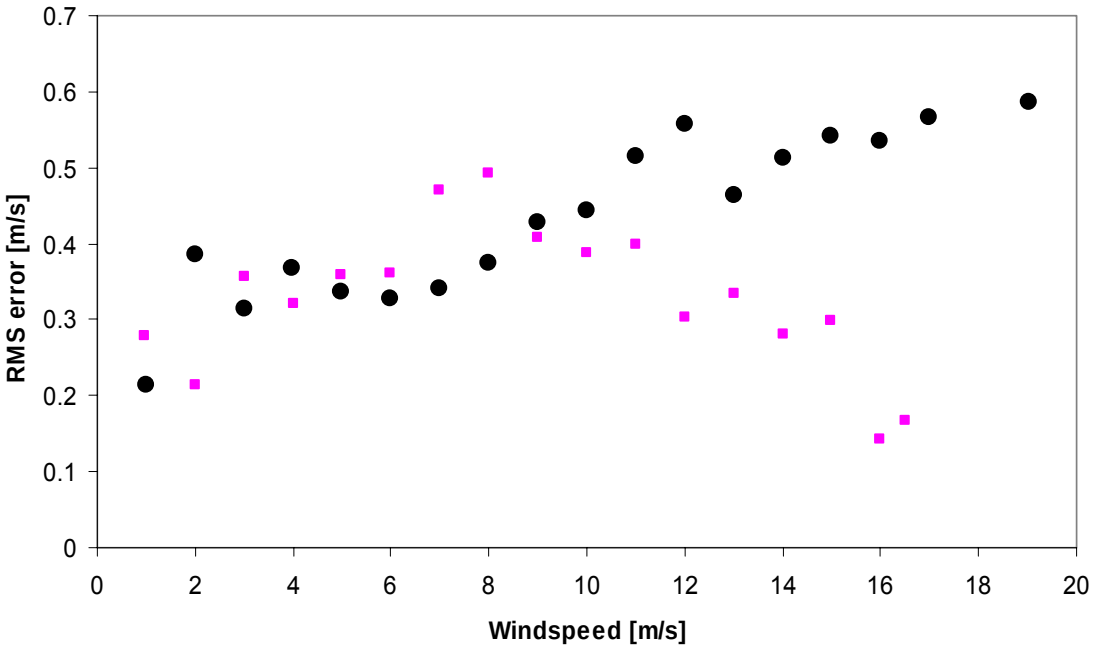

Figure 23. RMS residual error (i. e. uncertainty in least-squares fitted windspeed) vs windspeed. Black circles: AV4000 vs cups at 60 m; pink squares: cups at 80 m vs cups at 60 m.

In Figure 23 the rms residuals for the mast-mast (i.e. cup-cup) comparisons are not distinctly different from the rms residuals for the SODAR-mast comparisons. For wind speeds up to 11 m s^{-1}, an F-test at the 95% level finds that the rms errors for the two fits are *not* significantly different.

This is an extremely important finding, since it suggests that there is *no difference* between SODAR-mast and mast-mast in terms of residuals, except at higher wind speeds. But importantly, the mast-mast comparison is between two sensors only 20 m apart, whereas the SODAR-mast comparison is for two sensors 70 m apart and not necessarily exposed to even the same wind stream. The implication is that the SODAR is measuring winds to at least as high a reliability as the mast cup anemometers.

Variations with height

The regression slopes, *m*, given in Table 4 should be independent of height if the SODAR is a well-designed wind-sensing tool and providing the calibrations have been conducted well. Figure 24 shows the slopes, or calibration coefficients, from Table 4. For the Metek, from (3.5) the out-of-level error would need to be at least 20° to explain the 6% calibration change. A tilt error of this magnitude would be easily visible just by inspecting the SODAR, and the level of the instrument was meticulously checked before and after the PIE field trials. Eq. (3.5) also shows, a little surprisingly at first glance, that tilt errors *always* cause underestimation of wind speed components for a 3-beam system. This is because any increase in radial velocity on a tilted beam is more than cancelled by the increase in radial velocity on the normally vertical beam. This means that the calibration factor >1 for the AV4000 *can not arise from out-of-level errors*. In the case of the AV4000, the calibration error of 8% can not reasonably be attributed to temperature errors, as expressed in Eq. 3.4, since this would require a 50°C error. Thus the absolute calibration errors of all three SODARs remain unexplained.

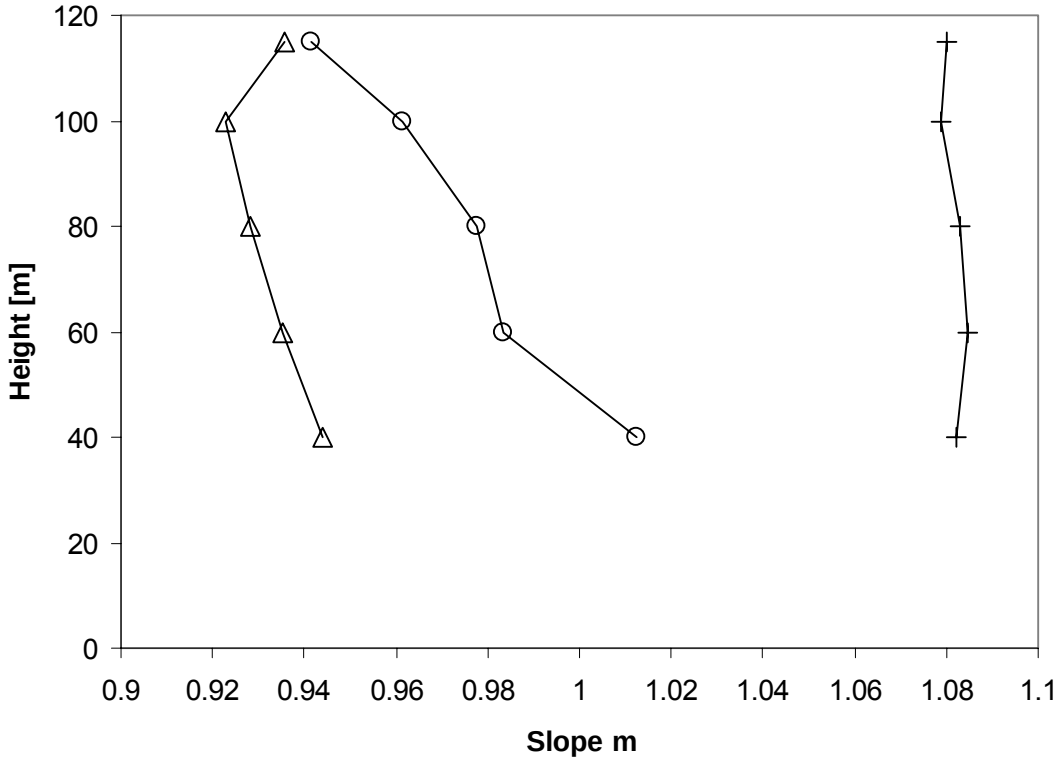

Figure 24. Variation in slope *m* with height. + = AV4000, △= Metek, ○ = Scintec.

If the SODAR measurements can be compared with windspeeds measured by well-calibrated cup anemometers at say 40 m, then it should be very easy to correct for any absolute calibration errors. This is shown in Figure 25 and Figure 26. Earlier, we noted that there is fixed echo contamination in the Metek data at 100m. If this is removed, then the dotted line is applicable to the Metek.

This means that, for 10-minute averaged data, both the AV4000 and the Metek give windspeed estimates good to within about 2% at all heights.

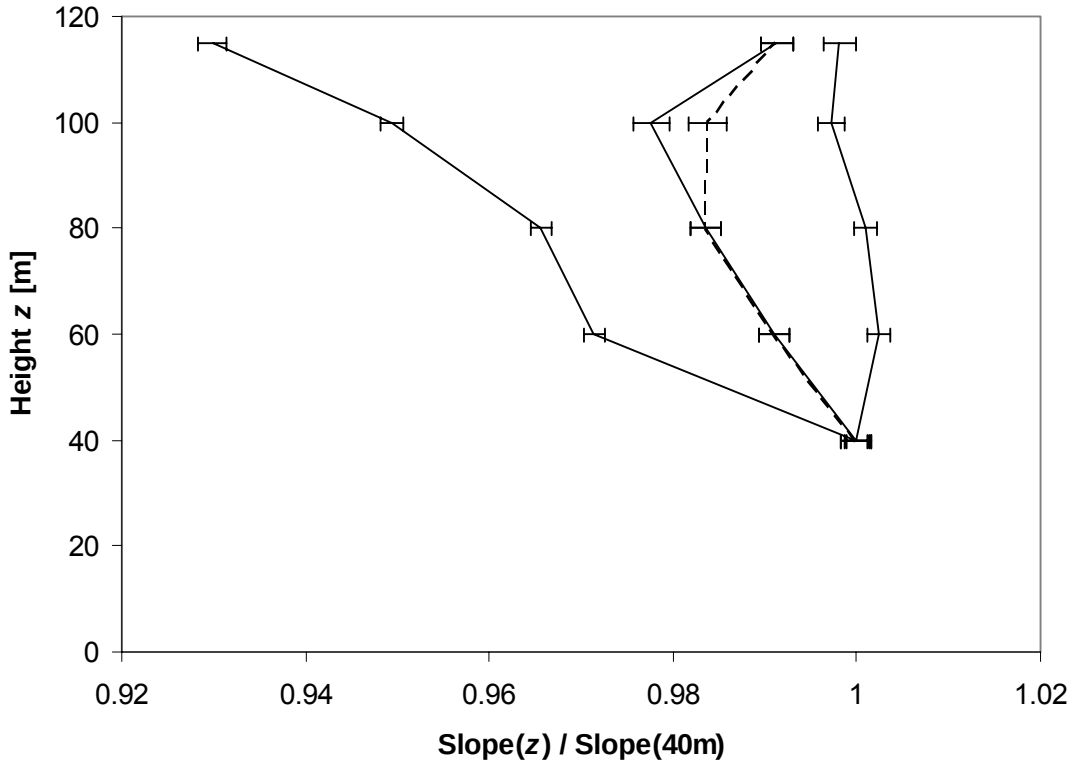

Figure 25 Slope (z) / slope(40m) vs height *z*. AV4000 (rightmost curve), Metek (central curve), Scintec (leftmost curve).

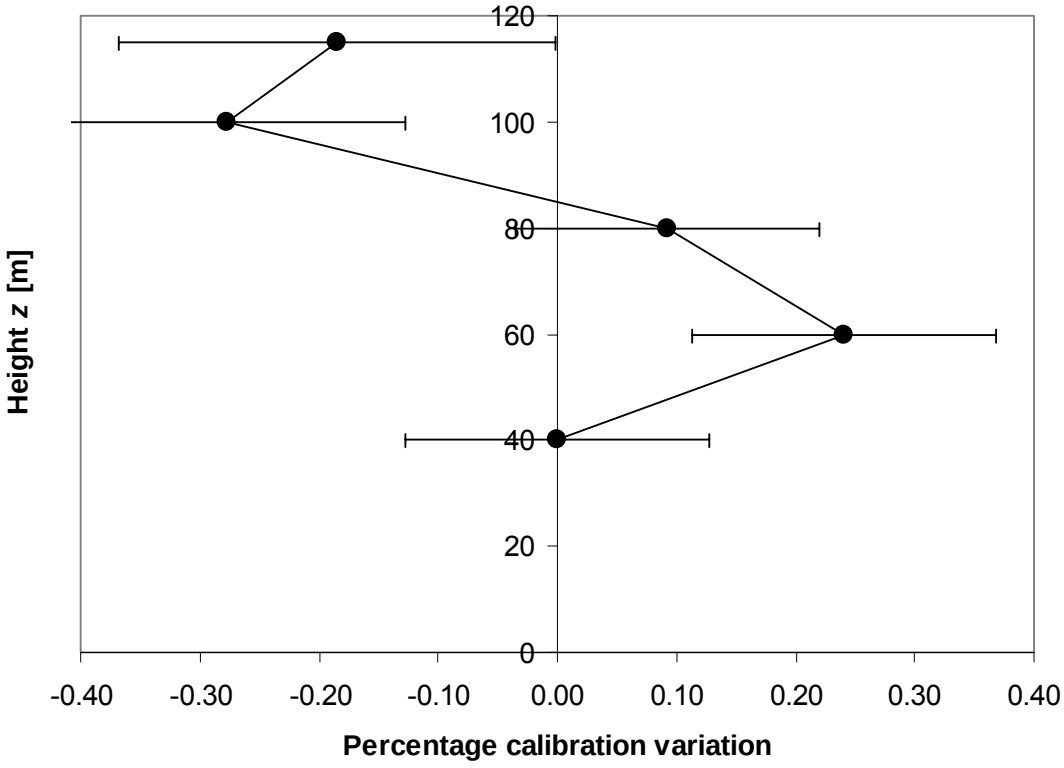

Figure 26 Expanded plot for the AV4000 showing the small variation of calibration with height.

Note that this level of accuracy is NOT achieved by the Scintec SODAR, and this SODAR also shows a significant change of calibration with height. This SODAR uses a combination of asymmetric opposing beams and a range of transmitted frequencies, with the lower frequencies being used preferentially for obtaining winds at greater heights. This could mean that the way in which data is handled is different at different heights (in the sense that different hardware is used and the software uses different parameters), and that this somehow causes the calibration change with height.

Non-linearity and Beam drift effects

As seen above, there is evidence of non-linearity through variation of residuals with height, but this is not readily explainable by the beam drift theory of Section 3.4. As a simple test of this theory, the radial wind components from opposing beams in the 5-beam Metek were compared. The regression shown in Figure 27 is between the opposing Beam 1 and Beam 4 radial velocity components.

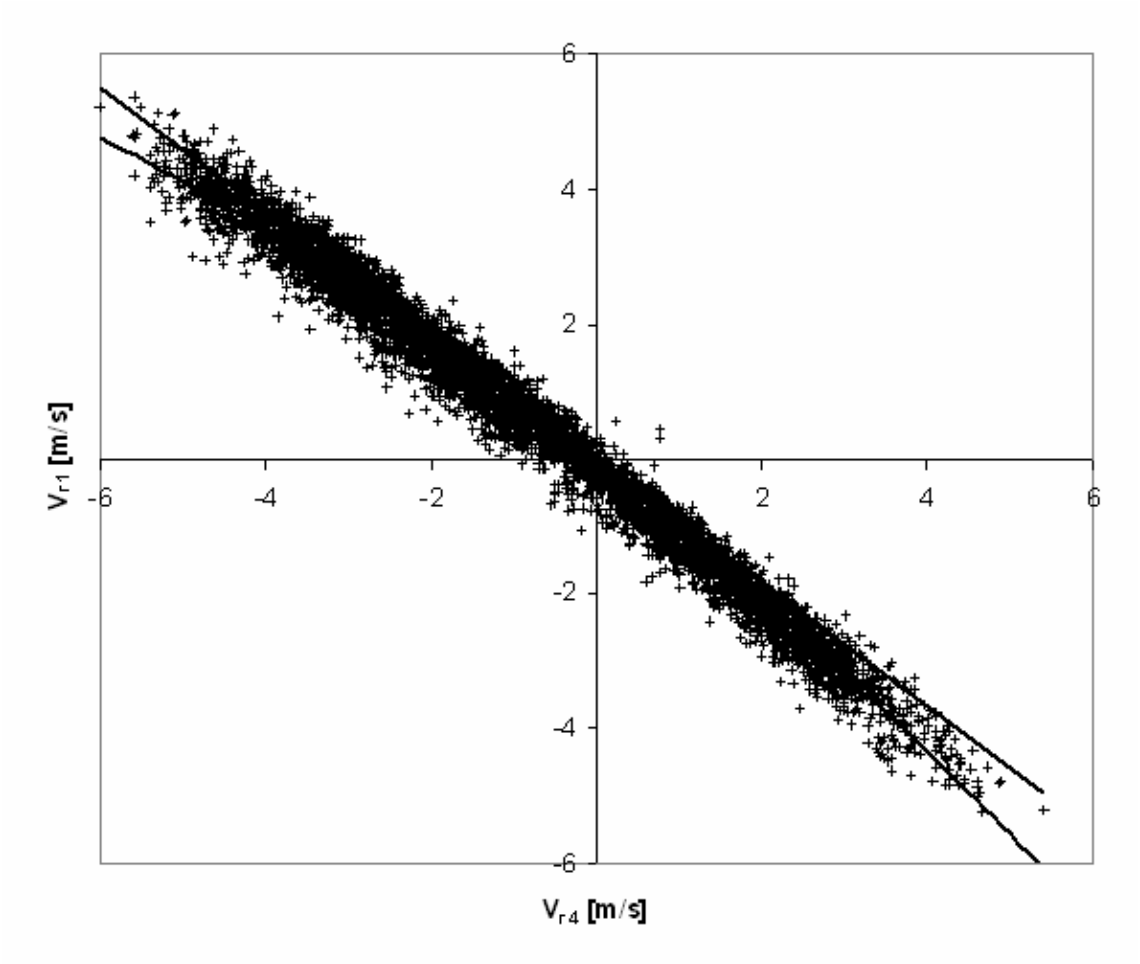

Figure 27 Radial velocities from Beam 1 and Beam 4 of the Metek SODAR at 28 m.

With exclusion of beam drift, $V_{r1} = -V_{r4} + 2w\cos\varphi$, and the inclusion of beam drift gives $V_{r1} = -V_{r4} + 2w\cos\varphi + 2\frac{V^2}{c}$. As a test, we have done regressions of the linear fit $V_{r1} = aV_{r4}$ and the quadratic fit $V_{r1} = aV_{r4} + bV_{r4}^2$, in both cases assuming w to be negligible. The quadratic fit here makes the assumption that V_{r4} is on average indicative of the wind strength. The results are shown in Table 5. Addition of the extra term in the regression does not explain much variance. The b coefficient can be a maximum of $\frac{2}{c\sin^2\varphi}$ ~0.06, but can be expected to be reduced because the wind is not solely in the Beam 4 plane. So the fitted coefficient is not unreasonable.

	r^2	a	b
Linear	0.973	-0.92	
Quadratic	0.978	-0.97	-0.03

Table 5. Parameters from linear and quadratic radial component regressions

5.5 Robustness of the calibration

The calibrations described in Section 5.4 cover the entire period of PIE and so are an average over all meteorological conditions encountered during that period. Five checks were performed on the robustness of the calibration to variations in conditions. Not all checks were performed on all SODARs.

1. divide the data set into even and odd hours. This should give two data sets with negligible difference in conditions, and is simply a test of the robustness of the regression process.
2. divide the data set into even and odd days. This should still provide considerable homogeneity in meteorological conditions.
3. divide data into different wind sectors. This would be expected to give very different meteorological conditions within the various sub-sets, and so is a good check that the calibration is not peculiar to a particular set of conditions.
4. divide the data into the first part of the PIE period and a later part. General seasonal climate differences can be tested.
5. perform calibrations elsewhere, using a SODAR similar to one of those in the PIE trials.

PIE tests for robustness

Regression results at 120 m are summarized in Table 6. There are no discrepancies in the first two tests (split hours and split days). There appear to be problems with the AV4000 and the Metek with variable meteorology. However, the Scintec data have had the wind data from the sector 325°-090° removed, on the basis that cup data are not good in this sector, and so it is necessary to compare the AV4000 and Metek with similar filtering.

	AV4000	Metek	Scintec
$m_{\text{odd hours}} / m_{\text{even hours}}$	1.002 ± 0.003	0.999 ± 0.001	0.997 ± 0.004
$m_{\text{odd days}} / m_{\text{even days}}$	0.998 ± 0.004		1.006 ± 0.004
$m_{305\text{-}325°} / m_{125\text{-}145°}$	0.961 ± 0.010	0.927 ± 0.013	1.007 ± 0.010
$m_{1/4/2004\text{-}20/6/2004} / m_{1/4/2004\text{-}20/8/2004}$	0.991 ± 0.004		

Table 6. Tests of calibration consistency through dividing the PIE data set in different ways

Effect of bad mast data

Because of shielding of the cup anemometer by the mast, there will be a sector of wind directions in which there is poorer mast wind data. If this sector is included in the data set for SODAR-Mast calibrations, then the spread of values and quality of regression will be poorer (this being due to the 'standard'). Table 7 gives regression parameters from the Metek-Mast correlation as a function of wind sector. For this mast the sector 325°-90° is contaminated. The table therefore shows the results of calibrations in this sector compared to the complementary 90°-325° sector at three heights. It can be seen that the slopes *m* vary by less than 1% between these two sectors. This suggests that the cup anemometers can be used quite successfully, for this mast, in all wind directions. On the other hand, Table 7 also shows the 'good' sector split into three parts: 90°-180°, 180°-270°, and 270°-325°. At all three heights the value of *m* is significantly higher (by ~2%) and the correlation coefficient also slightly higher for winds in this sector. This is unlikely to be an artifact of the SODAR. The results at 40 m are also shown in Figure 28. The dashed line shows the average over the 90°-325° "good" sector.

Height [m]	Sector	*m*	r^2
40	325°-90°	0.948	0.970
	90°-325°	0.957	0.984
	90°-180°	0.958	0.982
	180°-270°	0.977	0.988
	270°-325°	0.948	0.984
60	325°-90°	0.943	0.937
	90°-325°	0.946	0.986
	90°-180°	0.947	0.983
	180°-270°	0.963	0.990
	270°-325°	0.938	0.987
80	325°-90°	0.943	0.927
	90°-325°	0.938	0.985
	90°-180°	0.931	0.978
	180°-270°	0.951	0.989
	270°-325°	0.935	0.987

Table 7. Regression paramters for various wind direction sectors and heights for the Metek SODAR.

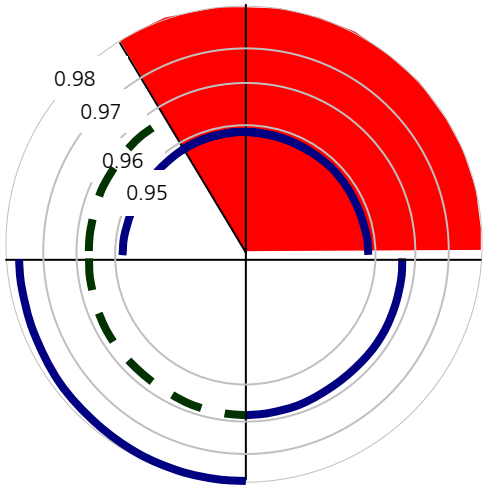

Figure 28: Variation of calibration with sector at 40 m height.

These effects are shown quite strongly in Figure 29, Figure 30, and Figure 31.

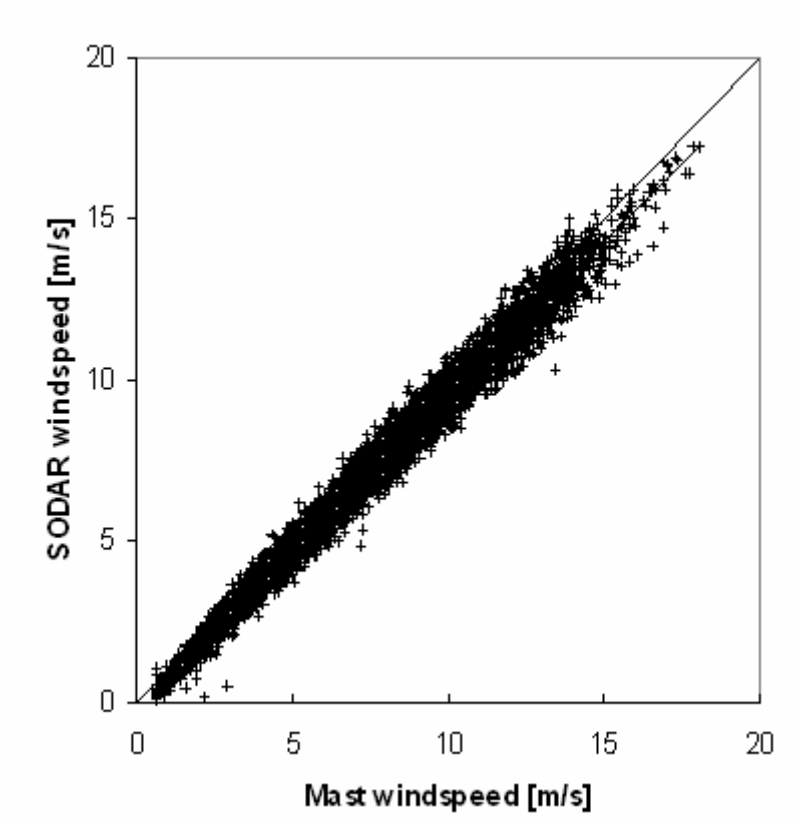

Figure 29: Regression at 40 m in the sector 90°-325°.

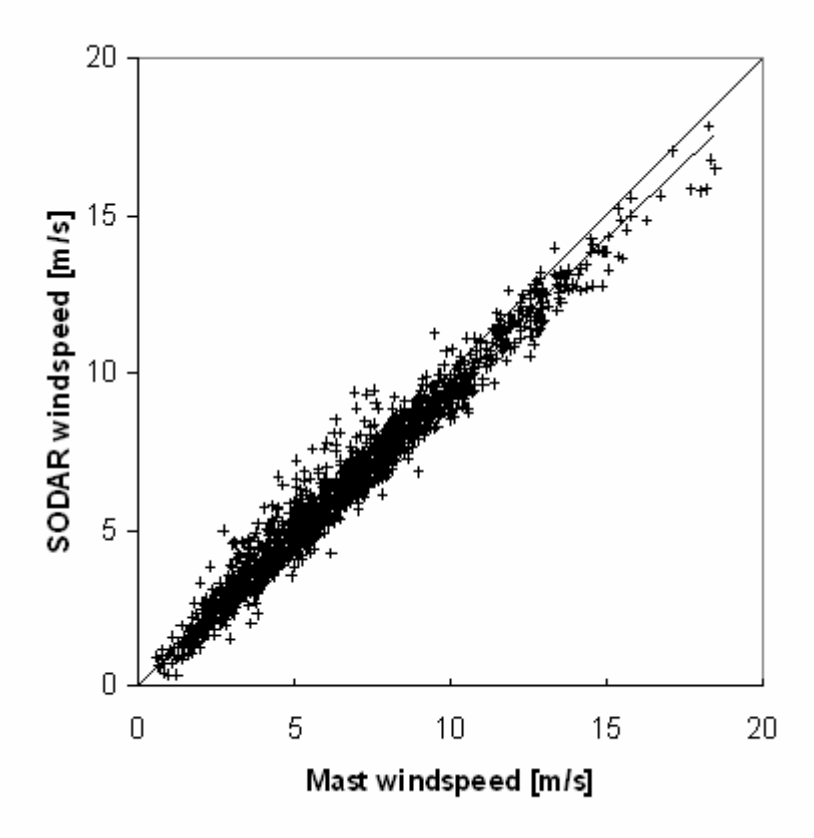

Figure 30: Regression at 40 m in the sector 325°-90°.

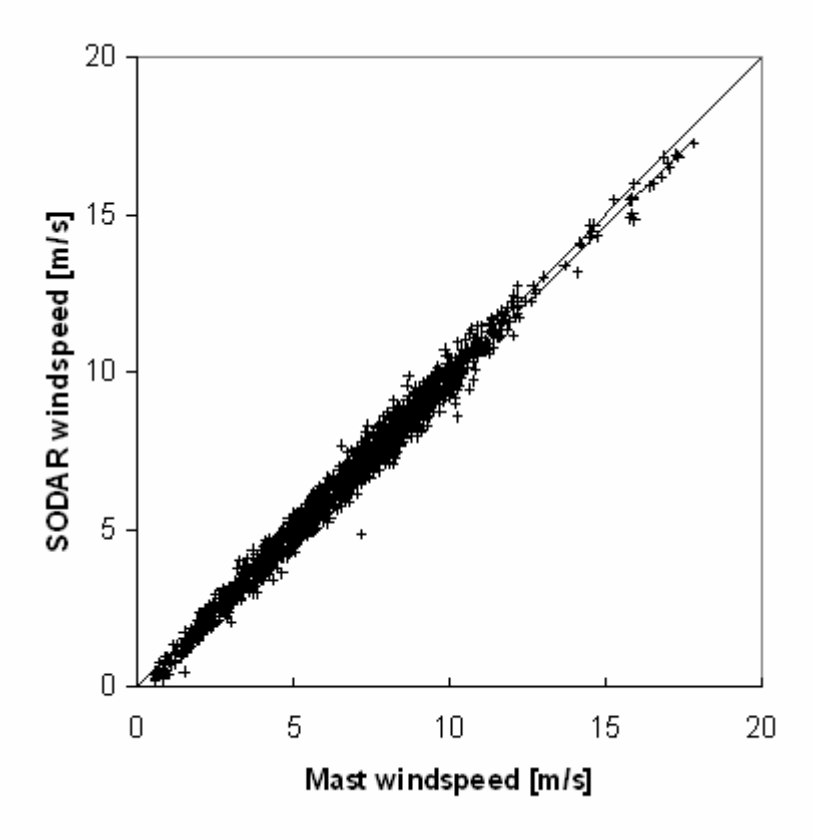

Figure 31: Regression at 40 m in the sector 180°-270°.

Calibrations elsewhere

Between 24 June and 10 August 2004 calibrations were performed between a different AV4000 system and the cup anemometer mounted on a 45m boom on the 108m tower at the ECN EWTW test site. Unfortunately not many high wind periods were included.
Only data satisfying the following criteria were retained:

- no rain detected
- wind direction within the sector of 40° - 260°
- $V_c > 4$ m/s (the calibration range for the cups)
- $\sigma_{Vc} < 2.7$ m s^{-1} for all beams
- $7 < \text{SNR} < 35$ for all beams
- $|V_s - V_c| < 2$ m s^{-1}

In Figure 32 the previously found regression line, having a slope $m = 1.08$ is shown superimposed upon the data from the different AV4000 SODAR. The slope is identical within the uncertainty of the regression.
When this regression slope is then used to predict the 'true' wind measured by a cup anemometer at 70m on the EWTW mast, the regression of predicted wind against mast wind at 70 m is found to be 1.004, or within 0.4%. The 45 m-corrected regression at 70 m is shown in Figure 33. Note again the tendency for this regression to slightly underestimate at higher wind speeds.
Applying the same regression method to correct the 70 m data during a different measurement period of 19 Dec 2003 – 27 Jan 2004, a regression of 0.982 was obtained. This echoes the finding in the section above, that the calibration varies with meteorological conditions (in this case by 2%). Some of this calibration change could be due to inadequate estimation of temperatures for computing beam tilt angles, since in the case of this AV4000 temperature estimates were based on a climatological table (there is the option to connect a temperature sensor).

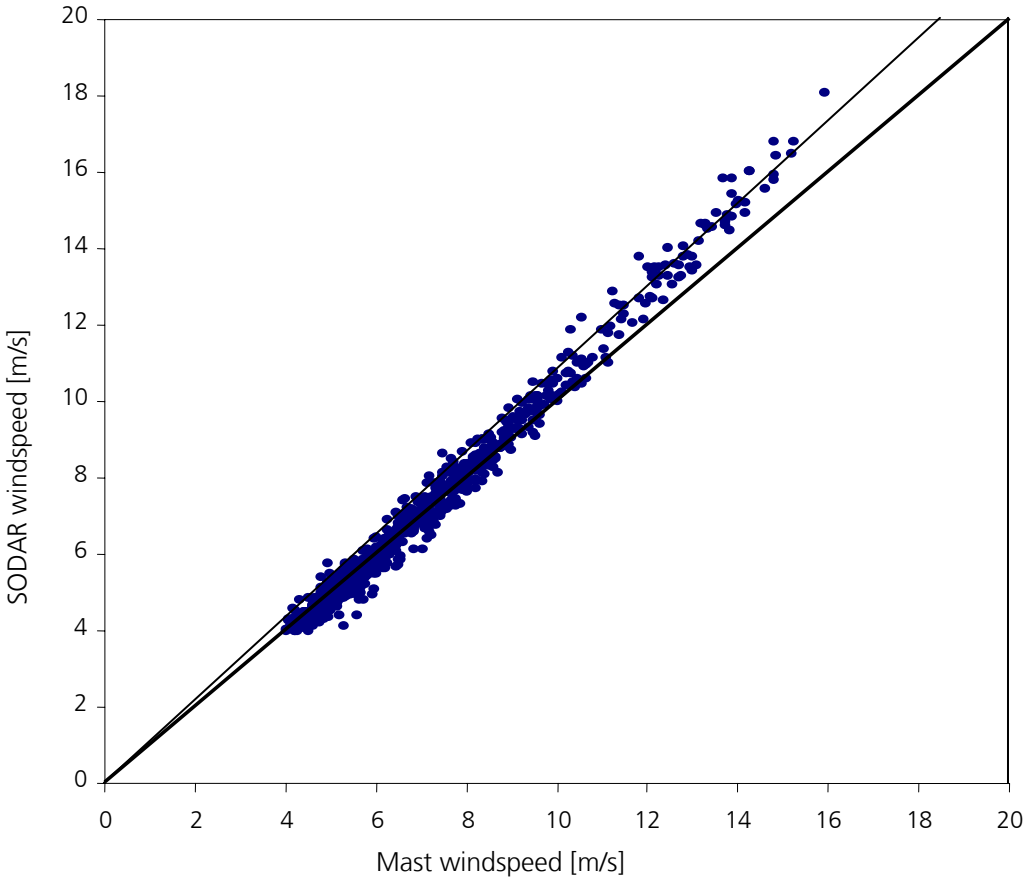

Figure 32 Calibration of the ECN AV4000 against a cup anemometer at 45 m.

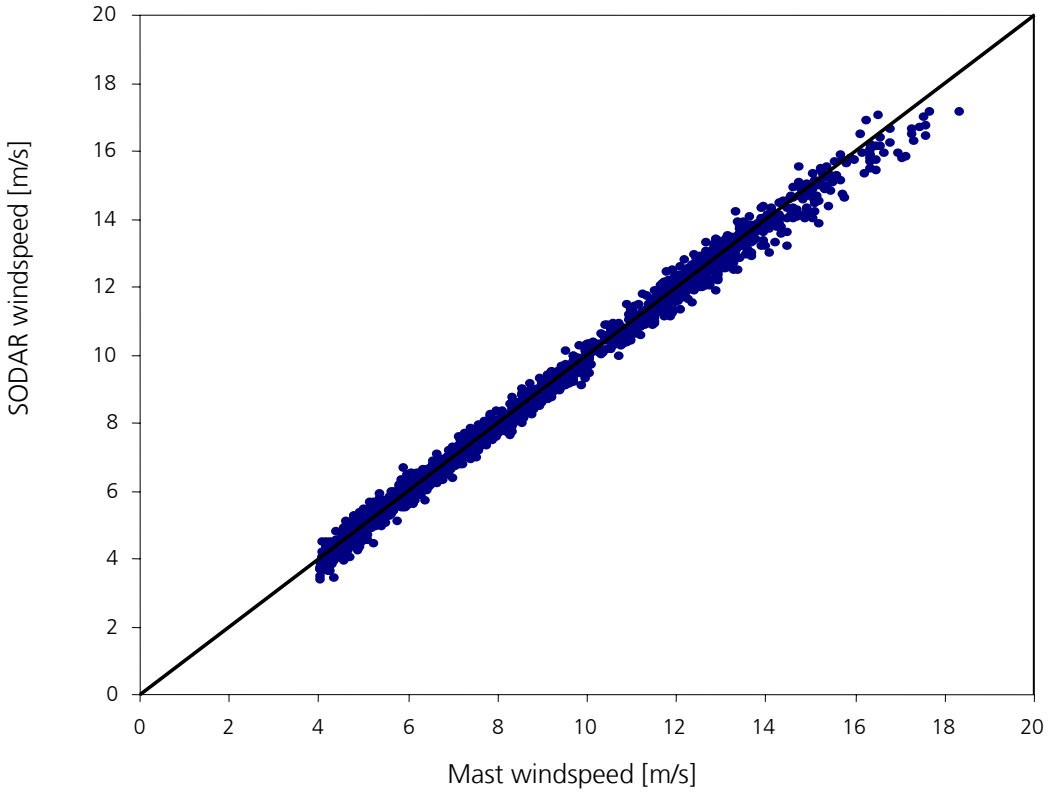

Figure 33 The regression at 70 m, corrected using the regression at 45 m.

5.6 Wind direction regressions

Monitoring wind direction is perhaps less important in wind energy applications, but regressions were also performed between SODAR directions and mast (wind vane) directions. Figure 34 and Figure 35 show correlations between Metek wind directions and the vanes at 60 m and 100 m on the Høvsøre mast. At 60 m the slope is 1.006±0.0004 and r^2 = 0.990 (8528 points), and at 100 m the slope is 0.989±0.003 and r^2 = 0.891 (3581 points). A fit through the origin for these data is a bit misleading, since the fit should be circular and repeat at 360°. Nevertheless, at 180° direction these fits predict errors of 1° at 60 m and 2° at 100 m, which are negligible for wind-energy support.

One curious artefact is that in the 100 m plot it is clear that for some points the sign of one of the individual wind components is wrong. This leads to a symmetric set of data points (e.g. mast -45°, SODAR +45°). It is not known what causes this occasional lapse, since it is not consistent with being due to fixed echoes.

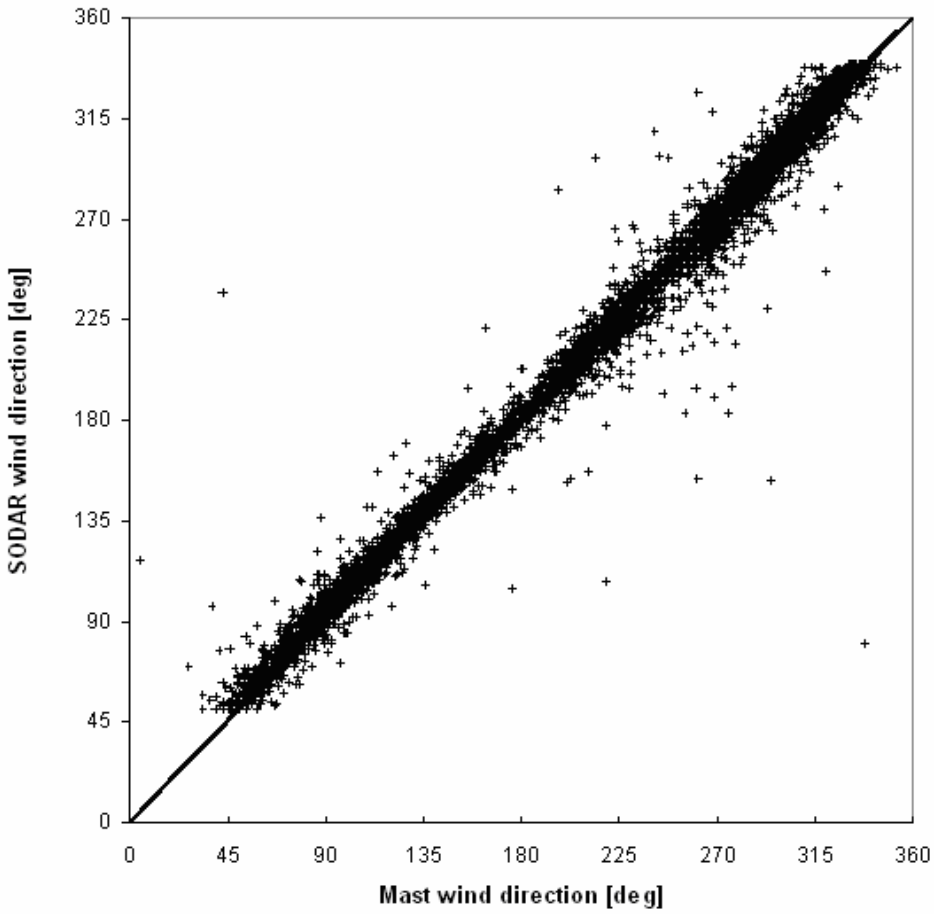

Figure 34 Regression of Metek-derived wind directions against the mast vane directions at 60 m.

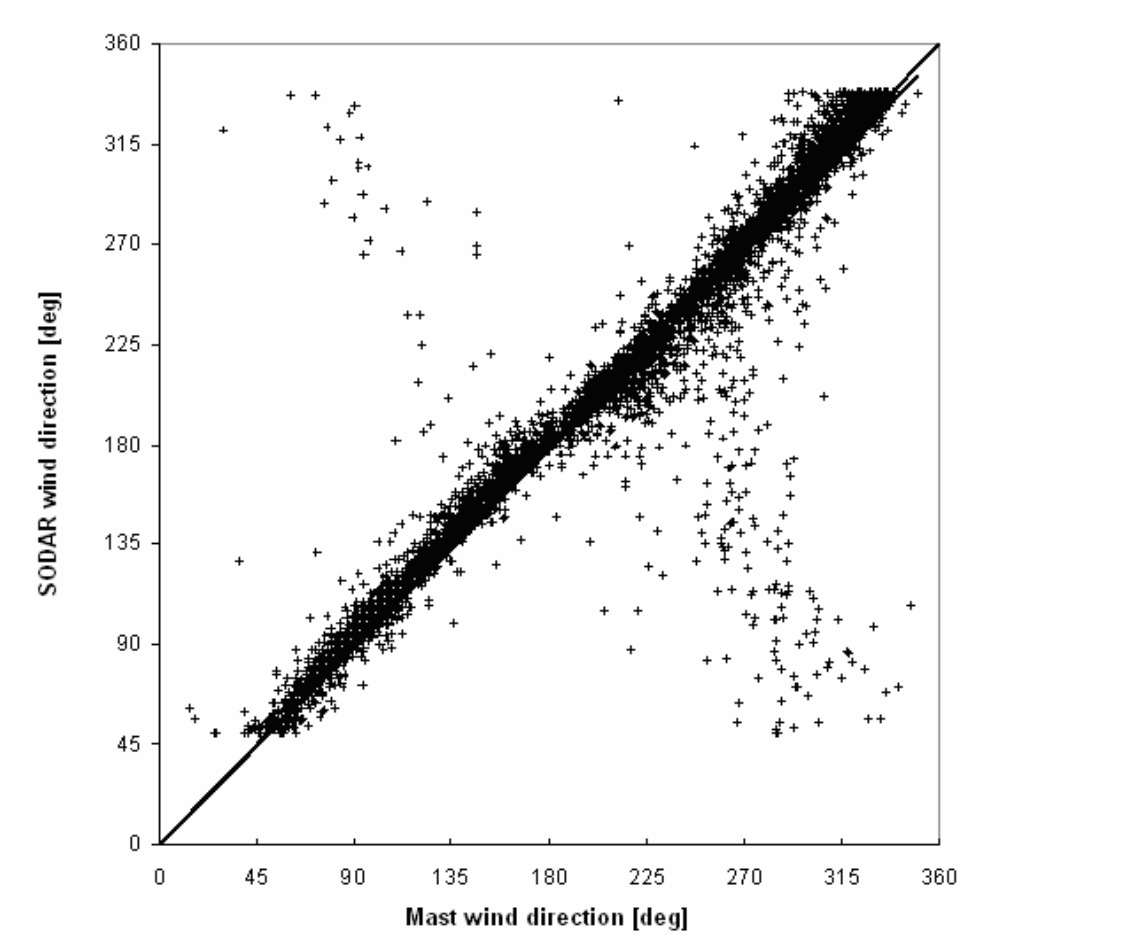

Figure 35 Regression of Metek-derived wind directions against the mast vane directions at 100 m.

6. Calibration transferability

The above sections describe a procedure in which a cup anemometer at 40 m height is used to provide a single-point 'absolute' calibration for a SODAR, and then the SODAR is used for wind finding at all other heights. The technique generally shows good potential, but the 40 m calibration does need to be repeated, at least seasonally, since there are some SODAR calibration shifts with changing meteorological conditions.

Since most SODARs are mobile, the question arises whether one SODAR can be used to periodically update the calibration of another fixed installation. The following describes SODAR-SODAR regressions, for the three SODAR systems at the PIE trials. Regressions are performed both with and without being forced through the origin.

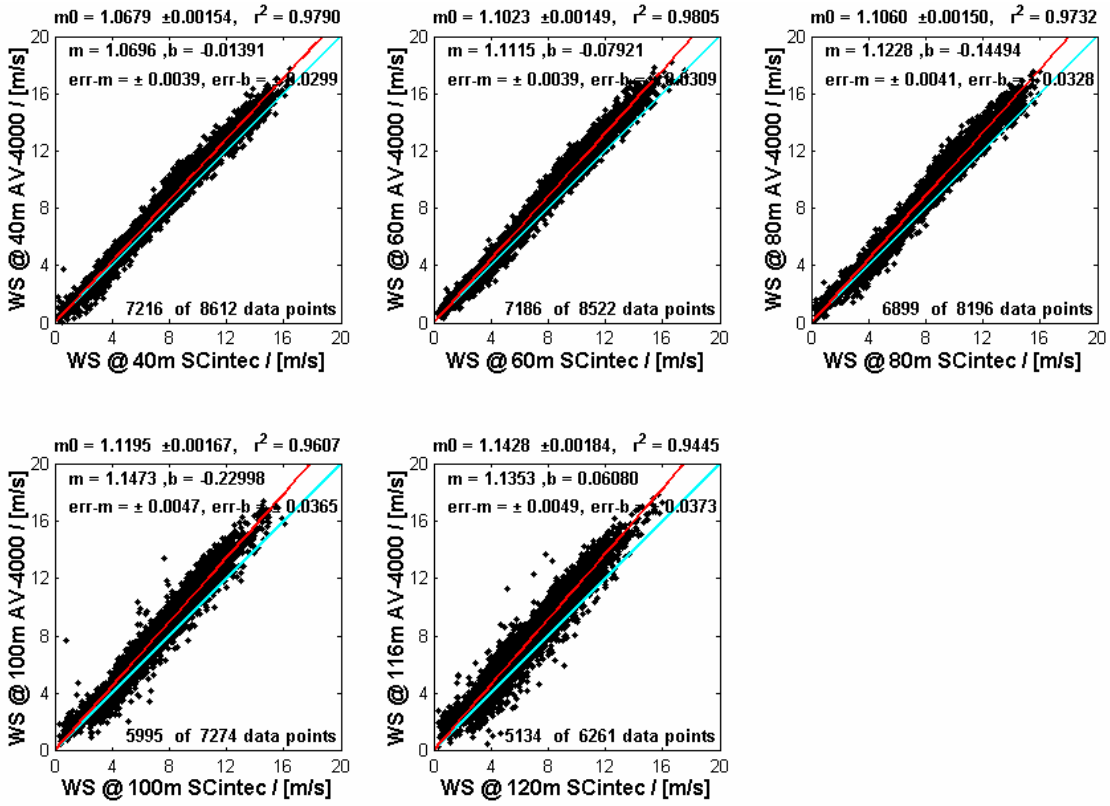

Figure 36. Windspeed correlation between AeroVironment and Scintec SODARs at a) 40 m, b) 60 m, c) 80 m, d) 100 m, and e) 120 m above ground level. All wind speeds and wind directions between 50° and 340° are included. m0 denotes the slope of the correlation with the intercept m0 denotes the slope of the correlation with the intercept set to zero, m is the slope, b the intercept, err-m the accuracy of the slope, err-b the accuracy of the intercept.

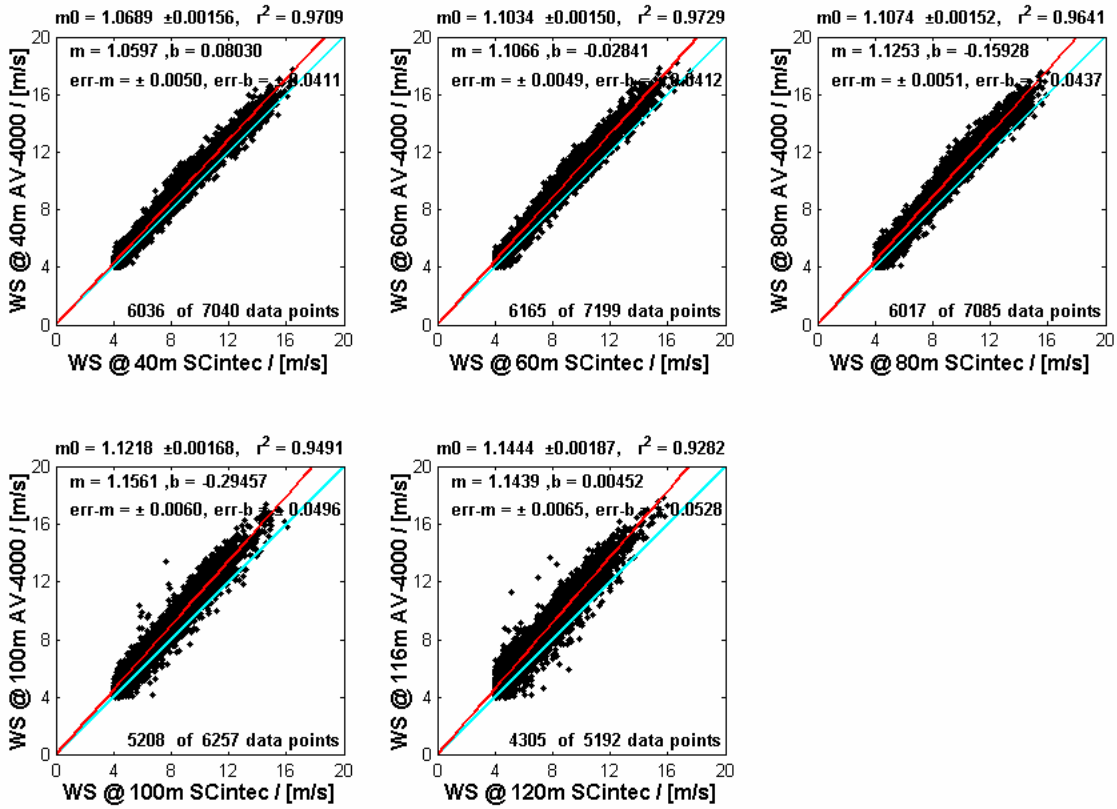

Figure 37. Windspeed correlation between Scintec and AeroVironment SODARs with windspeeds below 4 m s^{-1} discarded. Wind directions between 50° and 340° are included.

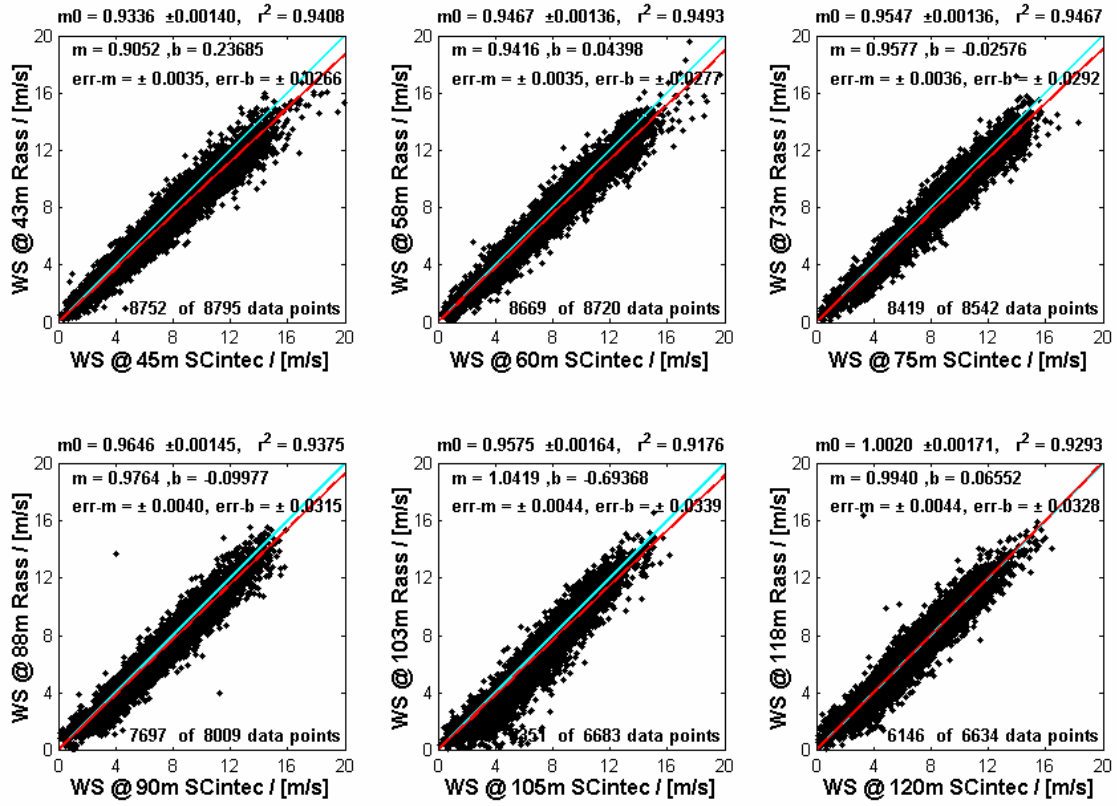

Figure 38: Windspeed correlation between Scintec and Metek (shown as 'RASS') SODARs. All wind speeds and wind directions between 50° and 340° are included..

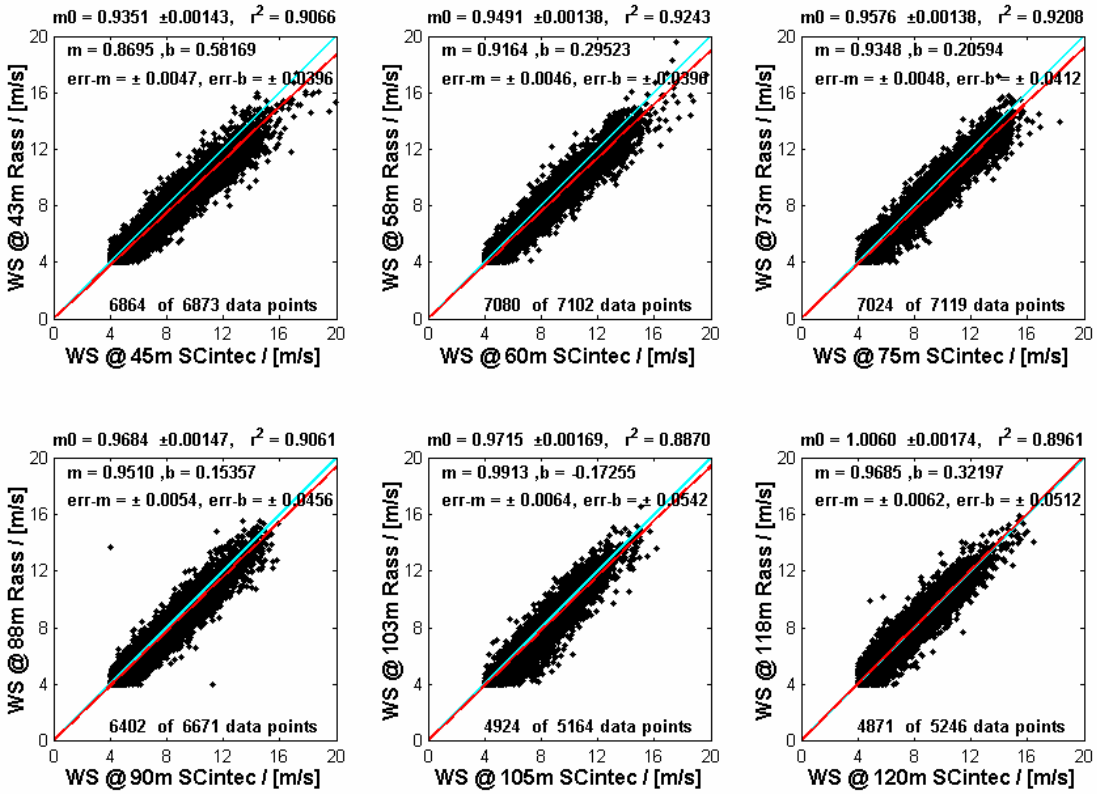

Figure 39:. Windspeed correlation between Scintec and Metek SODARs with windspeeds below 4m s^{-1} discarded. Wind directions between 50° and 340° are included.

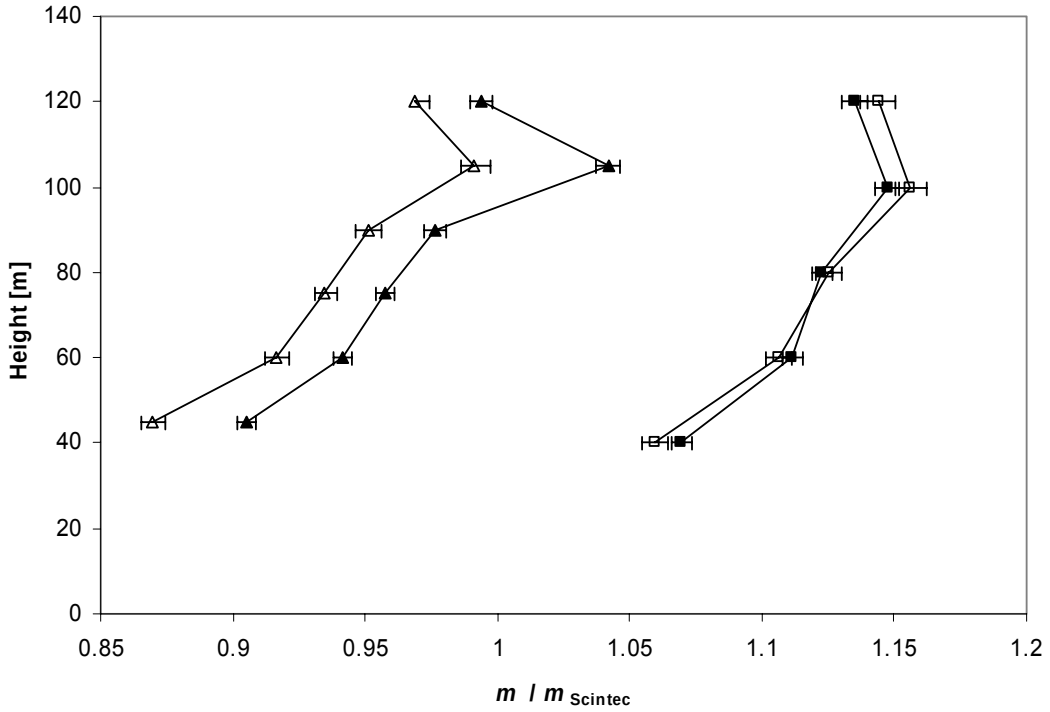

Figure 40:. Ratios of correlation slopes of Scintec and AeroVironment SODARs (squares) and Scintec and Metek SODARs (triangles) with non-zero intercepts. Closed symbols denote correlations that include all wind speeds, open symbols denote correlations which discard wind speeds smaller than 4 m s^{-1}.

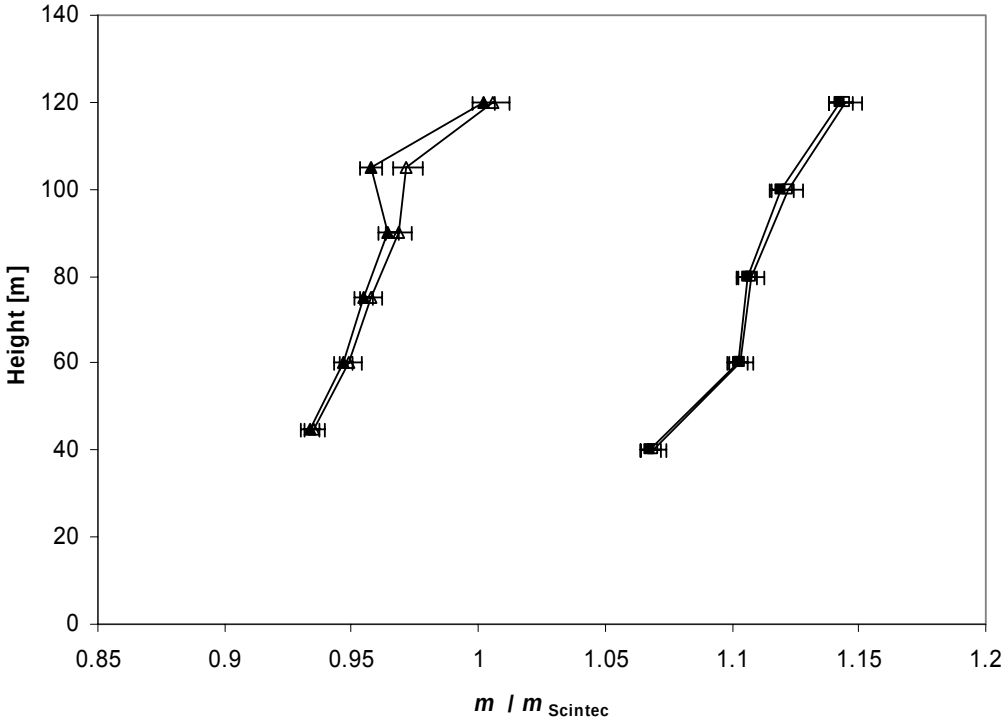

Figure 41: Ratios of correlation slopes of Scintec and AeroVironment SODARs (squares) and Scintec and Metek SODARs (triangles) with the regressions through the origin. Closed symbols denote correlations that include all wind speeds, open symbols denote correlations which discard wind speeds smaller than 4 ms^{-1}.

Figure 40 and Figure 41 are derived from Figure 36, Figure 37, Figure 38, and Figure 39. There are a number of very obvious features:

1. percentage differences in slope are typically ± 5-10%
2. the ratio of slopes increases with height
3. there is less effect of including winds below 4 m s^{-1} for regressions through the origin
4. the Metek data show a fixed echo problem near 100 m, consistent with previous plots.

From these data it is also possible to plot m_{Metek} / m_{AV4000} as shown in Figure 42, using the same scales. This shows that the variation in slope with height is due to the Scintec SODAR. Figure 42 is also consistent with the AeroVironment overestimating winds by about 8% (slope of 1.08 from Figure 24) and the Metek SODAR underestimating winds by about 5% (slope of 0.957 from Figure 28).

Note that these regressions are *performed without reference to the mast data*, although for clarity we show the regression slopes as m_{AV4000} / $m_{Scintec}$ and m_{Metek} / $m_{Scintec}$. Comparison between this ratio, shown in Figure 40 and Figure 41, with that derived from Table 4, serve to indicate the extent to which the variability in regressions against the mast data are contributed by the SODAR or the cup anemometer uncertainties.

	40m	60m	80m	100m	120m
AV4000-Mast/Scintec-Mast	1.068	1.103	1.107	1.123	1.146
AV4000-Scintec	1.068	1.102	1.106	1.120	1.143
Metek-Mast/Scintec-Mast	0.932	0.950	0.949	0.960	0.994
Metek-Scintec	0.934	0.947	0.955	0.958	1.002

Table 8. Comparison between SODAR-SODAR and Mast-SODAR calibrations.

It is clear from Table 8 that the SODAR-SODAR calibrations provide essentially the same information as the SODAR-Mast calibrations. This means that the calibration is transferable, using a 'standard SODAR'. However, some care will be required to ensure that the SODAR used as a standard does not have calibration varying with meteorological conditions, or that a 40 m cup anemometer is also used from time to time.

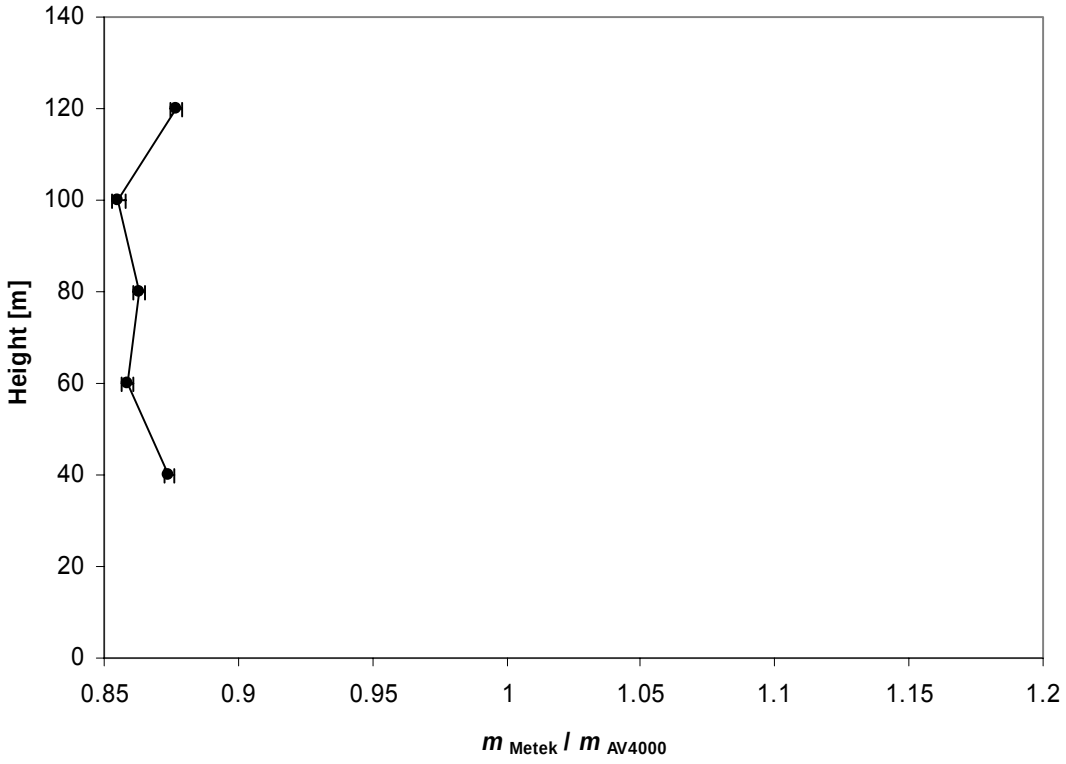

Figure 42: Ratios of correlation slopes of Metek and AeroVironment SODARs (through the origin).

The Metek and AeroVironment SODARs, if calibrated against a 40 m mast, have consistent calibration with each other and with the mast at all altitudes, with a calibration error of about ±1%.

7. The SODAR as a 'Turn key Instrument'

The above calibrations indicate that there is often an absolute calibration error for a SODAR, which can be as much as 6% or 8%, but that the relative or statistical calibration errors are typically less than 2% and may be as low as 0.4%. Errors in estimating wind speed from a *single* SODAR 10-minute windspeed are typically 0.4 m s^{-1} or 4% at 10 m s^{-1}.

If the SODAR is deployed *without any calibration* what errors can be expected? The estimation of rms errors, shown in Figure 23, is repeated for the AV4000 at 60 m, assuming that the calibration slope is unity. The result is shown in Figure 43. This shows that the estimation error, for this AV4000 SODAR, will be around 0.8 m s^{-1}, if no calibration is performed, and no assumptions made about systematic effects. This corresponds to an 8% error at 10 m s^{-1}, which is unacceptable for wind energy applications.

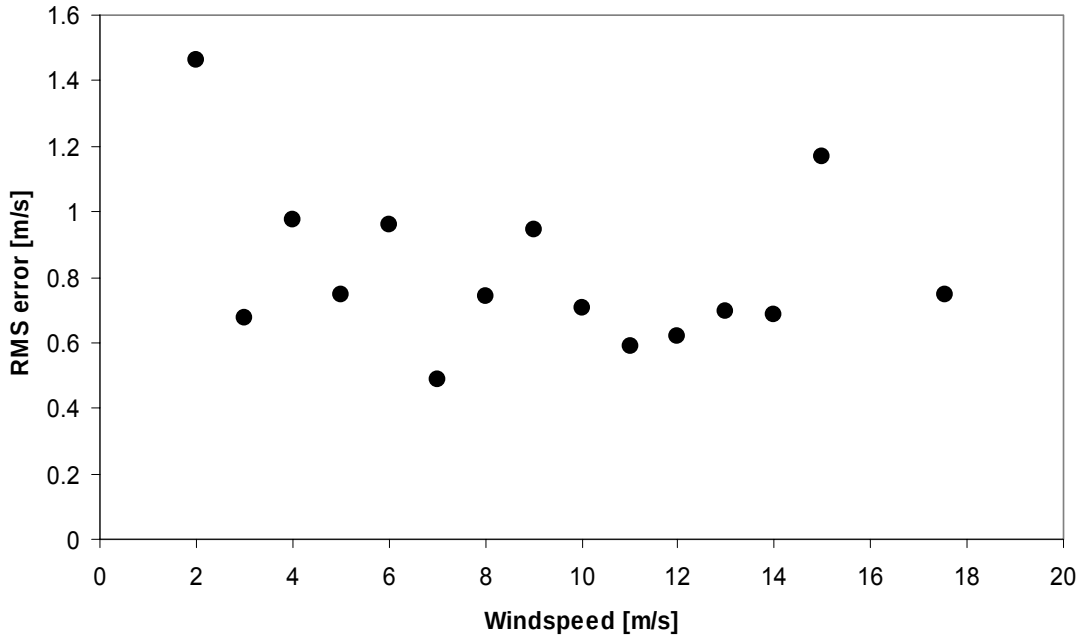

Figure 43: Rms errors in 1 m s^{-1} bands, assuming the calibration slope is 1.

8. Conclusions and recommendations

This Report is concerned with the errors which might occur in calibrating SODARs for wind energy applications, and also in evaluating an actual calibration experiment involving a number of SODARs from leading manufacturers.

8.1 SODAR Error budget

The various errors examined in Section 3 may be combined to provide an error budget for SODAR measurements of wind speed. In summary, the various error contributions are

ID	Source	Parameter	Slope error $\frac{\hat{u}}{u}-1$	Parameter range	Error range
1	Temperature	ΔT [K]	$+\frac{\Delta T}{2T}$	±20 K	± 3 %
2	Out of level	$\Delta\varphi$ [radian]	$-\frac{1}{2}(\Delta\varphi)^2$	±15° (±0.3 rad)	-3.5 % to 0 %
3	Fixed echoes	Δx [m]		0 to 500 m	0 to -100%
4	Rain	R [mm/h]		0 to 50 mm/h	20 - 30 m s^{-1}
5	Beam spread	σ_φ [radian] φ [radian]	$+2\frac{\sigma_\varphi^2}{\sin^2\varphi}$	4°-8° (0.07-0.14 rad) 15°-24° (0.26-0.42 rad)	+6 % to +25 %
6	Beam drift	u/c	$\pm\sqrt{2}\frac{u}{c}$	0 to ±0.06	0 % to ±8.5 %
7	Beam separation	$\rho(\Delta x)$	-(1-ρ)	0.8? to 1	-20 % to 0 %
8	Vector averaging	z_0 [m] z [m]	$\frac{1}{2\left(\ln\frac{z}{z_0}\right)^2}$	0.01 to 2 m 10 to 1000 m	0 to 10 ?
9	Peak position	$\sigma_{\Delta f}$ [Hz] φ [radian] f_T [Hz]	$\pm\frac{c}{\sqrt{2}\sin\varphi}\frac{\sigma_{\Delta f}}{f_T}$	±0.5 Hz 15°-24° (0.26-0.42 rad) 1000 to 6000 Hz	0 to 10

Table 9. Error sources and estimates for SODARs

All except for the error 9 can be systematic (rain and fixed echo errors vary with conditions, but when present can lead to persistent errors which are non-random).

Errors caused by poor setting-up

Errors labelled 1, 2 and 3 are due to poor setting up of the SODAR. Errors 1 and 2 are generally limited to about ± 3%, but should be much less than this. A strong fixed echo can give a zero m s^{-1} wind speed, although SODAR software will in many cases filter out fixed echo contamination.

Some care in siting and establishing the SODAR is desirable. The temperature measured or assumed by the SODAR hardware/software should be checked against ambient temperature using the temperature readout which is (hopefully) provided as a software menu item. The SODAR does not have to be on level ground, but the transponder array should be level, for directly upward transmitting arrays. It may not be adequate to assume that the array is parallel or perpendicular to

some other face on the SODAR (such as a baffle). For SODARs which reflect the sound upward (to protect speakers from rain), levelling is much more difficult, and it is important to carefully follow the manufacturers instructions. The angle of the reflector from the horizontal should equal half the angle of the array to the vertical, plus 45°.
Whenever possible, the tilted beams should be oriented away from any tall structures such as turbines or masts. The SODAR should also be run for say one week with a turbulence intensity "facsimile" display to see if any persistent horizontal lines indicate presence of fixed echoes. If such horizontal lines are apparent, then the wind speed and direction profiles should be carefully checked to see if there appears to be any significant change in profile at the height indicated by the facsimile display.
Beam separation error may be a significant problem in complex terrain, such as a site on the ridge of a hill.

Errors fixed through SODAR design

Errors due to rain should be identified as bad data by SODAR software, but there may be residual contamination during light rain. For this reason, having a sensitive rain gauge also recording is a good idea.
Errors 5, 6, 7, and 8 are fixed through SODAR design. A narrow beam SODAR, with a moderate tilt angle, will generally have small beam spread error and beam separation error.
Beam drift error is inescapable, but generally also negligible over common wind ranges.
Some of the errors are larger for beams having a greater tilt angle, but the peak detection resolution is improved if the Doppler spectrum is more spread, which occurs for larger tilt angles.
It appears from Figure 5 that 3-beam SODARs may perform better at lower height ranges (when the SNR is higher and the more rapid cycling around beams is advantageous) but 5-beam SODARs are better at greater heights (when more redundancy is useful in case of bad data). If the interest is primarily in lower altitudes, it may be better to select only 3 beams if using a 5-beam system (the beams selected would be based on minimising fixed echoes).

8.2 Calibration procedures and limitations

Section 8.1 summarized the sources and magnitudes of errors which might affect SODAR calibrations. Within WISE WP3 the efficacy of various calibration techniques was also evaluated and, having chosen the most appropriate procedure, the outcome of a multi-platform calibration and its limitations were investigated.

Choice of calibration method

The calibration *method* should be easily replicated and checked. Calibration between several SODARs should obviously be consistent (it is undesirable to have distinct calibration methods for different SODAR models). The following methods were considered.

Method	Sensor	Advantage	Limitation
Self-calibration	Speaker/microphone	Simple check of SODAR circuits	No check on response to winds
Transponder	Robotic speaker/microphone or array	PC generation of echoes based on actual transmissions	Technologically challenging to develop
Free balloon sonde	Radar tracking	Well-established technology	Short observation period
Tethered balloon sonde	Propeller anemometers	Continuous direct sensing	Inaccurate due to swinging
Tall mast	Cup anemometers	Accurate	Expensive and not mobile
Short mast	Cup anemometers	Accurate, inexpensive	Limited height range

Table 10. Advantages and limitations of calibration methods considered

Of these, the last two offer accurate, existing, methods. It was resolved to use the tall-mast method to develop and check the short-mast method for routine calibration of SODARs.

Calibration best practice

The procedure for calibration using the tall-mast method is to site a number of different SODAR models near to a 120 m mast. The following is recommended.

1. The mast should extend above hub height for most current turbines. This is so calibration results will be of relevance to wind energy requirements
2. The mast be instrumented with well-calibrated cups and vanes at at least 6 sites spaced through the mast height. This ensures that any variation of SODAR calibration with height can be detected.
3. At least 3 different SODAR models be deployed. This is so that variations in calibration due to SODAR hardware/software design variations can be explored.
4. The SODARs operate simultaneously and continuously and without cross-interference.
5. The inter-comparison should continue through a typical range of weather patterns. This is to make sure that temperature and wind variations do not significantly affect calibrations. In practice this means a field campaign of several months.
6. The SODARs be sufficiently close to the mast that there should be a high correlation between mast and SODAR wind profiles, but sufficiently far away that fixed echoes are not a major feature of the SODAR data. In practice this means a distance of about 50-100 m for low-elevation objects, and even further for elevated objects such as masts
7. Both real time filtering and post processing be applied for bad data (low SNR), rain, excluded sector influenced by the mast, and low wind speeds below the cup calibration recommendations. These filters are described in Section 5.3.
8. Care be applied in setting up the SODARs, as described in Section 8.1.

Following calibration against cup anemometers on a tall mast, calibration against a short mast was investigated. For this method to be successful:

1. The mast must extend above the lowest couple of range gates of common SODARs. This is to ensure that valid data is obtained at mast top, unaffected by antenna ringing or ground interference problems. In practice this means a mast height of around 40 m.
2. A high-quality well-calibrated cup and vane be installed at the top of the mast.
3. The tall-mast calibration should prove that the calibration obtained at 40 m can be extended reliably to above hub height through knowledge of generic SODAR characteristics.
4. If the tall-mast work demonstrated calibration dependence on wind or temperature extremes, then the short-mast calibration will need to encompass a similar range of weather.
5. The SODAR be placed within about a mast height of the mast (40 m, say). Closer than this will be likely to cause fixed-echo errors; further away could cause larger residuals.
6. Filtering be applied for bad data (low SNR), rain, excluded sector influenced by the mast, and low wind speeds below the cup calibration recommendations. These filters are described in Section 5.3.
7. Care be applied in setting up the SODARs, as described in Section 8.1.

8.3 Testing of calibration procedures

Testing of the tall-mast and short-mast methods was conducted in two separate experiments: PIE; and ECN EWTW. Testing during PIE also included SODAR-SODAR "calibrations". The main conclusions from these experiments are as follows.

PIE SODAR-Tall mast calibrations

1. Raw SODAR data is contaminated by fixed echoes, rain, and bad records. Strong filtering, using manufacturers' methods are first required before finding calibration slopes

2. Although there is some evidence for non-linearity and for offsets, the model $V_s = mV_c + \varepsilon$ describes, with high correlation (>0.96), the relationship between SODAR wind speed V_s and cup wind speed V_c.
3. Estimates of slope, m, are not biased by variations in the distribution of wind speed, so that generally higher winds at greater heights do not cause non-linearity
4. Neutral atmospheric conditions give poor data availability, particularly at greater heights. In practice it is possible to approximately relate data availability to either Richardson number or Obhukov-Monin length.
5. Three very different SODAR designs (AeroVironment, Metek and Scintec) were compared. These in practice gave three very different slope calibrations, if treated as isolated instruments, emphasizing the need for routine calibration against a low mast.
6. RMS residual errors σ_ε in wind speed for all SODARs was around 0.4 m s^{-1}. This was not significantly different from the rms residual errors when two cup anemometers were compared at the same site and under the same wind conditions.
7. the AeroVironment SODAR overestimates wind speed by about 8% and the Metek SODAR underestimates wind speed by about 5%
8. When account is taken of a fixed echo at 100 m, both the AeroVironment and Metek SODARs have a calibration slope essentially independent of height
9. The Scintec SODAR has very good estimation of wind speed at 40-60 m, but the increasingly underestimates wind speed at higher altitudes
10. There is no diurnal variation (i.e. temperature variation) in calibration evident
11. There is weak evidence for calibration dependence on weather conditions
12. Selecting the appropriate direction sector for mast-SODAR comparisons is vitally important
13. Mast and SODAR directions show good agreement

PIE SODAR-Low mast calibrations

1. AeroVironment and Metek SODARs can be calibrated successfully against a low mast to obtain wind speeds at all heights to within about ± 1%
2. In this inter-comparison experiment, and for the AeroVironmnet and Metek SODARs, there is no statistically significant difference between variations in SODAR-cup calibrations and cup-cup calibrations.
3. The Scintec SODAR has a calibration which varies with height in these experiments, and so can not be successfully calibrated against a 40 m mast under the assumption that that calibration holds at all heights

Tests of calibrations in an alternative situation

1. Comparison between mast-SODAR calibrations on two different AeroVironment SODARs at two different sites show no significant differences
2. SODAR-SODAR regression slopes are consistent with SODAR-mast regression slopes, and demonstrate the possibility of calibrating one SODAR against a mast and then using that SODAR as a secondary standard for calibration of other SODARs
3. Use of a SODAR without any calibration is unreliable for wind-energy applications

8.4 Interpretation of errors recorded during PIE

There are two significant questions arising from the PIE calibration:

1. Why does the AeroVironment underestimate wind speed and the Metek overestimate?
2. Why is the Scintec slope close to 1 at 40 m but decrease with height?

If the wind speeds reported by the AeroVironment software are based on calculated (or even measured) beam tilt angles, then the beam spread weighting (described in Section 3.3) could readily explain an overestimation in wind speed of about 8%. The Metek is less affected, having a larger tilt angle: the reason for this is not known. The only error sources which could give an

underestimation for the Metek are temperature errors (a temperature sensor is installed, although the Salford SODAR was testing a new design which experienced some problems) or an out-of level error (but considerable care was taken by the Salford team to get the speaker array surface level). The Scintec uses pairs of opposing beams (+19° with -24°, -19° with +24°) which will give rather spatially separated sampling volumes, particularly with increasing altitude. It is suspected that this feature gives decreasing *m* with increasing altitude, as predicted by (3.65) in Section 3.9.

Estimated range of various errors from Table 9 are combined with calibration results from Figure 24 in Figure 44.

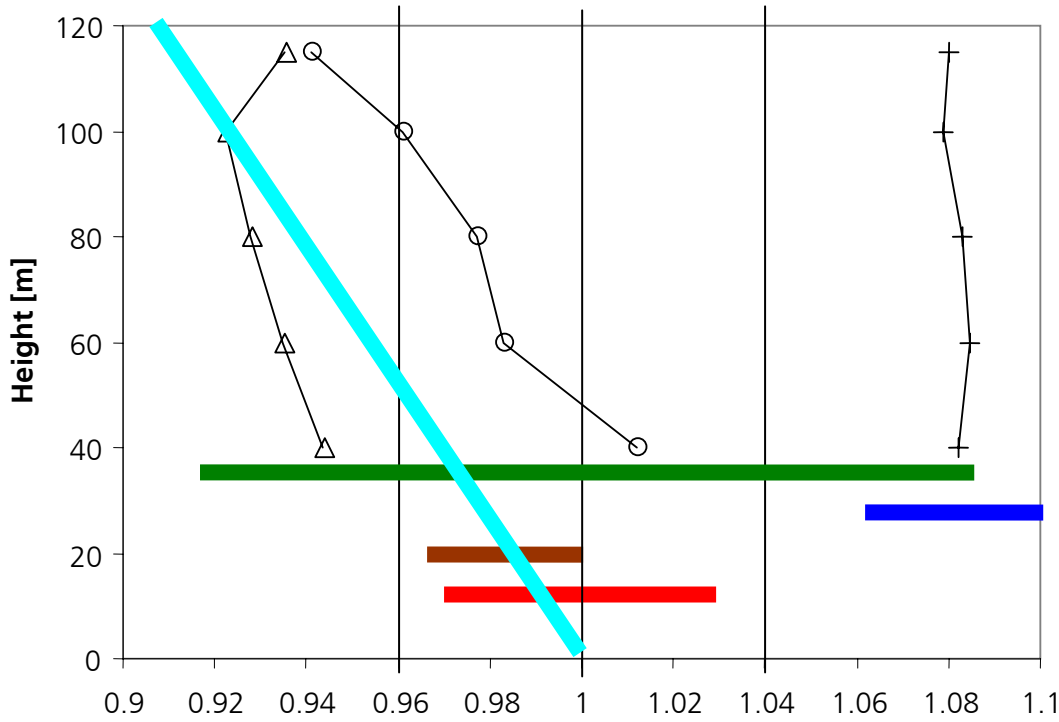

Figure 44. Regions of applicability of various errors, compared with calibrations from Figure 24. Temperature (red); out of level (brown); beam spread (dark blue) ; beam drift (green); beam separation (light blue).

This reinforces that

1. The overestimation of wind speeds by the AeroVironment SODAR is possibly due to beam spread error
2. The underestimation of wind speeds by the Metek SODAR is possibly due to combined out-of-level and temperature errors (beam drift errors are only significant at high wind speeds)
3. The decrease of calibration slope with height for the Scintec SODAR is possibly due to beam separation error.

8.5 Recommendations for improvements in SODARs for wind energy applications

This Report has shown that

1. SODARs can be calibrated to within the standard required for wind energy applications, and which is currently provided by mast-mounted cup anemometers.
2. There are differences between SODAR designs which may limit applicability of some designs

3. The proposed technique of calibrating against a 40 m mast cup anemometer is successful providing care is taken with siting of the SODAR, setting it up, and filtering of the SODAR data

What can be done to develop even better calibration techniques and/or more reliable and continuous SODAR operation?

1. Development of a means of self-calibration
2. Improved SNR by simultaneous transmission on several beams to obtain more averages per unit time and to improve data availability particularly in near-neutral conditions
3. More sophisticated digital signal processing and filtering to remove bad data
4. A rain rejection scheme (and preferably a scheme to obtains valid winds during rain)
5. Good diagnostics and information dissemination to the user
6. Automatic measurement of air temperature for beam tilt calculations
7. Detection of out-of-level
8. Designing with 5-beam capability
9. Attention to beam separation errors in tilt design

8.6 SODARs used in this study

It should be noted that the SODARs used in the PIE experiment are only three of many available commercial designs. They are from three manufacturers among those prominent in the market place, and between them typify most common design features while also having individual and specialised characteristics.

The three SODARs compared were owned by the research institutions involved in WISE, and there has been no attempt to select SODARs from across the full range of available models.

The PIE field trials were essentially conducted by the WISE partners, and not by the SODAR manufacturers, and so represent results which might be obtained by other well-informed users of SODARs. Although the participants attempted to obtain consistent, quality results from the field trials, any superior features, problems, or errors identified in this Report are not necessarily endemic within a particular SODAR model. This Report therefore does not imply either support or criticism for any specific SODAR model or manufacturer's products.

9. References

Antoniou I. and H. E. Jørgensen, 2003. Comparing SODAR to cup anemometer measurements. EWEA Wind Energy Conference and Exhibition, Madrid.

Antoniou I, H. E. Jorgensen, F. Ormel, S. G. Bradley, S. von Hünerbein, S. Emeis and G. Warmbier, 2003. On the theory of sodar measurement techniques Risø-R-1410 (EN), 59pp.

Dissanaike, Gishan and Wang, Shiyun, 2003. A critical examination of orthogonal regression. http://ssrn.com/abstract=407560

Antoniou I., H. E. Jorgensen, T. Mikkelsen, T. F. Pedersen, G. Warmbier and D. Smith, 2004. Comparison of wind speed and power curve measurements using a cup anemometer, a LIDAR, and a SODAR. EWEC Wind Energy Conference, London.

Georges, T. M. and Clifford, S. F., 1972. Acoustic sounding in a refracting atmosphere. *J. Acoust. Soc. Am.*, **52**, 1397-1405.

Georges, T. M. and S. F. Clifford, 1974. Estimating refractive effects in acoustic sounding. *J. Acoust. Soc. Am.*, **55**, 934-936.

Kindler, D., I. Antoniou, Hans. E. Joergensen, and M. de Noord. Operational Characteristics of SODARs – External Meteorological Influences . Proc. 12th International Symposium on Acoustic Remote Sensing and Associated Techniques of the Atmosphere and Oceans, Cambridge, UK, July 2004.

Ostashev, V. E., 1997. Acoustics in moving inhomogeneous media. Spon, London. ISBN 0 419 22430 0, 259pp.

Panofsky, H. A., H. Tennekes, D. H. Lenshow and J. C. Wyngaard, 1977. The characteristics of turbulent components in the surface layer under convective situations. *Bound. Layer Met.*, **11**, 355-361.

Phillips, P. D., H. Richner and W. Nater, 1977. Layer model for assessing acoustic refraction effects in echo sounding. *J. Acoust. Sco. Am.*, 62, 277-285.

Schomburg, A. and D. Englich, 1998. Analysis of the effect of acoustic refraction on Doppler measurements caused by wind and temperature. *Proc. 9th Int. Symp. Acoust. Rem. Sens., Vienna*.

Werkhoven, C. J., S. G. Bradley, 1997. The Design of Acoustic Radar Baffles. *J. Atmos. Oceanic Technol.,* **14**, 360-367.

Bibliographic Data Sheet

Title and authors

SODAR calibration for wind energy applications

Stuart Bradley (ed.), Ioannis Antoniou, Sabine von Hünerbein, Detlef Kindler, Manuel de Noord, and Hans Jorgensen.

ISBN 0-9541649-1-1

Pages	Tables	Illustrations	References
68	10	44	12

Abstract

The method traditionally used for measuring the wind speed and direction for wind energy purposes is to record the output from cup or propeller anemometers at several heights on a mast. As turbines have grown in height, this method has become increasingly more expensive and difficult, and new methods have been sought.

One alternative method for measurement of wind speed and direction over depths of around 200m is the SODAR (SOund Detection And Ranging). This instrument is installed on the ground and every few seconds transmits a short pulse of sound upward into the atmosphere. As the sound propagates upward, some acoustic energy is continuously reflected back to the ground by the variable atmospheric turbulence encountered. By analysing the Doppler frequency shift of echoes received from sound transmitted at a small angle to the vertical, wind speed components are estimated as a function of height.

SODAR technology is well established as a tool for visualising and quantifying atmospheric dynamics in the lowest few hundred meters. At the same time, use of SODAR technology as a replacement for cup or propeller measurements in wind energy applications has a number of potential drawbacks. These include the need to calibrate much more rigorously than generally required for other applications, and the requirement that the SODAR operates with well-specified performance over the full range of atmospheric conditions relevant to wind turbine operations. Furthermore, SODAR performance should be portable from one physical site to another, and instruments supplied by a variety of manufacturers should be able to be deployed with known characteristics.

Within the WISE (WInd energy SODAR Evaluation) project (EU project number NNE5-2001-297), work package WP3 described in this report, is concerned with:

a) An estimation of the uncertainties in calibration which arise from SODAR design and operation.
b) Description of calibration procedures established by the WISE project and an evaluation of their limitations.
c) Testing of the calibration procedures against other methods of measurement.
d) Suggestions for improvements in SODAR design.

Items (a), (b), and (c) comprise Project deliverable D4 (Report on calibration of SODAR and inter-comparison before and after calibration). Item (d) comprises Project deliverable D5 (Notes on possible improvements of SODAR hardware/software for easier and better calibration).

The central conclusions of this work are

1. Care and understanding of SODAR error sources are required in order to adequately calibrate SODARs
2. A reliable calibration method is to calibrate a SODAR against a cup anemometer mounted at the top of a 40 m mast, and to use this calibration to correct SODAR wind speeds at other heights.
3. When compared with quality cup anemometers, corrected SODAR wind speeds show similar rms fluctuations to those exhibited between two cup anemometers
4. SODAR wind directions show good agreement with mast mounted vanes
5. Variations between SODARs of the same design appear to be small
6. Design changes could improve SODAR operation for wind energy applications.

Descriptors INIS/EDB

SODAR CALIBRATION; WIND MEASUREMENT; WIND ENERGY; SODAR ERRORS; WIND TURBINES; ACOUSTIC REMOTE SENSING; ANEMOMETER

ISBN 0-9541649-1-1

Research Institute of the
Built and Human Environment
The University of Salford,
Brindley Building
Salford, Greater Manchester
M5 4WT. United Kingdom